UNIVERSITÄT OSNABRÜCK

Magnetic properties and proton spin-lattice relaxation in molecular clusters

Dem Fachbereich Physik der Universität Osnabrück
zur Erlangung des Grades eines

Doktors der Naturwissenschaften

vorgelegte Dissertation von

Dipl.–Phys. Mohammed Allalen

aus Tizi-Ouzou, Algerien

Osnabrück, 03/05/2006

Betreuer : Apl. Prof. Dr. Jürgen Schnack
Prof. Dr. Klaus. Bärwinkel
Apl. Prof. Dr. Heinz-Jürgen Schmidt.

Heisenberg, wearing a tuxedo for the wedding of one of his youth movement comrades in the late 1920s.

The leading theory of the atom when Heisenberg entered the University of Munich in 1920 was the quantum theory of Bohr.

All of my meagre efforts go toward killing off and suitably replacing the concept of the orbital path which one cannot observe.

–Heisenberg, letter to Pauli, 1925

The present paper seeks to establish a basis for theoretical quantum mechanics founded exclusively upon relationships between quantities which in principle are observable.

–Heisenberg, summary abstract of his first paper on quantum mechanics

Contents

List of Figures

List of Tables

1. Introduction

The continued interest in the fabrication and optimization of miniaturized magnetic devices [1], where quantum effects become important makes it essential to understand the interaction between the classical properties of the macroscale and the quantum properties of the microscale. Richard Feynman said in 1959 that:*"the principles of physics do not speak against the possibility of maneuvering things atom by atom. It would be possible for a physicist to synthesize any substance that the chemist writes down"*. Recently, the impact of chemistry in the field of magnetism, which is one of the most challenging properties observed in nature, has dramatically increased with the development of magnetic molecular clusters, where the techniques of molecular chemistry are exploited in order to design and to synthesize a new classes of magnets based on molecules rather than on metals or oxides.

Molecular magnets are the smallest particle of a pure chemical substance that still retains their chemical composition and properties, which possess, even in the absence of external magnetic fields, stable magnetic moments associated with certain chemical building blocks [2, 3, 4]. The word molecule usually refers to an assemblage of multiple atoms held together by covalent bonds. A molecule consists of two or more atoms joined by shared pairs of electrons in a chemical bond. It may consist of atoms of the same chemical element, as with oxygen (O_2), or of different elements, as with water (H_2O) [5, 6]. As described below, many dynamical properties have been discovered, which are derived from easy handling nature and the quantum effects, and these studies are different from those of inorganic magnetic materials that are expected to provide intense magnetization. The studies of molecular magnets have started in order to discover static ferromagnetism in organic materials. However, since deeper microscopic understanding of the mechanisms of ferromagnetic and antiferromagnetic interactions has been achieved, the researches have consequently provided a new frontier field of dynamical magnetism such as ferromagnetic-antiferromagnetic switchings. Controlled magnetism, namely the material design for easy handling of magnetization, is now one of the most attractive subjects [7]. Moreover, in molecular magnets, the spin structure can be often designed artificially, this leading to successful preparation of many model magnets that contribute to the development of the theory of magnetism [8]. Typical good examples are one-dimensional Haldane magnets, two-dimensional Kagome antiferromagnets with spin frustration [9], etc.

In the last few years, high-spin cluster complexes have extensively been designed and synthesized, and much attention has been paid to a special quantum effect observed uniquely in these systems: Magnetization reversal by quantum tunneling was inherently predicted in single-domain magnets of small particles. It is recognized, however, that recent intensive researches in this field could not be realized without discovery of the cluster complexes [10, 11, 12]. Considering such progress, it is easily expected that the molecular magnet researches can be extended to the microscopic field, namely the nanomagnet researches. Capability of structural design in molecules may allow one to develop new nano-magnets containing, for instance, supramolecules or hierarchical structure. Such high-order nano-magnets are interestingly related to biomagnets such as nano-magnets in magnetic bacteria and iron oxides in ferritin protein. Molecular magnets can be regarded not only as magnetic materials but as open-shell active species. Considering that many organic radicals appear as reaction intermediates, understanding of intermolecular interaction between organic radicals should contribute to clarification of the functionalities and the reaction mechanism of radical species in living systems [13].

On the other hand, the observation of resonant tunneling of magnetization in Mn12-Acetate has focused significant attention on a novel class of spin-ordered organometallic molecules. These molecules have evolved into one of the most attractive research areas in the field of molecule-based magnets. These molecular magnets consist of approximately 50 - 400 atoms and are typically composed of 4 - 20 transition metal ions locked in place by organic ligands and anions. Several reviews are available documenting the chemical and technological implications of this field of molecular nanomagnets [2, 14, 15, 16, 17, 18].

Although these new materials exhibit a number of unusual phenomena of scientific interest, some have potential for practical applications. These materials appear as macroscopic samples, i.e. crystals or powders, some have a cage-like structure that resembles fullerenes (the soccer-ball like molecule named giant Keplerate $\{Mo_{72}fe_{32}\}$ [5], see figure: 1.1), while others are shaped like tubes, called nanotubes ... etc... The intermolecular magnetic interactions are utterly negligible as compared to the intramolecular interactions. Therefore, measurements of their magnetic properties reflect mainly ensemble properties of single molecules. In addition to very interesting chemistry and physics, such molecular systems could form the basis of future nanoscale devices. Their magnetic properties promises potential applications including high-density magnetic storage devices[1], magneto-chemistry, and tunable high-frequency radiation sources, biomedical imaging, biology and material sciences [3, 4]. Tunneling and quantum coherence are also interesting in components for possible use in q-bits for quantum computing [20, 21], while local thermo-induced

[1] single-molecule "domains" → up to 40 Tbits/sq. inch;

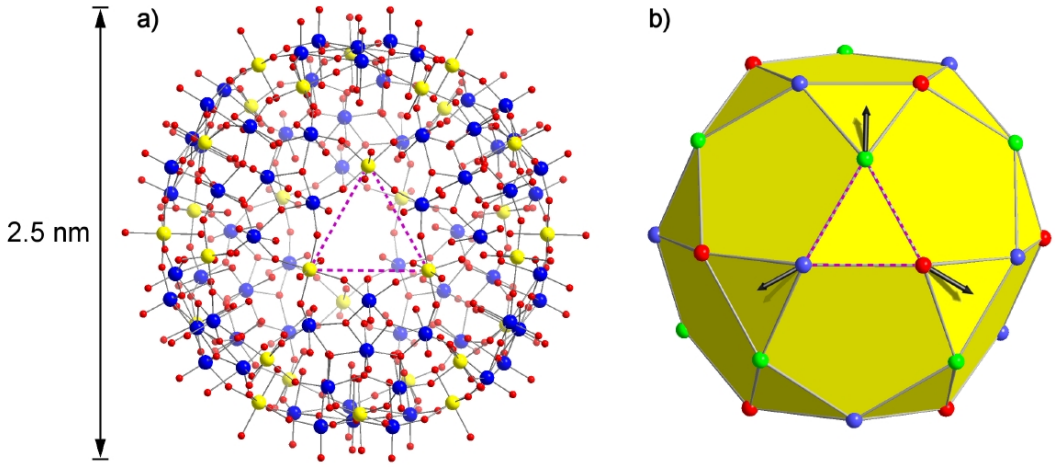

Figure 1.1.: The structure of the $\{Mo_{72}Fe_{30}\}$, a giant keplerate molecule where 30 iron are placed at the vertices of an icosidadecahedron [19].

spin-crossover transitions may bring revolutionary progress in the design of large-size displays due to spin dependence of the color of some magnetic molecules [4]. The use of magnetic molecules in biomedicine is growing rapidly. An example is the use of such molecules to enhance the NMR relaxation rate in specific target areas where greater contrast is needed for magnetic resonance imaging [6].

A major part of the study of molecular structure is the description of the chemical bonds which are formed between atoms. A stable compound occurs if the total energy of the combination has lower energy than the separated atoms. The two extreme cases of chemical bonds are: *Covalent bond*, in which one or more pairs of electrons are shared by two atoms. *Ionic bond*, in which one or more electrons from one atom are removed and attached to another atom, resulting in positive and negative ions which attract each other. Other types of bonds include metallic bonds [2] and hydrogen bonding [3]. In addition to novel isolated (except for dipole interactions) magnetic molecules, there exist a number of inorganic materials composed of well defined clusters of magnetically active atoms. Typically these clusters are separated far enough apart to ensure intra-cluster couplings to be dominant, but inter-cluster couplings are not negligible. These systems provide the possibility to study how many-spin systems interact dynamically among each other with weak to moderate inter-cluster coupling strengths. It appears that the majority of these molecules is rather well

[2] Where the atoms possess strong bonds with the electrons that can move freely in all directions in a metal.

[3] It is a force of attraction between a hydrogen atom in one molecule and a small atom of high electronegativity in another molecule. That is, it is an intermolecular force, not an intramolecular force as in the common use of the word bond.

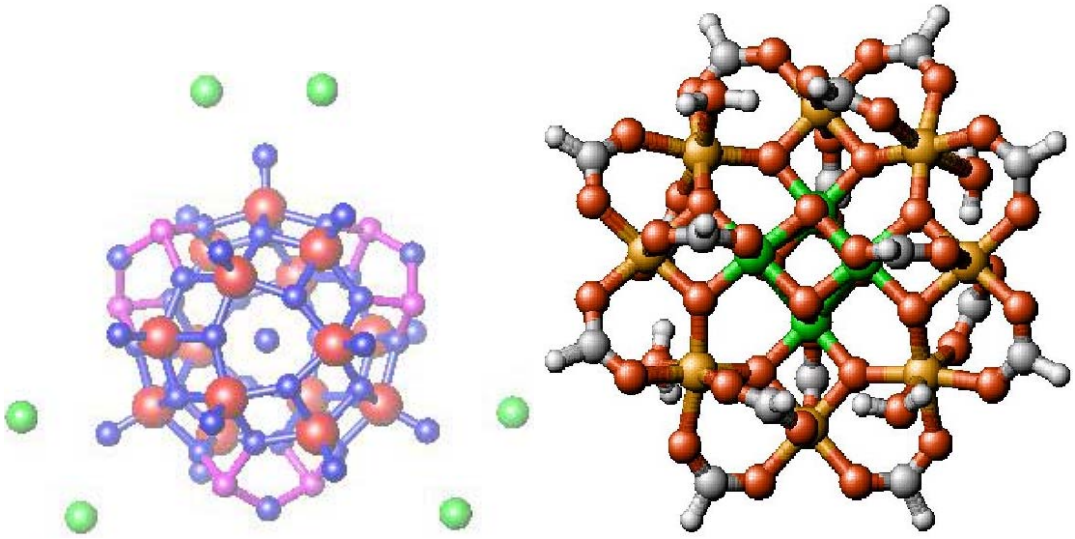

Figure 1.2.: Structure of $[V_{15}As_6O_{42}]K_6$ (l.h.s) [22] and $Mn_{12}O_{12}(CH_3COO)_{16}$ (r.h.s) [23] molecular magnets.

described by the Heisenberg model with isotropic nearest neighbor interaction sometimes augmented by anisotropy terms [24, 25, 26, 27]. Thus, the interest in the Heisenberg model, which is already known, but used mostly for infinite one-, two-, and three-dimensional systems, was renewed by the successful synthesis of magnetic molecules. Studying such spin arrays focuses on qualitatively new physics caused by the finite size of the system.

Training in molecular magnetism and the ability to proceed with careful measurements and theoretical methods from small molecules to larger clusters represents a wonderful laboratory with which to follow correlation and exchange interactions across important length scales, and means learning techniques which can be used for the different scientific areas mentioned above, using statistical mechanics, which includes mathematical tools for dealing with large populations, to the field of mechanics, which is concerned with the motion of particles or objects when subjected to a force. It provides a framework for relating the microscopic properties of individual atoms and molecules to the macroscopic or bulk properties of materials that can be observed in every day life, therefore explaining thermodynamics as a natural result of statistics and mechanics (classical and quantum). In particular, it can be used to calculate the thermodynamic properties of bulk materials from the spectroscopic data of individual molecules.

Significance and necessity of this project:

1. The first major goal of the present work was to explore the magnetism and to reexamine earlier susceptibility measurements for a new class of materials the wheel-shaped Tungstophosphate $[Cu_{20}Cl(OH)_{24}(H_2O)_{12}(P_8W_{48}O_{184})]^{25-}$ ($Cu_{20}P_8W_{48}$) [28], the dodecanuclear cluster $[Ni_{12}CO_3(OMe)_{12}(OAc)_9(\text{trans-tach})_6]$, and the heterometallic $\{Cr_7M\}$ wheels [29], in which one of the Cr^{III} ions of Cr_8 has been replaced by a Fe, Cu, Zn, Ni ion where this extra-spin acts as local probe for the spin dynamics. Such systems have been synthesized recently and they are well described using the Heisenberg spin Hamiltonian with a Zeeman term of an applied magnetic field along the z-axis. The magnetic ions in these molecules can interact ferromagnetic or antiferromagnetic through intervening O^{2-} ions. Using the numerical exact diagonalization method (Sec. 3.1), we calculate the energy spectrum and the eigenstates for different compounds, and use them for reexamining the available experimental susceptibility data to determine the values of exchange parameters. The results of this exchange energy will be used to extract much more information from these new materials, to provide the thermodynamic properties such as magnetization and susceptibility or heatcapacity.

2. This part focus on the low temperature regions where the molecular magnets act as individual quantum nanomagnets and can display super-paramagnetic phenomena like macroscopic quantum tunneling, ground state degeneracy, level-crossing. Here, we investigate how the various heterometallic rings would behave when probed by Nuclear Magnetic Resonance (NMR), using the theory of the interaction between the nuclear spin and the electron spin. We aim at the principle structure of the relaxation rate T_1^{-1} as a function of the applied magnetic field strength at low temperatures as it is measured in Nuclear Magnetic Resonance (NMR) experiments. The relaxation rate is expected to increase drastically whenever two levels approach each other due to possible resonant energy exchange with the surrounding protons. In contrast to this expectation it appears that $\{CuCr_7\}$ and $\{NiCr_7\}$ show an unexpectedly reduced relaxation rate at certain level crossings which should experimentally be observable.

The outline of the present work is as follows. In chapter 2, we will discuss and explore how quantum theory deals with molecular magnets. Chapter 3 gives a brief description of the symmetry used in heterometallic $\{Cr_7M\}$ wheels and the application for different rings by means of exact numerical diagonalization techniques. We evaluate the energy spectrum, eigenstates and the exchange parameters by fitting the experimental susceptibility of different rings. In chapter 4, once the calculated energy and the eigenvectors for different rings and the values of exchange parameters are well defined, we will proceed with the coupling between magnetic molecular levels and nuclear spins to explain the phenomena of level-crossing at specific magnetic field values, where we investigate the theoretical framework used to study the proton spin-lattice relaxation rate (T_1^{-1}) and to describe semiquantita-

tively the results of T_1^{-1} versus applied magnetic field B and temperature T. Chapter 5 and 6 contain the study of the magnetic properties of the dodecanuclear cluster $[Ni_{12}CO_3(OMe)_{12}(OAc)_9(\text{trans-tach})_6]$ presented recently by Geoffrey J. T. Cooper *et al.* and the wheel-shaped Tungstophosphate $[Cu_{20}Cl(OH)_{24}(H_2O)_{12}(P_8W_{48}O_{184})]^{25-}$ ($Cu_{20}P_8W_{48}$) [28], respectively. Chapter 7 summarises the main results of the present work and provides an outlook.

2. Quantum theory of Molecular Magnetism

In this chapter, many of the basic concepts and tools of quantum theory of molecular magnetism are discussed only at an introductory level and without providing much of the background needed to fully comprehend them. Most of these topics are magnetic properties, the thermodynamic properties, and spin dynamics in molecular magnets. In the end, we will give a brief description about the experimental method such us NMR and ESR used to study the spin dynamics properties. The purpose of the present Chapter is to give an overview of the field that one can understand the details and applications of the later chapters.

2.1. Magnetic order in magnetic materials

Molecular magnetic clusters are currently considered among the most promissing electron spin based quantum systems for storing and processing of quantum information [30]. Each molecule, hence, forms a magnet. Thus if a magnetic field is applied to these molecular magnets, they will arrange themselves and align to increase this effect. The magnetic moments of the ions in those cluster order at low temperatures anti-parallel or parallel to each other. These ordered states are called ferromagnetic [31] and antiferromagnetic [32, 33] systems and have attracted an increasing interest [34].

2.1.1. Diamagnetism and paramagnetism

2.1.1.1. Diamagnetism

Diamagnetic materials are often defined as substances which are lifted out of the magnetic field region and they possess a negative value of magnetic susceptibility of the order of χ_{mol} = -10 x 10^{-9} m^3 mol^{-1}. In this type of magnetic order the susceptibility is a temperature independent quantity, all electrons are paired. The observed diamagnetism reflects the fact that the ground state is a singlet and there are no thermally populated states of higher spin multiplicity. The properties of diamagnetic systems are:

- $\chi < 0$ and M < 0 owing to small additional currents attributable to the precession of electron orbits about the applied magnetic field (shown by all substances);
- χ usually independent of both T and B for purely diamagnetic materials (closed shell systems);
- Allowed for as diamagnetic correction in the evaluation of experimental susceptibility data of open shell systems.

Some substances exhibiting diamagnetic behavior can switch to a paramagnetic state when the temperature is increased, table 2.1. However, paramagnetic excited states are populated and the substance shows an increased positive magnetic susceptibility.

substance class	Molar susceptibility	range (cm^3mol^{-1})	localized electrons	itinerant (Free)
diamagnets	$\chi < 0$	$-10^{-4} \ldots -10^{-6}$	closed shell atoms, Langevin	Landau
vacuum	$\chi = 0$			
paramagnet	$\chi > 0$	$-10^{-2} \ldots -10^{-5}$	open shell atoms Langevin, Curie law	Pauli

Table 2.1.: Substance class of magnetic order

2.1.1.2. Paramagnetism

As opposed to diamagnetic substances, paramagnetic ones are those which are directly proportional to the applied magnetic field, and inversely proportional to the temperature (Curie's law). Their magnetic susceptibility is positive and temperature dependent. The properties of such types of magnetic order are

- $\chi > 0$ and $M > 0$ owing to net spins and angular momentum polarized in direction of the applied field;
- Observed in various forms, differing in magnitude and dependency on T and B:
- Curie paramagnetism: χ inverse dependency on T, independence on B at weak applied fields, but inverse dependency at strong fields (paramagnetic saturation)

- temperature independent paramagnetism: weak forms of paramagnetism, called Pauli paramagnetism (of conduction electrons observed in metals) and Van Vleck paramagnetism (TIP, second order effect involving mixing with the first excited multiplet by the applied field; example: Eu^{3+}).

In paramagnetism the tendency for angular momenta to be aligned parallel with the field direction is in competition with the thermal disorder. Therefore, the greater the temperature the greater the thermal disorder, the lower the degree of alignment and the susceptibility drops inversely with temperature, which correspond to Curie's law.

Curie law
Magnetization M is given as a function of magnetic field B and temperature T as

$$\chi_{mol} = \frac{M_{mol}}{H} = \frac{C}{T} \qquad \text{where C is a constant} \qquad C = \mu_0 \frac{N_A \mu^2}{3K_B}. \tag{2.1}$$

2.1.2. Ferromagnetic systems

The atomic spins in ferromagnetic materials interact with each other, each of them trying to align the others in its own direction. This effect between them is relativistically quantum mechanical properties of spins, as axiom the existence of such a force which tries to align spins, by the so-called *exchange energy* between spin $\vec{S}_i$ and spin $\vec{S}_j$, which is proportional to $\vec{S}_i \cdot \vec{S}_j$ [35], where the case $i = j$ is excluded, because the spins do not interact with themselves, and including the inetraction energy with an applied field. The best known ferromagnets are the metals Fe, Co and Ni. Such materials are characterized by a possible permanent magnetization, and generally have a profound effect on magnetic fields. The energy levels of the $3d$-electrons which give rise to the spin magnetic moments in these metals form a band, like those of the conduction electrons. The low energy properties of small ferromagnetic systems are in good approximation described in terms of the total spin S of the system. For illustration, consider a ferromagnetic system with total spin S described by the spin Hamiltonian $\underset{\sim}{H}$ in the absence of an external magnetic field, which can be written as:

$$\underset{\sim}{H} = -D\underset{\sim}{S_z}^2 + E\left(\underset{\sim}{S_+^2} + \underset{\sim}{S_-^2}\right) \tag{2.2}$$

with $D >> E > 0$, (D, E are the parallel and transverse anisotropy, repectively), $\underset{\sim}{S_\pm} = \underset{\sim}{S_x} \pm i\underset{\sim}{S_y}$ and $\underset{\sim}{S_\alpha}$ with α =x,y,z are the components of the spin operator. Due to E, the $\underset{\sim}{S_z}$ eigenstates $|\, m \,\rangle$ with m = -S, -S+1, ... , S-1, -S are not energy eigenstates. Rather, $E \neq 0$ gives rise to a mixing of states $|\, m \,\rangle$ and $|\, n \,\rangle$ with $|m-n|$ / 2 integer.

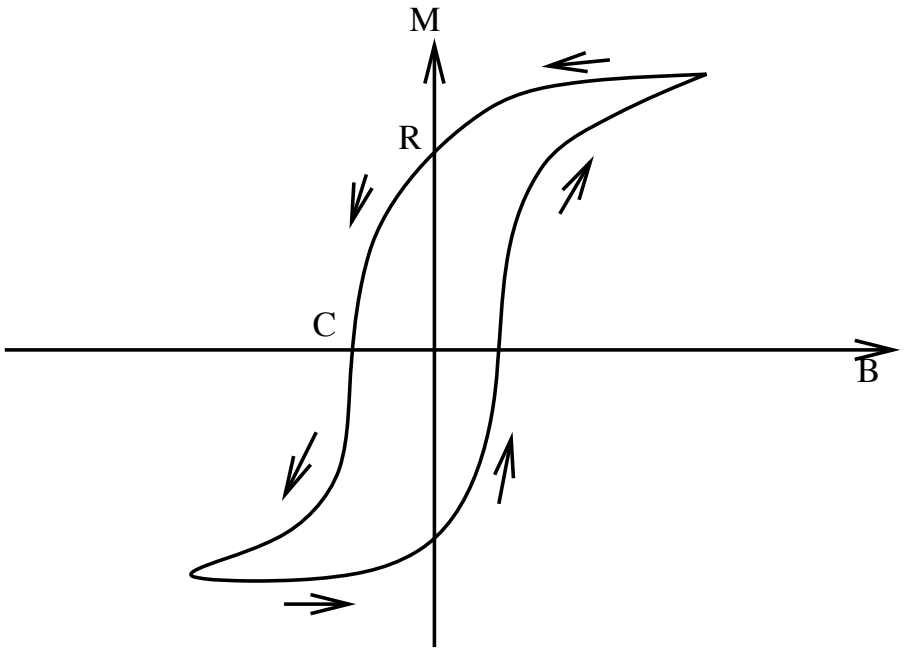

Figure 2.1.: Hysteresis loop of a ferromagnetic material.

More specifically, for $S = 1$, in the basis of $\underset{\sim}{S_z}$ eigenstates,

$$\underset{\sim}{H} = \begin{pmatrix} -D & 0 & 2E \\ 0 & 0 & 0 \\ 2E & 0 & -D \end{pmatrix} \tag{2.3}$$

The transverse anisotropy E$\neq$ 0 lifts the degeneracy between $|-1\rangle$ and $|1\rangle$. The energy eigenstates are $|0\rangle$ and $|e_\pm\rangle = (|-1\rangle \pm |+1\rangle)/\sqrt{2}$ with energies E_0 =0, and $E_\pm = -D \pm 2E$, respectively. The quantum spin system exhibits a rich and interesting behavior when a magnetic field B is applied,

$$\underset{\sim}{H} = -D\underset{\sim}{S_z^2} + E\left(\underset{\sim}{S_+^2} + \underset{\sim}{S_-^2}\right) + g\mu_B\left(B_x\underset{\sim}{S_x} + B_z\underset{\sim}{S_z}\right). \tag{2.4}$$

The longitudinal field B_z allows one to establish or destroy the tunneling resonance between two given levels $|m\rangle$ and $|n\rangle$. The transverse field B_x gives rise to intriguing effects such as Berry phase oscillations which can be traced back to the geometrical phase acquired by a spin tunneling in a transverse magnetic field [36, 37].
Ferromagnetic materials are used either to channel magnetic flux (e.g., around transformer circuits) or as sources of magnetic field (permanent magnets). For use as a permanent magnet, the material is first magnetized by placing it in a strong magnetic field. It is vitally important that a permanent magnet should possess both a large

retentivity or called also remanence (R) and a large coercivity (C), Figure 2.1. It is generally a good idea for the ferromagnetic materials used to channel magnetic flux around transformer circuits to possess small remanences and small coercivities.

2.1.3. Antiferomagnetic systems

When the magnetic susceptibility increases with temperature up to the critical point called the Néel temperature or the antiferrromagnetic Curie temperature, beyond which the susceptibility decreases in the normal paramagnetic fashion. This phenomenon is called antiferromagnetism where it tends to align the neighboring spins anti-parallel to each other, which can also give rise to certain order at low temperatures. These phenomena are contrasted with the "magnetically dilute" situation in paramagnetism in which there is no or very little interaction between spins [38, 39].

The theory of this phenomenon was presented by Louis Néel (French physicist, who in 1936 gave one of the first explanations of antiferromagnetism), even before it was first observed experimentally [40] (Nobel lecture). This spontaneous anti-parallel coupling of atomic magnets is disrupted by heating and disappears entirely above a certain temperature, called the Néel temperature, characteristic of each antiferromagnetic material. Usually these temperatures are low. The Néel temperature for manganese oxide (MnO), for example, is 122 K (or -151 C^0). Below the Néel temperature the susceptibility depends on the direction of the external field relative to the easy axis, which is defined by the minimum of the anisotropy energy.

The occurrence of this Nèel temperature may be visualized in the following way: At very low temperatures, an alternating "up and down" type of spin arrangement is established in the absence of any external field (Fig: 2.2). A strong negative magnetic interaction is said to exist between the plus and minus spin which decreases the tendency of all spins to be magnetized with decreasing temperature. As the temperature is increased, the uncoupling of magnetic spins facilitates greater and greater magnetization up to the Nèel point; then, as with normal paramagnetism, with further increase in temperature beyond this point, the susceptibility decreases due to thermal-randomization of spins. The theoretical description of antiferromagnetic system is more challenging than that of their ferromagnetic counterparts which are well described in terms of a single large spin. The main reason for this is that, in contrast to the ferromagnetic system, for the anstifferomagnet the Néel ordered state is not an energy eigenstate of the quantum spin system [41]. Let's consider two antiferromagnetically coupled spins $\underset{\sim}{s_1}$ and $\underset{\sim}{s_2}$ with spin quantum number s and an easy axis anisotropy,

$$\underset{\sim}{H} = J\vec{s_1}.\vec{s_2} - K_z\left(\underset{\sim}{s}^2_{1,z} + \underset{\sim}{s}^2_{2,z}\right) \tag{2.5}$$

$$= \frac{J}{2}\left(\underset{\sim}{S}^2 - 2s(s+1)\right) - K_z\left(\underset{\sim}{s}^2_{1,z} + \underset{\sim}{s}^2_{2,z}\right) \tag{2.6}$$

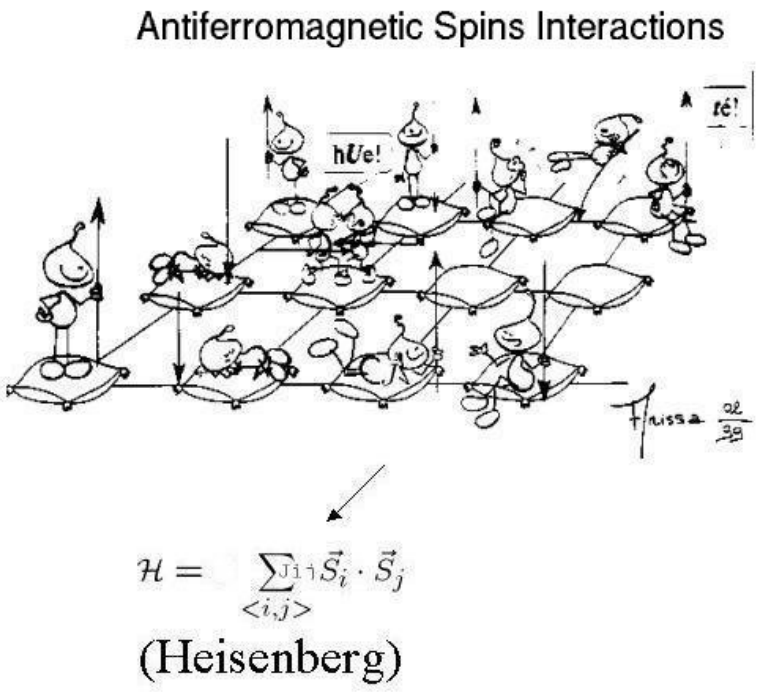

Figure 2.2.: Schematic sketch of the arrangement of the antiferromagnetically coupled ions.

Where, $\vec{S} = \vec{s_1} + \vec{s_2}$ is the operator of total spin.

For $K_z = 0$, $[\vec{S}, \underset{\sim}{H}] = 0$ and the total spin is a good quantum number. Diagonalization of the Hamiltonian is greatly simplified in such cases with spin symmetry. For $K_z \neq 0$, the Hamiltonian is no longer block diagonal in the S-subspaces whereas $\underset{\sim}{S}_z$ remains a good quantum number in absence of a magnetic field. Perturbation theory in the anisotropy term in Eq. (2.5) is valid as long as the typical energy scale of the anisotropy term, $2\mathrm{K}_z\mathrm{s}^2$, is small compared to J, the characteristic energy scale of the exchange term. For $2\mathrm{K}_z\mathrm{s}^2 \gtrsim \mathrm{J}$, the energy eigenstates must be determined from the diagonalization of the full Hamiltonian Eq. (2.5) in the various subspaces with given S_z.

2.2. Exchange interaction

From sec. 2.1, it is well known that the antiferromagnet and ferromagnet in ionic crystals originates from the interaction between spins of magnetic ions; the interaction is written as:
-J$_{ij}$ $\vec{S}_i \cdot \vec{S}_j$. An interaction of this type is called the exchange interaction; the coupling constant J_{ij} is the exchange integral. It originates from the a quantum exchange term of the Coulomb interaction between d electrons on neighboring ions and Pauli exclusion principle [1]. It has been studied since the early days of quantum mechanics [42, 43] and has been reviewed in some classic references [44, 45]. Recently, a promising proposal [46] has emerged to use exchange interaction as a tunable qubit-qubit interaction in a quantum computer, with the individual spins of electrons acting as qubits.

2.3. Theoretical models

In recent years several models and theories were proposed to study molecular magnets and to understand the mechanism of the exchange interaction between the ion spins in molecular clusters. The large molecular magnetic clusters can now be synthesized in bulk quantities by chemical techniques and arranged in crystal lattice, so that each constituent magnetic object has perfectly defined size and structure [47]. The molecular clusters with antiferromagnetic exchange interactions are particularly appealing not only from an esthetical point of view. Rather, the high symmetry of these compounds limits the number of parameters in the microscopic spin Hamiltonian. It is also found that antiferromagnetic interactions are favored in most molecules leading to nontrivial ground states. The magnetic system is well modeled by a system of spins located at certain positions in a lattice, where the interaction of neighboring spins contributes to the total energy of the system.

Simple Model for Magnetism:
In the case of unpaired electron spins, which are coupled and aligned. The sum of their magnetic fields gives macroscopic magnetism.

$$\bigstar \text{low temperature} \rightarrow \begin{cases} \rightarrow \text{alignment} \\ \rightarrow \text{large magnetization} \end{cases}$$

[1] Only two electrons with opposite spin may share the same orbital.

★ high temperature → disorder (thermal fluctuations) $\begin{cases} \rightarrow \text{random alignment} \\ \rightarrow \text{spins and fields cancel} \\ \rightarrow \text{no magnetization} \end{cases}$

2.3.1. Heisenberg model

Usually, in the majority of these molecular magnets, the interaction between the localized single-particle magnetic moments can be rather well modeled and described via the most common theoretical approach in this field which is called the Heisenberg Hamiltonian or Heisenberg model, with isotopic (nearest neighbor) interaction and an additional anisotropy term [24, 25, 26, 27]. Further on, dipolar interaction are usually of minor importance, and the Zeeman term added, yielding

$$\underset{\sim}{H} = \underset{\sim}{H}_{Heisenberg} + \underset{\sim}{H}_{Anisotropy} + \underset{\sim}{H}_{Zeeman} \ . \tag{2.7}$$

$$\underset{\sim}{H} = \sum_{i,j}^{N} J_{ij} \vec{S}_i \cdot \vec{S}_j - \sum_{i=1}^{N} d_i (\vec{e}_i . \vec{S}_i)^2 + g\mu_B \vec{B} \cdot \sum_{i=1}^{N} \vec{S}_i \ , \tag{2.8}$$

Where J_{ij} is a symmetric matrix containing the exchange parameters between spins at sites i and j. $\vec{S}_i$ is the spin vector at site i with spin quantum number S, J_{ij} nearest neighbor exchange interaction, where the notation as above corresponds to $J_{ij} > 0$ for antiferromagnetic coupling. The second term is the anisotropy term, which usually simplifies to a large extend, for instance for spin rings, where the site-dependent directions $\vec{e}_i$ are all equal, e.g. $\vec{e}_i = \vec{e}_z$ and the strength is the same for all sites d_i = d (z the uniaxial anisotropy axis). The third part (Zeeman term) in the full Hamiltonian describes the interaction with the external magnetic field $\vec{B}$. J_{ij} remain to be determined experimentally, for example, from the measurement of the magnetization curve as function of the magnetic field and the angle between the magnetic field and the ring axis of the molecules [48, 49]. For most antiferromagnetic molecular rings synthesized to date, J has been well established by various experimental techniques including electron spin resonance [27], specific heat [50], torque magnetometry and magnetic susceptibility [26], inelastic neutron scattering [51, 52], and spin relaxation in nuclear magnetic resonance [53].

2.3.2. Evaluating the spectrum

Product basis

The Hamiltonian has eigenstates $|\psi_n>$ with a corresponding set of eigenvalues E_n

$$\underset{\sim}{H}|\psi_n> = E_n|\psi_n> \tag{2.9}$$

These eigenstates form a basis of the Hilbert space of the system, and can be constructed by so called product basis given by

$$|\vec{m}> = |m_1, m_2, \ldots, m_u, \ldots, m_N> , \tag{2.10}$$

which are eigenstates of all $\underset{\sim}{S}_z(u)$.

$$\underset{\sim}{S}_z(u)|m_1, m_2, \ldots, m_u, \ldots, m_N> = m_u|m_1, m_2, \ldots, m_u, \ldots, m_N> , \tag{2.11}$$

The Hamiltonian (2.8) for systems with a finite number of spins can be expressed in a basis such as (2.11), these states sometimes called Ising states. They construct the full Hilbert space in which the Hamiltonian matrix elements defined, and diagonalized them exactly either analytically [54, 55] or numerically [56, 57, 58, 24, 59] with high accuracy to obtain all the eigenvalues and eigenstates. The applicability of this approach is limited to small-size systems, since the dimensionality of the Hilbert space increases exponentially with the size of the system ($\dim(H)=(2^*S+1)^N$). We restrict ourselves to working inside invariant subspaces with reduced dimensionality using the basis (2.11) to construct symmetry-related basis states.

Symmetries of the problem

Usually the total dimension of the Hilbert space ($\dim(\mathcal{H})= (2^*S+1)^N$) is very large. There exist symmetry operations which transform the system into a symmetric configuration identical with an initial one because of spin symmetries or space symmetries, where the symmetry elements (axis, plane,...) remain unchanged. The Hamilton matrix can be decomposed into a block structure following this symmetry operation of the system. The isotopic Heisenberg Hamiltonian includes only a scalar product between spins. This operator is rotationally invariant in spin space. Nevertheless, it commutes with $\underset{\sim}{\vec{S}}$ and thus also with $\underset{\sim}{S}_z$. In the case where anisotropy is negligible and the applied magnetic field can be assumed to point into z-direction for vanishing anisotropy the Zeeman term automatically also commutes with $\underset{\sim}{H}$, $\underset{\sim}{S}^2$ and $\underset{\sim}{S}_z$.

$$\left[\underset{\sim}{H}, \underset{\sim}{S}^2\right] = 0, \qquad and \qquad \left[\underset{\sim}{H}, \underset{\sim}{S}_z\right] = 0. \tag{2.12}$$

Since M is a good quantum number the Zeeman term does not need to be included in the diagonalization but can be added later, and the Hilbert space can be decomposed into mutually orthogonal subspaces $\mathcal{H}(M)$.

$$\mathcal{H} = \bigoplus_{M=-S_{\max}}^{+S_{\max}} \mathcal{H}(M), \ , \qquad \text{With: } , \qquad S_{\max} = \sum_{u=1}^{N} S(u) \ . \tag{2.13}$$

For given values of M, N and of all S(u) the dimension dim[$\mathcal{H}(M)$] can be determined as the number of product states [60], which constitute a basis in $\mathcal{H}$(M), with $\sum_u(m_u)$ = M. The solution of this combinatorial problem can be given in closed form [61]:

$$\dim[\mathcal{H}(M)] = \frac{1}{(S_{\max} - M)!} \left[\left(\frac{d}{dz} \right)^{S_{\max}-M} \prod_{x=1}^{N} \frac{1 - z^{2s(x)+1}}{1 - z} \right]_{z=0} . \tag{2.14}$$

For equal single-spin quantum numbers $S(1) = \ldots = S(N)$, and thus a maximum total spin quantum number of S_{max} =Ns [62] the dimension dim[$\mathcal{H}(M)$] simplifies to

$$\dim[\mathcal{H}(M)] = f(N, 2s+1, S_{max} - M)$$

$$\text{with} \qquad f(N, \mu, \nu) = \sum_{n=0}^{\lfloor \nu/\mu \rfloor} (-1)^n \begin{pmatrix} N \\ n \end{pmatrix} \begin{pmatrix} N - 1 + \nu - n\mu \\ N - 1 \end{pmatrix} \tag{2.15}$$

In both formulae (2.14) and (2.15), M may be replaced by $|M|$ since the dimension of $\mathcal{H}$(M) equals those of $\mathcal{H}$(-M). $\lfloor \nu/\mu \rfloor$ in Eq. (2.15) symbilizes the greatest integer less or equal to ν/μ [61].

If the Hamiltonian commutes with $\underset{\sim}{\vec{S}}^2$ and all individual spins are identical the dimensions of the orthogonal eigenspaces $\mathcal{H}$ (S,M) can also be determined. The simultaneous eigenspaces $\mathcal{H}$ (S,M) of $\underset{\sim}{\vec{S}}^2$ and $\underset{\sim}{S}_z$ are spanned by eigenvectors of $\underset{\sim}{H}$ more details about it see [63].

For spin rings

The translational symmetry found in the case of molecular rings of N spins, with $\underset{\sim}{S}_{N+1} = \underset{\sim}{S}_1$ is represented by the cyclic shift operator $\underset{\sim}{T}$ [64, 65]:

$$\underset{\sim}{T} \, | \, m_1, \ldots, m_u, \ldots, m_N \, \rangle = \, | \, m_N, m_1, \ldots, m_N - 1 \, \rangle, \tag{2.16}$$

$\underset{\sim}{T}$ is defined by its action on the product basis [60], and shifts all spins by one position. This means that the eigenstate common for the operator $\underset{\sim}{H}$ is shifted into another,

and the shift operations can be repeated N times.
The eigenvalues of $\underset{\sim}{T}$ are the N-th roots of unity

$$z_k = e^{-i\frac{2\pi k}{N}}, \qquad k = 0, \ldots, N-1, \qquad P_k = 2\pi k/N \ . \tag{2.17}$$

where k will be called translational (or shift) quantum number and P_k momentum quantum number. The shift operator $\underset{\sim}{T}$ commutes not only with the Hamiltonian but also with total spin. Any $\mathcal{H}$ (S,M) can therefore be decomposed into simultaneous eigenspaces $\mathcal{H}$ (S,M,k) of $\underset{\sim}{S}^2$, $\underset{\sim}{S}_z$ and $\underset{\sim}{T}$. A special decomposition of $\mathcal{H}$(S,M) into orthogonal subspace can be achieved by starting with the product basis of Eq. (2.16). The cycle is defined as the linear basis vectors giving by this formula.

$$|\,\psi_k\,\rangle = \frac{1}{\sqrt{N}} \sum_{\nu=0}^{N-1} \left[\exp\left(i\frac{2\pi k}{N} \right) \underset{\sim}{T} \right]^{\nu} |\,\psi_1\,\rangle \ , \qquad \text{With:} \quad |\,\psi_1\,\rangle = |\,m_1, m_2, \ldots, m_N\,\rangle \ . \tag{2.18}$$

which are eigenstates of $\underset{\sim}{T}$ with the respective shift quantum number k. Evidently the dimension of a cycle can never exceed N.
The obviously orthogonal decomposition of $\mathcal{H}$ into the cycles is compatible with the decomposition of $\mathcal{H}$ into the various $\mathcal{H}$(M).

$$\begin{cases} \left[\underset{\sim}{T}, \underset{\sim}{H}\right] & = 0 \\ \\ \left[\underset{\sim}{H}, \underset{\sim}{S}_z\right] & = 0 \end{cases} \qquad - - - > \qquad \mathcal{H}\,(S, M) - - > \mathcal{H}\,(S, M, k)$$

We may finally decompose the complete Hilbert space into the mutually orthogonal subspaces, where all energy eigenvalues and eigenvectors can be computed using the *Numerically Exact Diagonalization*.

For general structure

In the case of complicated molecular structures and larger systems, we can define other symmetry operators and decompose the Hilbert space into orthogonal subspaces which make the numerical exact diagonalisation method feasible. But the disadvantage of the numerical exact diagonalization method is in the case of very large molecules where we can not find some symmetry operations. There, due to the very large size of the related Hilbert space, we approximate the spin system by a smaller one or we must switch to the other methods. One can still use numerical methods to evaluate low-lying energy levels and the respective eigenstates. But one cannot get the full energy spectrum, we can just describe the ground state energy or some other properties of the compound under consideration. A simple method is the

projection method [59] which rests on the multiple application of the Hamiltonian on some random trial state. Another method to diagonalize a huge matrix was proposed by Cornelius Lanczos [66, 67], which also uses a random initial vector. The DMRG technique [68] has the main idea is to reduce the Hilbert space while focusing on the accuracy of a target state. It give also the properties of the ground state for the huge system. Quantum and Classical Monte Carlo (CMC[2], QMC[3]), where we can simulate big systems and give the information about the magnetic order in the compound, ... etc..
Currently the most popular way to include the effects of electron correlation in these calculations is density functional theory. This method is in principle exact, in reality fast and often very accurate, but does have a certain number of well-known limitations. In particular, with only limited knowledge available concerning the exact mathematical form of the so-called exchange-correlation functional, the accuracy of the approximate form of the theory is non-uniform and non-universal, and there are important classes of materials for which it gives qualitatively wrong answers. An important and complementary alternative for situations where accuracy is paramount is the Quantum Monte Carlo (QMC) method, which has many attractive features for probing the electronic structure of real systems. It is an explicitly many-body method which takes electron correlation into account from the outset. It gives consistent, highly accurate results while at the same time exhibiting favorable scaling of computational cost with molecular size.

2.3.3. Quantum Monte Carlo (QMC) simulation method

To calculate sums (or integrals, if the spins are continuous-valued) over a large number of degrees of freedom, to obtain its complete physical description, we resort to Monte Carlo techniques. One introduces an artificial dynamics on phase space which is based on random numbers. MC simulations are very powerful and popular for static properties. As with the MC integration mentioned earlier, we could just generate configurations at random, and approximate the real thermal averages. The problem is calculating the quantum-mechanical thermal (equilibrium) expectation value of an

[2]Samples are drawn from a probability distribution, often the classical Boltzmann distribution, to obtain thermodynamic properties, minimum-energy structures and/or rate coefficients, or perhaps just to sample conformers as part of a global conformer search algorithm
[3]Random walks are used to compute quantum-mechanical energies and wavefunctions, often to solve electronic structure problems, using Schroedinger's equation as a formal starting point)

operator $\underset{\sim}{A}$,

$$< \underset{\sim}{A} > = \frac{1}{Z} Tr \left\{ \underset{\sim}{A} e^{-\beta \underset{\sim}{H}} \right\}$$

$$= \frac{1}{Z} \sum_n \langle\, n \,|\, e^{-\beta \underset{\sim}{H}} \underset{\sim}{A} \,|\, n \,\rangle \tag{2.19}$$

where $\underset{\sim}{H}$ is the Hamiltonian, $\beta = 1/\mathrm{k}_B\mathrm{T}$, the states $|\, n \,\rangle$ form a complete orthonormal basis set, and Z the partition function.

$$Z = Tr \left\{ e^{-\beta \underset{\sim}{H}} \right\} = \sum_n \langle\, n \,|\, e^{-\underset{\sim}{H}/kT} \,|\, n \,\rangle \tag{2.20}$$

As the Hamiltonian generally consists of non-commuting terms,

$$\underset{\sim}{H} = \sum_{i=1}^{M} \underset{\sim}{H}_i \tag{2.21}$$

with

$$\left[\underset{\sim}{H}_i, \underset{\sim}{H}_j \right] \neq 0 \quad \text{for some} \quad i, j \tag{2.22}$$

direct evaluation of the operator $\mathrm{e}^{-\beta \underset{\sim}{H}}$ is impossible, which is the density matrix, except for small systems for which the Hamiltonian can be diagonalized numerically. The method need to find a mapping of the quantum partion function to a classical problem. Several Monte Carlo algorithms to evaluate the traces in (2.19) and (2.20) have been proposed. This task is possible with the Feynman path integral [4] approach (Feynman and Hibbs, 1965) [69] (more details about path-integral see appendix A), or with (SSE) Stochastic Series Expansion (high temperature expansion). To understand the physics of QMC with a very good description I would recommend to read the flowing reviews [70, 71, 72, 73, 74], and for applications in solids [75] and molecules [76].

2.4. Thermodynamic observables

The thermodynamics properties of the magnetic systems can be all extracted from Z called the partition function, which contains all of the essential information about the system under consideration. It is the fundamental quantity in statistical mechanics.

$$Z = Tr(e^{-\beta \underset{\sim}{H}}) \tag{2.23}$$

[4] time-dependent perturbation theory in imaginary time

where $\underset{\sim}{H}$ is the Hamiltonian for the system, T is the temperature, $\beta = 1/k_B T$, and k_B is Boltzmann's constant. All thermodynamics quantities of interest are not fixed, but have a statistical distribution about a mean or expected value.
In this section, we state the relationships between the partition function and the various thermodynamic parameters of the system as function of temperature T and magnetic field B.

• If $\left[\underset{\sim}{H}, \underset{\sim}{S}_z\right] = 0$, which mean that the energy eigenvectors $|\,\psi_\nu\,\rangle$ can be chosen as simultaneous eigenvectors of $\underset{\sim}{S}_z$ with eigenvalues $E_\nu(B)$ and M_ν. The energy dependence of $E_\nu(B)$ on B is simply given by the Zeeman term given as

$$E_\nu(B) = E_\nu(B=0) + g\mu_B B M_\nu \ . \tag{2.24}$$

• In the case, $\underset{\sim}{H}$ and $\underset{\sim}{S}_z$ do not commute the respective traces for the partition function have to be evaluated. If all the particles in a system or ensemble are distributed over the accessible states according to the canonical distribution (Boltzmann probability) given by

$$p_i = \frac{e^{-E_i/k_B T}}{\sum e^{-E_i/k_B T}} = \frac{e^{-\beta E_i}}{Z}. \tag{2.25}$$

(Here E_i are the energy eigenvalues of the system)
then all the thermodynamic functions can be related to the partition function Z. Since the mean energy per particle is

$$\bar{E} = \sum_i p_i E_i = \frac{\sum E_i e^{-\beta E_i}}{Z}, \tag{2.26}$$

and noting

$$\sum E_i e^{-\beta E_i} = -\sum \frac{\delta}{\delta\beta} e^{-\beta E_i} = -\frac{\delta Z}{\delta\beta}, \tag{2.27}$$

it follows that

$$\bar{E} = -\frac{1}{Z}\frac{\delta Z}{\delta\beta} = -\frac{\delta ln Z}{\delta\beta}, \tag{2.28}$$

from this it can be shown also that the entropy which measure the disorder present in a system can be given by

$$S = k(lnZ + \beta\bar{E}) = klnZ + \frac{\bar{E}}{T}, \tag{2.29}$$

where k is a constant (and is really just a choice of measurement units).
For N particles, the Helmholtz free energy becomes

$$F = U - TS = -kTlnZ, \tag{2.30}$$

where U is the internal energy of the system ($\approxeq \bar{E}$).
By the same reasoning that gave $\bar{E}$ it is seen that the magnetization is related to the strength of the applied magnetic field B

$$M(T,B) = -kT\frac{\delta lnZ}{\delta B}. \tag{2.31}$$

Using the trace for the partition function, the magnetization being defined as:

$$M(T,B) = -\frac{1}{Z}Tr\left\{e^{-\beta \underset{\sim}{H}} g\mu_B \underset{\sim}{S}_z\right\} = -\frac{g\mu_B}{Z}Tr\left\{\underset{\sim}{S}_z e^{-\beta \underset{\sim}{H}}\right\}\ , \tag{2.32}$$

with $\underset{\sim}{H} = \underset{\sim}{H}(B)$. If $|\,\nu\,\rangle$ is eigenstate of $\underset{\sim}{H}$ then $\underset{\sim}{H}\,|\,\nu\,\rangle = E_\nu\,|\,\nu\,\rangle$. Substituting the result in (2.32), one obtains

$$M(T,B) = -\frac{g\mu_B}{Z}\sum_\nu \langle\,\nu\,|\,\underset{\sim}{S}_z\,|\,\nu\,\rangle e^{-\beta E_\nu(B)}, \tag{2.33}$$

comparing equation (2.31) with equation (2.30) yields

$$M = -\frac{\delta F}{\delta B}, \qquad\qquad \chi = \mu_0\frac{\delta M}{\delta B} = -\mu_0\frac{\delta^2 F}{\delta B^2}. \tag{2.34}$$

Magnetic susceptibility is one of the most important tools to understand whether ordering occurs between spins in a crystalline, molecular "magnetic" solid. The zero-field magnetic susceptibility is given by:

$$\chi_B(T,B) = \frac{\partial M(T,B)}{\partial B} = \beta(g\mu_B)^2\left\{<< \underset{\sim}{S}_z^2 >> - << \underset{\sim}{S}_z >>^2\right\}. \tag{2.35}$$

For $[\underset{\sim}{S}_z, \underset{\sim}{H}] = 0$ and using the equations (2.26) and (2.33), the magnetic susceptibility can be given by

$$\chi_B(T,B) = \frac{(g\mu_B)^2}{KT}\left\{\frac{\sum_\nu M_\nu^2 e^{-\beta E_\nu(B)}}{\sum_\nu e^{-\beta E_\nu(B)}} - \left(\frac{\sum_\nu M_\nu e^{-\beta E_\nu(B)}}{\sum_\nu e^{-\beta E_\nu(B)}}\right)^2\right\}\ . \tag{2.36}$$

Analogously the internal energy and the specific heat are evaluated from first and second moments of the Hamiltonian

$$U(T,B) = -\frac{1}{Z}Tr\left\{\underset{\sim}{H}e^{-\beta \underset{\sim}{H}}\right\} \tag{2.37}$$

$$= -\frac{1}{Z}\sum_\mu E_\mu(B)e^{-\beta E_\mu(B)}, \tag{2.38}$$

$$C(T,B) = \frac{\partial U(T,B)}{\partial B}. \tag{2.39}$$

$$\tag{2.40}$$

Using a partition function Z, one easy shows that the specific heat can be written

$$C(T,B) = \frac{1}{k_B T^2}\left\{\frac{1}{Z}\sum_{\mu}(E_\mu(B))^2 e^{-\beta E_\mu(B)} - \left(\frac{1}{Z}\sum_{\mu} E_\mu(B) e^{-\beta E_\mu(B)}\right)^2\right\}. \quad (2.41)$$

2.5. Spin dynamics and relaxation

Quantum spin dynamics in microscopic magnets has received much attention over the recent years, both from experiment and from theory [77, 78]. In particular, a number of nanosized particles in the paramagnetic regime have been identified as promising candidates for the observation of macroscopic quantum phenomena such as tunneling of the magnetization out of a meta-stable potential minimum, or, more strikingly, macroscopic quantum coherence, where the magnetization tunnels coherently between classically degenerate directions over many periods. On the one hand, these phenomena are interesting from a fundamental point of view as they extend our understanding of the transition from quantum to classical behavior. On the other hand, the measurement of quantities such as the tunnel splitting provides independent information about microscopic parameters such as anisotropies and exchange constant.

2.5.1. Spin quantum tunneling

The quantum aspects of molecular magnets are encountered by considering non diagonal anisotropy terms like $E(S_X^2\text{-}S_Y^2)$, which describes a hard-axis anisotropy caused by a rhombic distortion, and $C(S_+^4\text{-}S_-^4)$ which is the lowest-order non diagonal term allowed by tetragonal symmetry. These terms do not commute with S_z, Figure 2.3.

Let us suppose that the field $\vec{B}$ is along the hard axis, S_x, and not too large. At first sight, as B_x is increased, it should be progressively easier for the spin to tunnel from a state localized in the potential well in the positive S_z hemisphere to the symmetrically located state in the negative hemisphere, Figure 2.3. The tunnel splitting between the ground states in the positive and negative S_z wells actually oscillates as a function of B_x, going to zero at periodically spaced B_x values [79]. Precisely these oscillations have been seen in Fe_8 by Wernsdorfer and Sessoli (WS) [80], and were initially explained in terms of an interference between instanton trajectories for the spin [79] and the observations on Fe_8 are very hard to explain by another mechanisms. The clincher is that WS see additional oscillations that were not predicted. To understand these, suppose $\vec{B}$ also has a nonzero z component so as to bring the first or second excited state in the positive S_z well into degeneracy with the ground state in the other well. One can then conceive of tunneling between these states. WS observe that the amplitude for this tunneling also oscillates with B_x, and that the

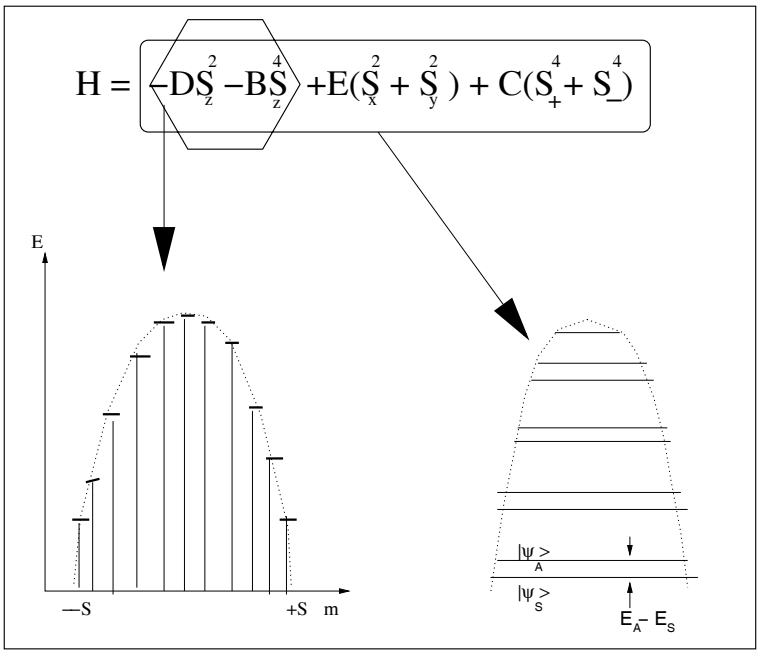

Figure 2.3.: Sketch of the energy levels scheme for the Hamiltonian, when considering only the diagonal terms (left) or including the non-diagonal ones (right).

oscillations are shifted by half a period for each excited state in the deeper well.
To understand more the evidence of tunneling effects, let us express $|\psi>$ in the basis of the eigenstates $|m>$ of S_z:

$$|\psi> = \sum_m C_m |m>, \qquad m = -S, \ldots, +S \tag{2.42}$$

one finds that each doublet now consist of a state $|\psi_s>$ with symmetric coefficients, $c_{+m} = c_{-m}$, and an antisymmetric state $|\psi_A>$ with $c_{+m} = -c_{-m}$, separated by an energy gap $\Delta = E_A - E_S$. In particular for the ground doublet, one finds to a very good approximation:

$$|\psi_S> = \frac{1}{\sqrt{2}}(|+S> + |-S>) \tag{2.43}$$

$$|\psi_A> = \frac{1}{\sqrt{2}}(|+S> - |-S>) \tag{2.44}$$

This means that a state localized on one side of the barrier, e.g.$|+S>$, must now be expressed as a superposition of the actual eigenstates

$$|+S> = \frac{1}{\sqrt{2}}(|\psi_S> + |\psi_A>) \tag{2.45}$$

It is clear from basic quantum mechanics that if one would prepare the system at t =0 in such a state, $|\psi(t=0)> = |+S>$, the time evolution should obey the Schrödinger equation

$$|\psi(t)> = \frac{1}{\sqrt{2}} e^{-i\frac{E_S+E_A}{2\hbar}t} \left(|\psi_S> e^{+i\frac{\Delta}{2\hbar}t} + |\psi_A> e^{-i\frac{\Delta}{2\hbar}t} \right) \tag{2.46}$$

This equivalent to having coherent oscillations of the cluster spin between the states $|+S>$ and $|-S>$ with frequency $\mathrm{w}_T = \Delta/\hbar$, which implies that the spin is tunneling back and forth through the anisotropy barrier. For this reason the energy gap Δ is called tunneling splitting.

2.5.2. Nuclear Magnetic Resonance (NMR)

NMR signals of protons are a phenomenon that provides a very suitable experimental tool for probing both static and dynamic properties of magnetic systems. First signals were observed in bulk matter independently by Felix Bloch *et al.* at Stanford and Edward Purcell at Harvard in 1946 (United States) [81]. Later discoveries with NMR included electric quadruple effects; an important shift of NMR frequencies in metals; and the splitting of energy levels in liquids resulting from variations in chemical structure and the influence of one nuclear spin on another. In NMR, unlike other types of spectroscopy, the quality of the sample has a profound effect on the quality of the resulting spectrum. So that the sample we prepare gives a spectrum in which useful information is not lost or obscured, we must follow a few simple rules, like to use the correct quantity of material. For ^{1}H spectra of organic compounds (except polymers) the quantity of material required is about 5 to 25 mg, remove all solid particles distort the magnetic field... etc. NMR spectroscopy probes the absorption of radio-frequency (RF) radiation by the nuclear spins of the molecule. The most commonly occurring spins in natural samples are ^{1}H (protons), ^{2}H(deutrons), ^{13}C and ^{15}N nuclei. In the presence of an external magnetic field $\vec{B}$ along the z-axis, each such nucleus has its spin states split in energy which is covered in more detail in Sec.2.5.3. In most NMR experiments, a fixed RF frequency is employed and the external magnetic field is scanned until the above resonance condition is met.

NMR spectrum is extremely rich in information about the nuclear spin density, the measurement of the nuclear spin-lattice relaxation rate T_1 which gives information about the low-frequency behavior of the spin fluctuations[82], the spin-spin relaxation time $1/\mathrm{T}_2$, molecular motions (such as diffusion and perfusion), and susceptibility effects. It provides information about the electronic environment local to that nucleus. It has proved to be a powerful tool to investigate the local spin dynamics in magnetic molecules, and a considerable body of results has accumulated over the past 10 years mostly on dependence of the proton spin-lattice relaxation rate ($1/\mathrm{T}_1$) on T and $\vec{B}$ [83].

2.5.3. Nuclear Magnetic moments

Nuclear magnetism of a nuclear spin system originates from the microscopic magnetic field associated with a nuclear spin $\vec{I}$, this magnetic field exist because a nucleus such as a proton has electric charges. The spin angular momentum and magnetic moment vectors are related to each other by:

$$\vec{\mu} = \gamma \vec{I} \tag{2.47}$$

where γ is a physical constant known as the gyromagnetic ratio, which is nucleus-dependent. For ^{1}H, $\gamma = 2.675\text{x}10^8$ rad/sT. I is nuclear spin quantum number [5].

To activate macroscopic magnetism from an object it is necessary to line up the vectors. By exposing the object to a strong external magnetic field $\vec{B}_z$ along a certain axis $\vec{z}$, the phenomenon of magnetic resonance results from the interaction of the magnetic moment $\vec{\mu}$ of an atomic nucleus with the external magnetic field.

2.5.4. Basics of pulse NMR

The Hamiltonian of a nuclear spin $\vec{I}$ placed in a magnetic field $\vec{B}_z$ is given by:

$$H = -\vec{\mu} \cdot \vec{B} = \hbar \gamma \vec{I} \cdot \vec{B}_z \tag{2.48}$$

where γ is the gyromagnetic ratio, and the eigenstates $|m>$ are the $2I+1$ projections of the spin along $\vec{z}$ axis, and having energies E_m, $m = -I, -I+1, \ldots, I+1, I$, separated from each other by the Zeeman splitting $E_{m+1} - E_m = \hbar \gamma B_z$, Which corresponds to the Larmor frequencies $\omega = \gamma B_z$ for the classical precession. Transitions between adjacent Zeeman levels can be produced by introducing a time-dependent field $\vec{B}_{rf}(t)$, provide that the matrix elements $\langle\, m \,|\, B_{rf} \,|\, m+1 \,\rangle \neq 0$, i.e. $\vec{B}_{rf}$ is not parallel to the direction $\vec{z}$. Considering for simplicity a spin $I = 1/2$ and taking $\vec{B}_{rf} = B_{rf} cos(\omega_N t)\vec{\text{x}}$, the expectation value of the z component of the magnetic moment will oscillate in time at a frequency $\omega_{Rabi} = \gamma B_{rf}$ (Rabi oscillations).

$$< \mu_z(t) > = < \mu_z(0) > cos(\omega_{Rabi} t) \tag{2.49}$$

This means in a classical picture that, if $\vec{\mu}(0) = \hbar \gamma I \vec{z}$, after a time $t_{\pi/2} = \pi/(2\gamma B_{rf})$ the magnetic moment has been turned 90 away from $\vec{z}$ axis and lies in the xy plane. For this reason, the application of such an alternating field of frequency ω_N for a time $t_{\pi/2}$ is called "$\pi/2$-pulse". The rotation angle can in fact take any value, by choosing the appropriate duration and strength of B_{rf}. After a $\pi/2$-pulse the state of

[5] If we look at the periodic table, we can extract the general rules: Even mass nuclei that have even number of neutron have $I = 0$ (not interesting from the NMR point of view), even mass nuclei that have odd number of Neutrons have an integer spin quantum number and odd mass nuclei have half integer spin quantum number.

the system is $|\psi\rangle = 1/\sqrt{2}(|+1/2\rangle + |-1/2\rangle)$, and the time evolution caused by the Hamiltonian (2.48) is equivalent to the classical Larmor precession of the magnetic moment within the xy plane, which produces a rotating magnetic field that can be detected via the electromotive force induced in a pick-up coil with axis parallel $\vec{x}$. In practice the same coil is used to produce B_{rf} and to detect the Larmor precession.

2.5.5. Electron spin resonance (ESR)

Electron spin resonance (ESR) is also known by the name electron paramagnetic resonance (EPR). It was first observed in 1944 by a Soviet physicist, Y.K. Zavoysky, in experiments on salts of the iron group of elements. ESR has made possible the study of such phenomena as the structural defects that give certain crystals their color, the formation and destruction of free radicals in liquid and solid samples, the behavior of free or conduction electrons in metals, and the properties of metastable states (excited states that are long-lived because energy transfer from them by radiation does not occur) in molecular crystals.

ESR serves as a valuable tool to experimentally probe the intrinsic spin dynamics of many systems. It is a very helpful method and provides more precise data even on the molecular orbital of the unpaired electron. In which a strong static magnetic field is applies to induce a splitting between the energies of different electronic spin states. An oscillating microwave field is applied to induce transition between these states, and one sweeps a second weak magnetic field until one finds the transition where radiation is absorbed by an electron-spin transition, and measures this absorption of radiation polarized perpendicular to the field direction which gives rise to an ESR spectrum. However, neither study was able to resolve spin-spin splitting from three electrons, or nuclear hyperfine structure using the low-frequency EPR [84] or only powder samples [85].

ESR measures the interaction between the spin density, which is the difference between the densities of the spin up and spin down electrons, and the spins of the nuclei in the molecule. This also indicates that closed shell molecules do not exhibit ESR spectra, because in this case the spin up equals the spin down density. The key problem in electron-spin resonance is, on one hand, to construct a mathematical description of the total energy of the interaction in the ligand field plus the applied magnetic field and, on the other hand, to deduce the parameters of the theoretical expression from an analysis of the observed spectra. The comparison of the two sets of values permits a detailed quantitative test of the microscopic description of the structure of matter in the compounds studied by ESR.

The theoretical description of electron spin resonance is the following: In the standard Faraday configuration, the ESR absorption intensity at frequency ω is propor-

tional to the Fourier transform of the transverse spin-spin correlation function of the total spin operator S [86, 87] given by

$$I(\omega) = \int dt e^{i\omega t} < S^+(t)S^-(0) > \tag{2.50}$$

where the static magnetic field points along the z axis and $\vec{S} = \sum_i \vec{S}_i$ is the total spin operator of the system under consideration. The Hamiltonian governing the spin interaction is

$$\underset{\sim}{H} = g_e\beta_e\vec{B}\cdot\vec{S} - g_N\beta_N\vec{B}\cdot\vec{I} - \vec{S}\cdot A\cdot\vec{I} \tag{2.51}$$

where g_e, g_N are the electronic and nuclear g-factor, respectively, β_e, β_N the Bohr (electronic) and nuclear magnetons, $\vec{B}$ the magnetic field at the atom, $\vec{S}$ the electron spin, $\vec{I}$ the nuclear spin, and A the hyperfine interaction tensor, which can separated into an isotropic part, independent of the molecules orientation in the magnetic field, and an anisotropy part, dependent on the molecular orientation.
Inserting a complete set of eigenstates $|\,\psi\,\rangle$ of $\underset{\sim}{H}$ in Eq.(2.50), the ESR intensity follows as

$$I(\omega) = \frac{1}{Z}\sum_{u,v} e^{-E_v/T}\delta\left(\omega - (E_u - E_v)\right)|\langle\,\psi_u\,|\,S^-\,|\,\psi_v\,\rangle|^2 \tag{2.52}$$

If the Hamiltonian $\underset{\sim}{H}$ Eq. (2.51) parallel to the z axis. In Eq.(2.52), $I(\omega)$ only receives contributions from matrix elements between eigenstates with equal total spins $S_u = S_v$. Then all states with $S_u^z = S_v^z - 1$ will contribute to form a δ-peak at frequency $\omega = B$. At zero temperature, the application of a magnetic field B, taken as large enough to overcome a spin gap possibly presents at $B = 0$, leads to a ground state with finite magnetization, $S_0 \neq 0$, and the states with $S_u^z = S_0^z - 1$ yield the δ-peak.

3. Anti-ferromagnetic molecular rings $\{Cr_8\}$ and $\{Cr_7M\}$

In this chapter, we study magnetic rings closely related to the new tetragonal crystal form of [Cr_8 F_8 Piv_{16}] $\approx \{Cr_8\}$ [88], which contains eight Chromium^{III} ions ($S_{Cr} = 3/2$), that lie at the corners of a regular octagon, figure 3.1. Each edge of the octagon is bridged by one fluoride ion and two privalate ligands. There is a large cavity at the center of the ring. Susceptibility measurements suggested an AF interaction between the Cr^{III} ions ($J = 1.5$ meV), resulting in an energy gap of about 0.8 meV [89] between the ground state ($S = 0$) and the first excited state ($S = 1$). Carretta *et al.* [89] have reported the results of inelastic-neutron-scattering (INS) measurements performed in zero magnetic field on a fully deuterated polycrystalline sample of $\{Cr_8\}$. This spectroscopic technique provides direct access to the energies and wave functions of the cluster's different spin states. Thus it is contributing information that can be very useful to build a comprehensive picture of the magnetic anisotropy in molecular magnets [90, 91].

We also report the study of spin ring systems comprising ions of different chemical elements. The breakthrough was already achieved with the synthesis of heterometallic $\{Cr_7M\}$ wheels [29], where one of the Chromium ions of the original $\{Cr_8\}$ ring [92, 93, 94, 95] is replaced by another element M=Mn, Fe, Co, Ni, Cu, and Zn. The possibility of a systematic study of these compounds has initiated first investigations on these compounds as there are susceptibility measurements [29] as well as neutron scattering on $\{Cr_7M\}$ wheels with M=Mn, Zn, Ni [51].

We explore and discuss the results of the Heisenberg exchange parameters from earlier susceptibility measurements by means of complete diagonalization (Sec. 3.1) for different molecular rings, where our results agree with first estimates given in Ref. [29], with the noticeable difference that we find that the exchange parameters of the iron ion to its neighboring chromium ions is rather different from the original chromium-chromium exchange, whereas it remains practically unchanged for the other paramagnetic ions.

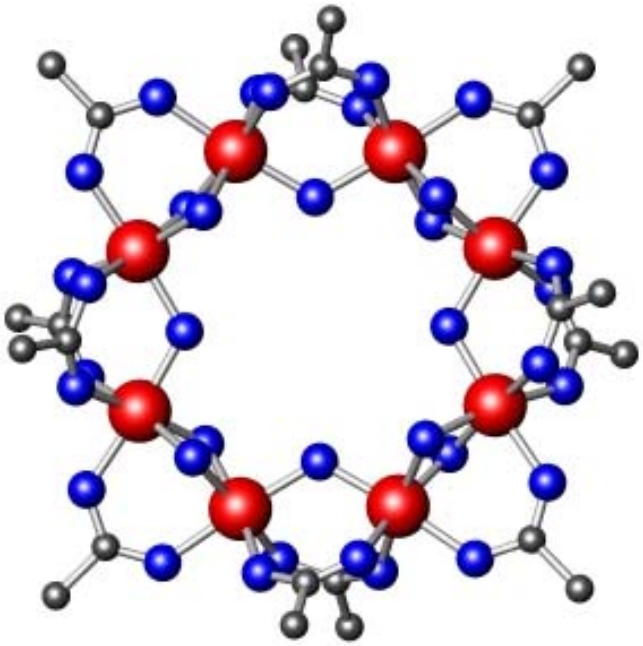

Figure 3.1.: The $\{Cr_8\}$ wheel. Eight Cr^{III} ions are arranged on a ring and coupled by antiferromagnetic exchange interactions.

3.1. Hamiltonian and observables

These systems are characterized by the existence of localized unpaired electrons, usually located on metallic ions. The properties of the material are governed by the interaction between the unpaired electrons on neighbor centers, which may be viewed as an effective interaction between site-centred spins, and well mapped and described using the Heisenberg spin Hamiltonian with Zeeman term of applied magnetic field along the z-axis

$$\underset{\sim}{H} = 2J_1 \sum_{i=2}^{N} \vec{S_i} \cdot \vec{S_{i+1}} + 2J_2 \left(\vec{S_1} \cdot \vec{S_2} + \vec{S_1} \cdot \vec{S_N} \right) + g\mu_B B \sum_{u}^{N} \underset{\sim}{S_z}(u), \tag{3.1}$$

where $N = 8$, and the total spin operator $S = \sum_i^N S_i$.

3.1.1. Symmetry used in heterometallic $\{Cr_7M\}$ wheels

Molecular symmetry originates in the fact that there exist symmetry operations transforming the molecule into a symmetric configuration identical with the initial one and the total Hilbert space of the Hamiltonian 3.1 can be decomposed into mutally orthogonal subspaces. The symmetry elements (axis, plane, inversion center) remain unchanged. In order to study the magnetic properties of the different antiferromagnetic spin rings, we have used the symmetry operation given by equation (2.16) for $\{Cr_8\}$ and for heterometallic $\{MCr_7\}$ wheels we have used the symmetry represented in Figure 3.2.

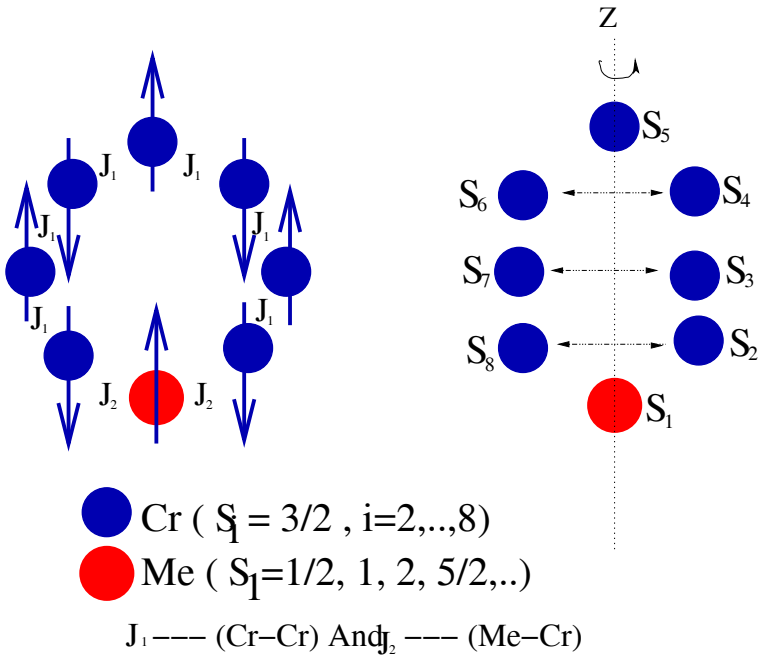

Figure 3.2.: Schematic representation of symmetry operations used in our calculations to study the molecular magnetic rings of heterometallic $\{Cr_7M\}$ wheels.

The spins are mirrored, the operator $\underset{\sim}{T}_M$ is represented by:

$$\underset{\sim}{T}_M \,|\, m_1, m_2, m_3, m_4, m_5, m_6, m_7, m_8 \,\rangle = \,|\, m_1, m_8, m_7, m_6, m_5, m_4, m_3, m_2 \,\rangle, \quad (3.2)$$

where the quantum number k Eq.(2.18) is equal to 0 or 1.

3.2. Exact diagonalisation of Cr_8 and $\{Cr_7M\}$

The Hamiltonian (3.1) for heterometallic systems with a finite number of spins can be expressed in a basis such as (3.2) and then diagonalized exactly to obtain all the eigenvalues and eigenstates.

3.2.1. $\{Cr_8\}$

The complete Hilbert space for $\{Cr_8\}$ rings contains $4^8 = 65536$ states. In a case where the anisotropy term is negligible in the equation (3.1) and the applied magnetic field can be assumed to point into z-direction for vanishing anisotropy, the Zeeman term automatically also commutes with $\underset{\sim}{H}_{Heisenberg}$, $\underset{\sim}{S}_z$ and $\underset{\sim}{S}^2$. Since M is a good

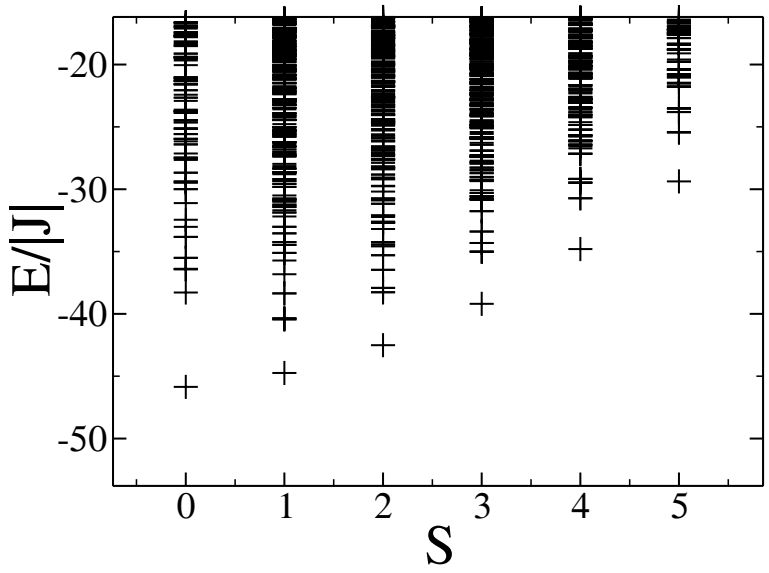

Figure 3.3.: Calculated low-energy eigenvalues as a function of total spin quantum number S for a $\{Cr_8\}$ ring described by the Heisenberg spin Hamiltonian. The spectrum shows that the ground state is in $S = 0$.

quantum number the Zeeman term does not need to be included in the diagonalization but can be added later. The figure 3.3 represent the energy spectrum for the molecular cluster rings $\{Cr_8\}$ containing eight Cr^{III} ions with ($S_{Cr} = 3/2$). It shows that the lowest energy levels (ground state) are not degenerate with total spin $S = 0$, and resulting energy gap of about 1.6 meV between the $|S = 0>$ ground state and the $|S = 1>$ first exited state [92].

3.2.2. Heterometallic $\{Cr_7M\}$ wheels

The symmetry operation used to study the $\{Cr_7M\}$ wheels is represented in Figure 3.2. For example, the complete Hilbert space contains $4^7 * 5 = 81920$ states for Fe^{II}-Cr_7 . The low-energy part of the spectrum for different physical systems $\{MCr_7\}$ (with M=Zn, Fe, NI, Cu) is represented in Figure 3.4.

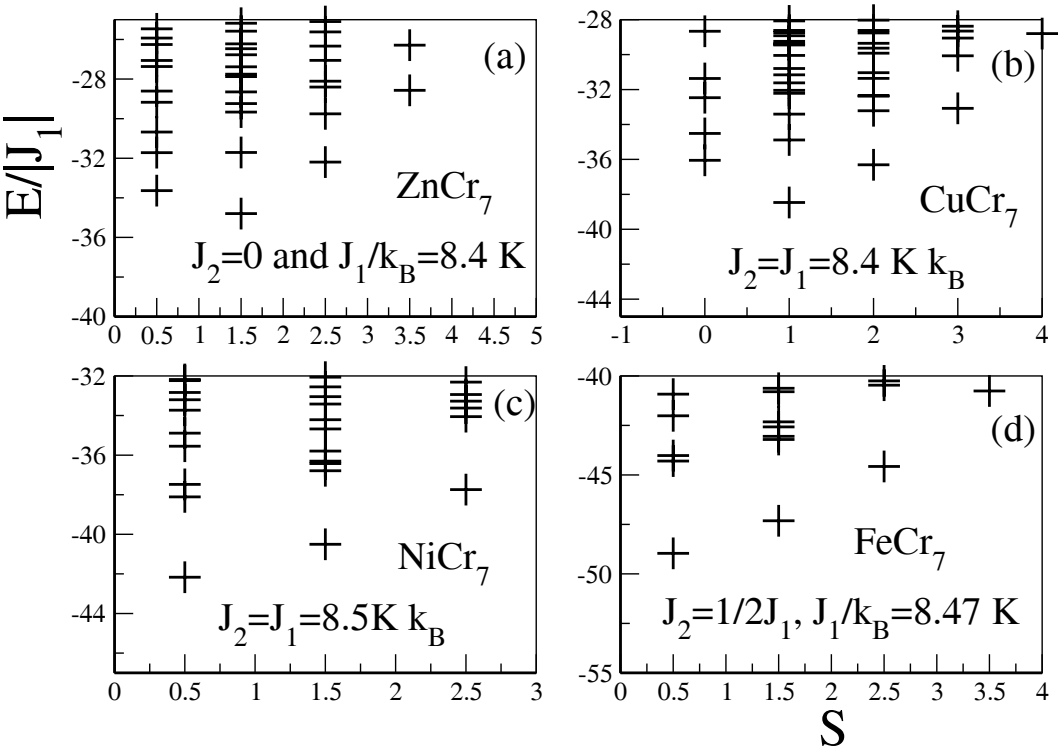

Figure 3.4.: Low-energy eigenvalues as a function of total spin quantum number S for a $\{MCr_7\}$ ring (with M=Zn, Fe, NI, Cu) described by the Heisenberg spin Hamiltonian. The spectrum shows that the ground state is in $S = 1/2$ for $\{FeCr_7\}$ and $\{NiCr_7\}$, and $S = 1$, 1.5 for $\{CuCr_7\}$ and $\{ZnCr_7\}$, respectively.

3.3. Low-field susceptibility

The low-field susceptibility $\mathcal{M}/B$ as well as $T\mathcal{M}/B$ of $\{CuCr_7\}$, $\{ZnCr_7\}$, $\{NiCr_7\}$, and $\{FeCr_7\}$ are shown in Figures 3.5-3.8. For the theoretical fits a g-value of $g = 2.1$ has been used for the molecular ring $\{NiCr_7\}$, and in all the other cases we

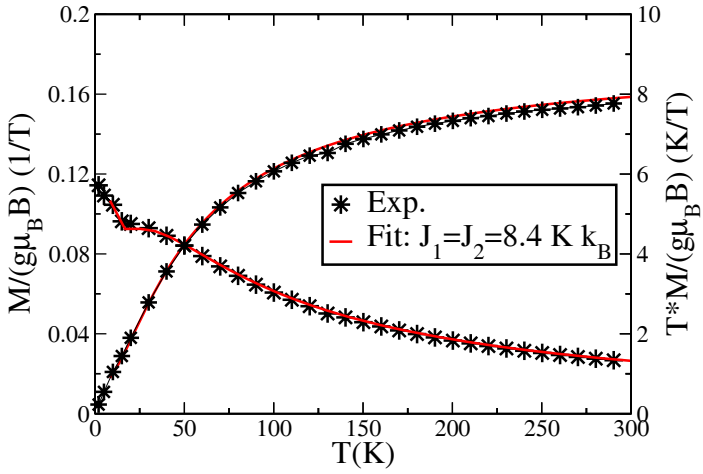

Figure 3.5.: Variation of $\mathcal{M}/B$ and $T\mathcal{M}/B$ as a function of temperature T for $\{CuCr_7\}$: The experimental data are given by black stars. The theoretical fit is depicted by a solid curve for $J_1 = J_2 = 8.4\ k_B$ K; $B = 1$ T and $g = 2$.

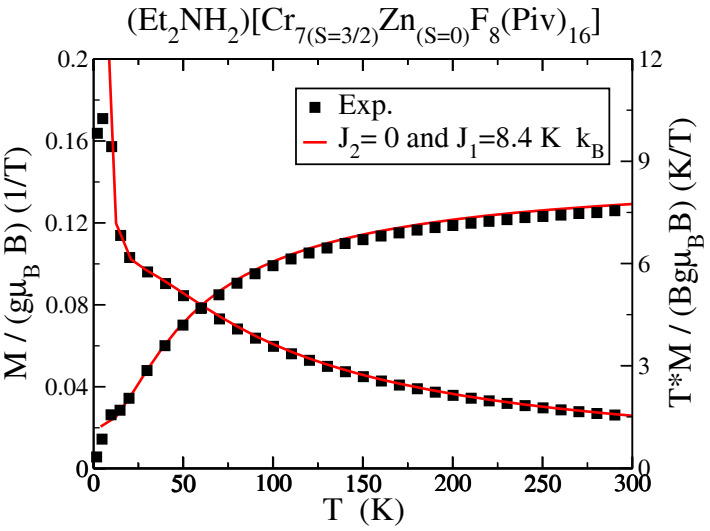

Figure 3.6.: Variation of $\mathcal{M}/B$ and $T\mathcal{M}/B$ as a function of temperature T for $\{ZnCr_7\}$: The experimental data are given by black squares. The theoretical fit is depicted by a solid curve for$J_1/k_B = 8.4$ K and $J_2 = 0$ K k_B; $B = 1$ T and $g = 2$.

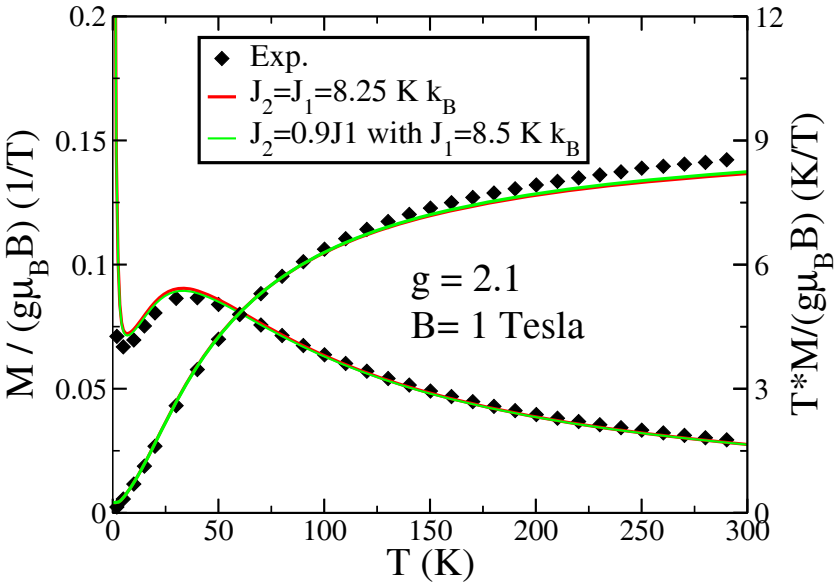

Figure 3.7.: Variation of $\mathcal{M}/B$ and $T\mathcal{M}/B$ as a function of temperature T for $\{NiCr_7\}$: The experimental data are presented by black diamonds. The theoretical fit for $J_1 = J_2 = 8.25\ k_B$ K is given by a red solid curve and for $J_1/k_B = 8.5$ K and $J_2/k_B = 7.425$ K by a green solid curve [96]. $B = 1$ T and $g = 2.1$.

assumed $g = 2$.
Reexamining the available experimental susceptibility data [29] in terms of complete numerical diagonalization of the Hamiltonian, we find the same qualitative behavior as in Ref. [29]. Depending on the spin of the dopant the resulting ground state spin S assumes the following values: $S = 1/2$ for M = Fe, $S = 1$ for M = Cu, $S = 1/2$ for M = Ni, $S = 1$ for M = Mn, and $S = 3/2$ for M = Zn.

3.4. Results and discussions

- **{Fe-Cr_7}**: The complete chemical formula is $[\{nBu_2NH_2\}\{\mathbf{Cr_7Fe}F_8(O_2CCMe_3)_{16}\}]$. Mössbauer spectroscopy indicates that only Fe^{II} ions are present [29]. The spectrum of this system is represented in Figure 3.4-d. The plot of $T * M/B$ shows a value close to zero at low temperatures and a maximum in plot M/B versus T at 30 K, Figure 3.5-3.8. This means that there is a weak anti-ferromagnetic interaction between the metal ions of this system. The theoretical fit curve

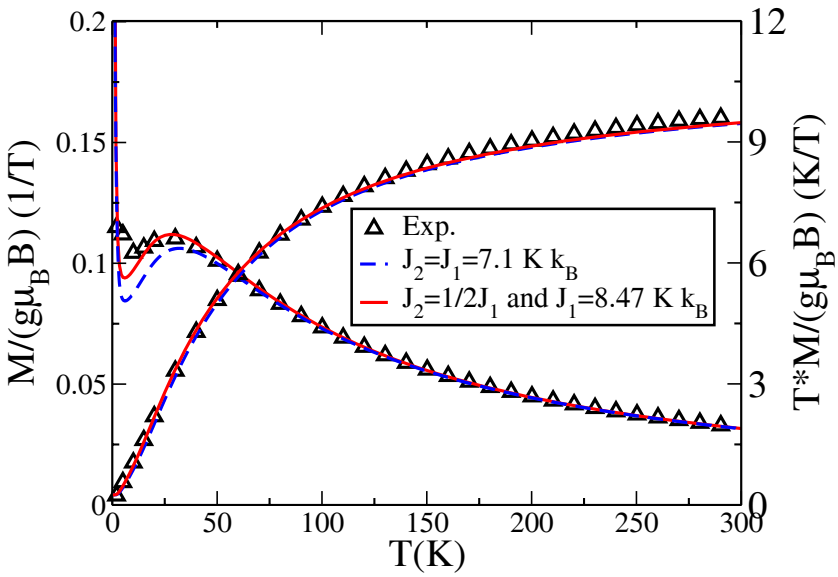

Figure 3.8.: Variation of $\mathcal{M}/B$ and $T\mathcal{M}/B$ as a function of temperature T for $\{FeCr_7\}$: The experimental data are depicted by black triangles. The theoretical fit for $J_1 = J_2 = 7.1\ k_B$ K is given by a dashed curve, and for $J_1/k_B = 8.47$ K and $J_2 = J_1/2$ by a solid curve. $B = 1$ T and $g = 2$.

using an isotropic Heisenberg model is given by a red and blue solid line for J_1 (Cr-Cr) = J_2 (Fe-Cr) = 7.1 k_B K and J_2 (Fe-Cr) = 1/2 J_1 (Cr-Cr) with $J_1/k_B = 8.47$ K, respectively, for the low magnetic field $B = 1$ Tesla and the value of $g = 2$ (estimated from EPR spectra and by means of vector coupling approach) [29, 97]. We found that the fit with $J2 = 1/2J1$ seems to be better than with $J2 = J1$, Figure 3.8.

- **{Ni-Cr$_7$}**: The complete chemical formula is $[\{Me_2NH_2\}\{\mathbf{Cr_7Ni}\,F_8(O_2CCMe_3)_{16}\}]$. In fact, the M/B versus T curves (Figure 3.7), indicate an antiferromagnetic interaction for Cr-Cr and Cr-Ni ions and an $S = 1/2$ ground state. The theoretical fit results in $J_2 = J_1 = 8.19\ k_B$ K, for $g = 2$.

- **{Zn-Cr$_7$}**: The Zn ion in this system is diamagnetic, therefore the ring simulated in this case contains seven spins and there is no interaction between Cr-Zn, $J_2 = 0$. The experimental data is fitted with the theoretical curve for

J_1/k_B = 8.4 K (Figure 3.6). The plot of $T * M/B$ versus T curves shows a value close to a zero at low temperatures.

	exchange parameters		
Compounds	J_1 (k_B K)	J_2 (k_B K)	Curves
$FeCr_7$	8.47	1/2 J_1	Red solid
$FeCr_7$	7.1	$=J_1$	Blue dashed
$CuCr_7$	8.4	$=J_1$	
$ZnCr_7$	8.4	0	
$NiCr_7$	8.25	$=J_1$	Red solid
$NiCr_7$	8.5	$0.9J_1$	Green solid [96]

Table 3.1.: Results of the exchange parameters J_2 and J_1 in antiferromagnetic molecular magnetic rings of heterometallic {Cr_7M} wheels

In table 3.1, we report the results of the exchange parameters J_2 and J_1. All susceptibility curves are compatible with antiferromagnetic exchange [98]. In the first example of {$CuCr_7$}, figure 3.5, a common exchange interaction explains the experimental data. This exchange is the same as in {Cr_8} [92], thus unchanged in the heterometallic compound. The second example of $ZnCr_7$, figure 3.6, constitutes a spin chain since the Zn ion is non-magnetic. Thus the original Cr-Cr interaction is not altered whereas the coupling to the Zn ion is $J_2 = 0$. The third example deals with $NiCr_7$, Figure 3.7. Here we find that the experimental data can either be described by common, but slightly reduced exchange interaction, or by an almost unchanged Cr-Cr interaction and a 10 % smaller Cr-Ni exchange. This has also been reported in Ref. [99]. The last example of $FeCr_7$, figure 3.8, shows the biggest deviation from the assumption of an common and almost unchanged exchange parameter. Although a single exchange constant provides a reasonable fit to the experimental data [29], a better approximation is given if one assumes that the Cr-Cr exchange is not much altered whereas the Cr-Fe exchange is reduced to half the size of the Cr-Cr exchange.
It should be mentioned that the value of the exchange interaction in this com-

pound is close to the value obtained in tetragonal crystal form of $[Cr_8F_8Piv_{16}]$, $(J = 1.5\ meV = 17.4\ K\ k_B) * 1/2 = 8.7\ k_B$ K [92, 93].

3.5. Conclusion

In conclusion we have presented the exchange parameters of molecular magnetic rings of heterometallic $\{Cr_7M\}$ wheels where M=Fe, Cu, Zn and Ni with spin $S = 2$, $S = 1/2$, $S = 0$ and 1, respectively. In order to study these different systems we have used a mirror symmetry operation around the doping ion. We have evaluated the different energy spectra and used these energy eigenvalues to adjust the curves of $T * M/B$ and M/B versus T with the measured data. We find, that in the case of $\{FeCr_7\}$, the iron-chromium exchange is different from the chromium-chromium exchange in contrast to the other cases.

4. Spin-lattice relaxation time T_1 in heterometallic $\{Cr_7M\}$ wheels

At low temperatures molecular magnets act as individual quantum nanomagnets and can display super-paramagnetic phenomena like macroscopic quantum tunneling, ground state degeneracy, level-crossing... etc. The coupling between magnetic molecular levels and the environment such as phonons or nuclear spins are a crucial issue to understand these phenomena. Furthermore, the measurement of the proton spin-lattice relaxation rate, T_1^{-1}, also called longitudinal relaxation time, is a powerful tool to investigate the spin dynamics, and to understand the degeneracy as well as level crossing effects [100, 101, 102], accuring at some critical field values B for which two levels of the magnetic spectrum intersect. For instance, the early observation of a strong field dependence of $1/T_1$ at high T [103], in one dimensional anti-ferromagnetic linear chains has revealed a long-time persistence of the various spin-spin time correlation functions [104].
In this chapter, we investigate T_1^{-1} for the heterometallic $\{Cr_7M\}$ wheel systems. We first need to discuss briefly the basics and some general aspects of T_1 in the context of magnetic molecule systems. Hence, we will provide a general theoretical framework of the interaction between the nuclear spin and the electron spin. We will use the calculated energy levels, eigenstates of the different rings and the values of the exchange interaction, well obtained from the fit of the magnetic susceptibility from chapter 3, to describe semiquantitatively the behavior of T_1^{-1} versus applied magnetic field B and temperature T. We will close the chapter with discussing the results and a summary.

4.1. T_1 in molecular magnets

4.1.1. Measurement of T_1

The relaxation time T_1 represents the "lifetime" of the first order rate process that returns the magnetization to the Boltzmann equilibrium along the Z axis, Figure 4.1. If at any time the longitudinal magnetization is not equal to Mz_0, it will exponentially

approach the equilibrium value. The time constant for this exponential approach toward Mz_0 is T_1. This time can be measured by various techniques (exp: NMR, Inversion Recovery Fourier Transform ($IRFT$), Progressive Saturation ($PSFT$)). The magnitude of the relaxation time depends highly on the type of nuclei[1] and on other factors like the physical state (solid or liquid state), on the viscosity of the solution, the temperature ... etc. In other words, the relaxation time depends on the motion of the molecule.
The measurement of the nuclear spin-lattice relaxation rate provides an effective technique for determining the low frequency part of the dynamics of the paramagnetic ions in magnetic molecules. It provides a powerful tool to investigate the spin dynamics, since the nuclei probe the fluctuation spectrum of the local field induced at the nuclear site, by the hyperfine interaction with the localized magnetic moments. For example in one-dimensional (1D) magnetic chains, T_1^{-1} measurements have proved the long time diffusive behavior of the two spin correlation function at high temperature [102]. Furthermore, in magnetic systems, the slowing down of the spin fluctuations, on approaching from high temperature side the phase transition to long range order, is manifested by a divergence of ${T_1}^{-1}$ [105].

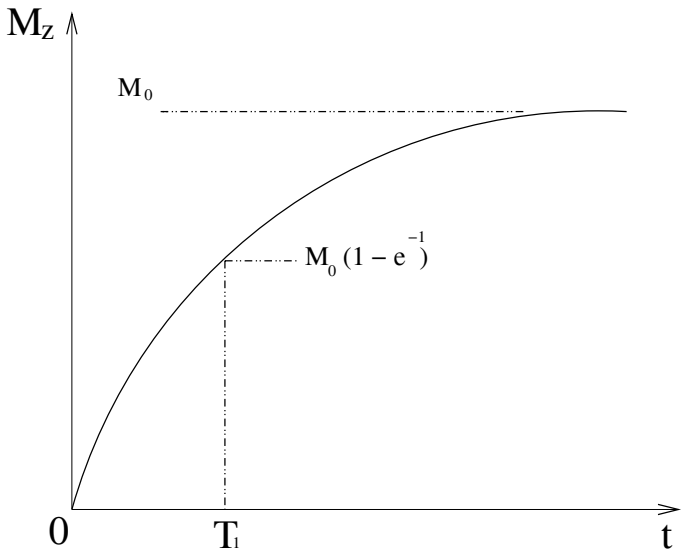

Figure 4.1.: Typical relaxation curve of the magnetization.

At equilibrium, the net magnetization vector lies along the direction of the applied magnetic field B_0 and is called the equilibrium magnetization M_0. In this configu-

[1] nuclei with spin 1/2 and low magnetogyric ratio have usually long relaxation times whereas nuclei with spin > 1/2 have very short relaxation times

ration, the Z component of magnetization, M_z, equals Mz_0. M_z is referred to as the longitudinal magnetization. There is no transverse (M_X or M_Y) magnetization. It is possible to change the net magnetization by exposing the nuclear spin system to radiation of appropriate frequency. If enough energy is put into the system, it is possible to saturate the spin system and make $M_z = 0$. The time constant which describes how M_z returns to its equilibrium value is called the spin lattice relaxation time (T_1), Figure 4.1. The equation governing this behavior is: if at time $t = 0$ the longitudinal magnetization is zero, the magnetization at time t after its displacement will be

$$M_z = M_0(1 - e^{-t/T_1}) \tag{4.1}$$

If the net magnetization is placed along the $-Z$ axis, it will gradually return to its equilibrium position along the $+Z$ axis at a rate governed by T_1. The equation governing this behavior as a function of the time t after its displacement is:

$$M_z = M_0(1 - 2e^{-t/T1}) \tag{4.2}$$

The spin-lattice relaxation time (T_1) is the time to reduce the difference between the longitudinal magnetization (M_z) and its equilibrium value by a factor of e .

If the net magnetization is placed in the XY plane it will rotate about the Z axis at a frequency equal to the frequency which would cause a transition between the two energy levels of the spin. This frequency is called the Larmor frequency.

4.1.2. Theoritical estimation of T_1

In the ground state, all nuclear spins are disordered, and there is no energy difference between them. When we apply a strong external magnetic field B, they orient either against or with it, there is always a small excess of nuclei (population excess) aligned with the field than pointing against it. Upon application of the external magnetic field we create an energy difference between nuclei aligned and against B. Each level has a different population, and the difference between the two is related to the energy difference which is produced by the Boltzmann distribution. To explain certain aspects of NMR, we need to refer to circular motion and we define the precession or Larmor frequency, ω_N.

According to the standard formula of Moriya [106], our theoritical modeling is based in the coupling between magnetic molecular levels of the system and nuclear spins. The total Hamiltonian $H_{dipolar}$ of a system described with dipole-dipole interaction between nuclear spin I and the fluctuations of the electron spin S_i(lattice) is defined as [107]:

$$H_{dip.}(S_i, I) = \underset{\sim}{G}^z \underset{\sim}{I}^z + \underset{\sim}{G}^+ \underset{\sim}{I}^- + \underset{\sim}{G}^- \underset{\sim}{I}^+ \tag{4.3}$$

with the operators $G^{\pm}$ and G^z discribing the electron spin defined by

$$\underset{\sim}{G}^{\pm} = \sum_i \left[D_0(i)\underset{\sim}{S}^{\pm}(i) + D_{\mp 1}(i)\underset{\sim}{S}^{z}(i) + D_{\mp 2}(i)\underset{\sim}{S}^{\mp}(i) \right],$$

$$\underset{\sim}{G}^{z} = \sum_{i=1}^{N} \left[\frac{2}{3} D_0(i)\underset{\sim}{S}^{z}(i) + D_{+1}(i)\underset{\sim}{S}^{+}(i) + D_{-1}(i)\underset{\sim}{S}^{-}(i) \right],$$

where

- $D_0(i) = \alpha_i(3\cos\theta_i - 1)$,
- $D_{\pm 1}(i) = \alpha_i \sin\theta_i \cos\theta_i \exp(\mp i\varphi_i)$,
- $D_{\mp 2} = 1/2\alpha_i \sin^2 \alpha_i \exp(\mp 2i\varphi_i)$

are the usual geometrical factors of the dipolar interaction, $\alpha_i = 3\gamma_N\gamma_S/(2r_i^3)$. θ_i and φ_i are the polar coordinates of the vector $\vec{r_i}$ describing the relative positions of the two spins.

Since the protons do not bond directly to the spins S_i of the ions, figure 4.2, we assume that the contact hyperfine interaction is negligible compared to the dipolar interaction. This is confirmed by the observation that the ^{1}H NMR line is broadened but not shifted by the magnetic interaction with ionic moments [83]. That means, in order to describe the nuclear spin-lattice relaxation time, in a magnetic system in the presence of a correlated spin dynamics, it is more convenient to express the nuclear T_1 in terms of the components of the electronic spins. We suppose that the fluctuation mainly arises due to the exchange interactions and omit the effect of the lattice vibrations. T_1^{-1} is given by [106]:

$$\frac{1}{T_1} = \left(1 + e^{-\hbar\omega_N/k_BT}\right) \int_{-\infty}^{+\infty} << \underset{\sim}{G}^{+}(t)\underset{\sim}{G}^{-}(0) >> e^{+i\omega_N t} dt \tag{4.4}$$

where ω_N is the nuclear Larmor frequency (resonance frequency) $\omega_N = \gamma_N B$.
The average term $<< \underset{\sim}{G}^{+}(t)\underset{\sim}{G}^{-}(0) >>$ describes the electron spin, which corresponds to a sum of exponentially decaying functions and can be obtained by expressing the correlation function, as in the following formula

$$<< \underset{\sim}{G}^{+}(t)\underset{\sim}{G}^{-}(0) >> = Tr\left\{ e^{-\beta\underset{\sim}{H}} e^{i\underset{\sim}{H}t/\hbar} \underset{\sim}{G}^{+} e^{-i\underset{\sim}{H}t/\hbar} \underset{\sim}{G}^{-} \right\} / Tr\left\{ e^{-\beta\underset{\sim}{H}} \right\}. \tag{4.5}$$

The decay $<< \underset{\sim}{G}^{+}(t)\underset{\sim}{G}^{-}(0) >>$ is not a single exponential. It can be written in

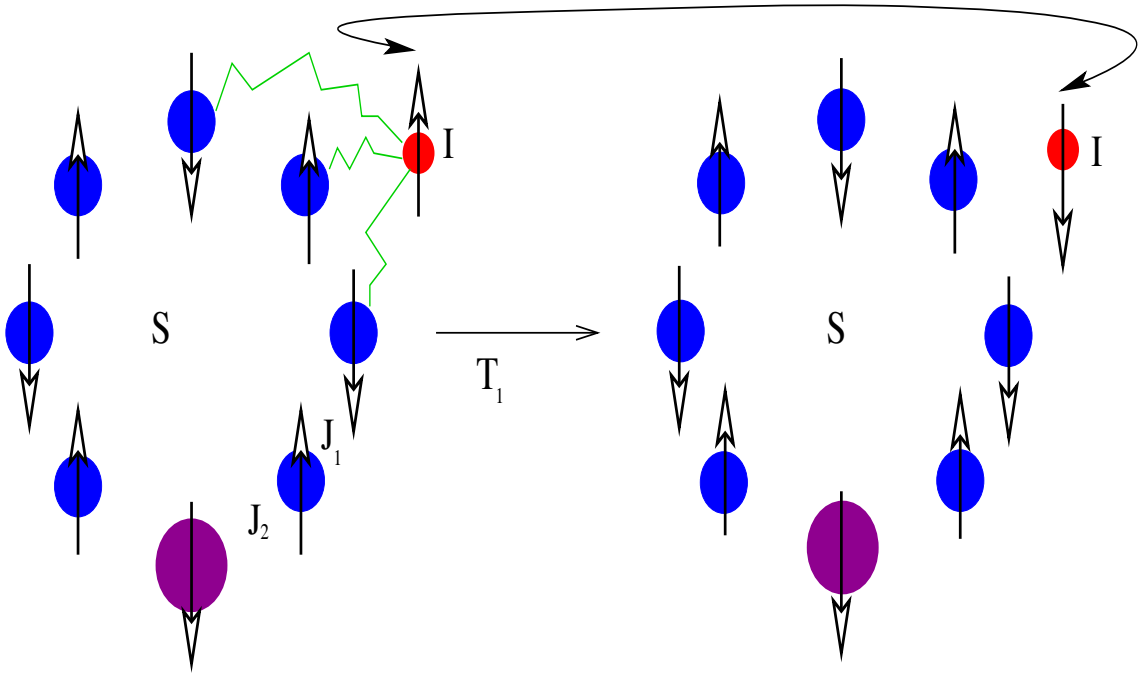

Figure 4.2.: Electron-Nucleus interactions.

terms of the matrix elements of the local spin components between eigenvectors of the total spin system

$$<< e^{i\frac{\underset{\sim}{H}t}{\hbar}}\underset{\sim}{G}^{+}e^{-i\frac{\underset{\sim}{H}t}{\hbar}}\underset{\sim}{G}^{-} >>= \frac{1}{Z}\sum_{\mu} < \psi_\mu|e^{i\frac{E_\mu t}{\hbar}}\underset{\sim}{G}^{+}e^{-i\frac{\underset{\sim}{H}t}{\hbar}}\underset{\sim}{G}^{-}|\psi_\mu > e^{-\beta E_\mu},$$

where

$$\underset{\sim}{H}|\psi_\mu >= E_\mu|\psi_\mu > \begin{cases} \mu = 1,\ldots,\text{Dim} \\ |\psi_\mu >= \sum_{\vec{m}_{\mu n},k_\mu} C_{\vec{m}_{\mu n}k_\mu}|\vec{m}_{\mu n},k_\mu > \\ n = 1,\ldots,N \end{cases} \quad \begin{array}{l} \text{Dim: dimension of Hilbert space} \\ \text{k: shift quantum number} \\ \text{N: number of spin} \end{array} \tag{4.6}$$

From chapter 2 the product basis $|\vec{m}_{\mu,n},k_\mu >$ are given by:

$$|\vec{m}_{\mu,n},k_\mu >= \frac{1}{\sqrt{N}}\sum_{j=0}^{N-1}\left(e^{\frac{i2\pi k}{N_c}}\underset{\sim}{T}_m\right)^j|\vec{m}_{\mu,n} > \quad \begin{cases} \underset{\sim}{T}_m: \quad \text{shift} \quad \text{operator.} \\ N_c \text{ number of cycle,} \end{cases}$$

with

$$|\vec{m}_{\mu n}>=|m_{\mu 1}, m_{\mu 2}, \ldots, m_{\mu N}> .$$

Substituting the result in (4.4), one obtains

$$\frac{1}{T_1}=\frac{1}{Z}\left(1+e^{-\hbar\omega_N/k_BT}\right)\int_{-\infty}^{+\infty}\sum_{\mu,\nu}e^{i\frac{E_\mu t}{\hbar}}<\psi_\mu|\underset{\sim}{G}^+|\psi_\nu>e^{-i\frac{E_\nu t}{\hbar}}<\psi_\nu|\underset{\sim}{G}^-|\psi_\mu>e^{-\beta E_\mu}e^{+i\omega_N t}dt, \tag{4.7}$$

which can also be written as

$$\frac{1}{T_1}=\frac{1}{Z}\left(1+e^{-\hbar\omega_N/k_BT}\right)\sum_{\mu,\nu}e^{-\beta E_\mu}<\psi_\mu|\underset{\sim}{G}^+|\psi_\nu><\psi_\nu|\underset{\sim}{G}^-|\psi_\mu>\int_{-\infty}^{+\infty}e^{i\frac{E_\nu-E_\mu}{\hbar}t+i\omega_N t}dt. \tag{4.8}$$

Using Fourier transformation, the integration can be represented by a $\delta-$function, the equation (4.8) can be easily put into the form

$$\frac{1}{T_1}=\frac{2\pi}{Z}\left(1+e^{-\hbar\omega_N/k_BT}\right)\sum_{\mu,\nu}e^{-\beta E_\mu}<\psi_\mu|\underset{\sim}{G}^+|\psi_\nu><\psi_\nu|\underset{\sim}{G}^-|\psi_\mu>\delta_\varepsilon\left(\omega_N-\frac{E_\nu-E_\mu}{\hbar}\right) \tag{4.9}$$

Where:

δ_ε is the delta function;
$\omega_N =\gamma_N B$ and $\gamma_N = g_N\ \frac{\mu_N}{\hbar}$;
γ_N: gyromagnetic ratio;
g_N: Landé factor of nuclear $\backsimeq 5.5854$;
μ_N: nuclear magneton = 5.0508 10^{-27} A m^2;

$$\frac{1}{T_1}=\frac{1}{Z}\left(1+e^{-\hbar\omega_N/k_BT}\right)\sum_{\mu,\nu}e^{-\beta E_\mu}\left(|<\psi_\mu|\underset{\sim}{G}^+|\psi_\nu>|\right)^2\delta_\varepsilon\left(\frac{g_N\mu_N B-\Delta E}{\hbar}\right) \tag{4.10}$$

The spin-lattice relaxation is a resonant process [107] which ideally should only occur if the transition energy $E_\mu - E_\nu$ in the spin system matches the nuclear Lamor frequency. Nevertheless, the interaction of the whole system with its surrounding broadens levels. In addition the experimental resolution is limited. We therefore allow transitions which deviate up to ε from strict energy conservation. This can be supported by transforming the $\delta_\varepsilon(\omega_N - \frac{E_\mu-E_\nu}{\hbar})$ using the Lorentzian function

$\left(\delta_\varepsilon(x) = \frac{\varepsilon/\pi}{x^2+\varepsilon^2}\right)$ or by a Gaussian distribution function $\left(\delta_\varepsilon(x) = \frac{1}{\varepsilon\sqrt{\pi}} \quad e^{-\frac{x^2}{\varepsilon^2}}\right)$. Such a function could in principle depend both on temperature and on applied field [108, 109]. Using a Gaussian function in the Eq. (4.10) can be written as

$$\delta_\varepsilon(g_N\mu_N * B - \Delta E) = \frac{1}{\varepsilon\sqrt{\pi}}\exp\left\{-\frac{(g_N\mu_N * B - \Delta E)^2}{\hbar^2\varepsilon^2}\right\} \tag{4.11}$$

We have neglected such possible dependencies and use the same function with ε that is constant and independent of both B and T.
The energy levels of the total system are given by

$$E_\mu = E_\mu(B=0) + g_e\mu_B B M_\mu \tag{4.12}$$

and likewise

$$\Delta E = E_\nu(B=0) - E_\mu(B=0) + g_e\mu_B B(M_\nu - M_\mu) \tag{4.13}$$

with:

g_e:Landé factor of the electron;
μ_B: electron magneton: $9,274\ 10^{-24}$ A m^2;

Substituting the equations (4.11) and (4.13) into equation (4.10) yields the spin latice relaxation rate which can be written as

$$\frac{1}{T_1} = \frac{1}{Z\varepsilon\sqrt{\pi}}\left(1 + e^{-\hbar\omega_N/k_BT}\right)\sum_{\mu,\nu} e^{-\beta E_\mu}\left(|<\psi_\mu|\underset{\sim}{G}^+|\psi_\nu>|\right)^2$$

$$\exp\left\{-\frac{(g_N\mu_N * B - E_\nu(B=0) - [E_\mu(B=0) + g_e\mu_B B(M_\nu - M_\mu)])^2}{\hbar^2\varepsilon^2}\right\} \tag{4.14}$$

Equation(4.14) is our final expression which shows that $\frac{1}{T_1}$ depends on applied magnetic field and temperature which we will discuss in Sec. 4.3 and 4.4 .

4.2. Level crossings in heterometallic wheels

The phenomenon of level-crossing and the situation of degeneracy between levels has interested many scientists in recent years. A famous theorem of quantum mechanics states that the interaction of two energy levels of a physical system is infinitely unlikely as a single parameter is varied [110]. The degeneracies that lie on the components B_x or B_z axes in the magnetic field space sec. 2.5.1 can be understand in terms

of symmetry allowed level crossings as per the von Neumann-Wigner theorem [111], but the newly discovered ones [80] lie off the axes, and cannot be so understood, which raises fundamental problems of quantum dynamics. However, in many cases it has been found that the relaxation time saturates at some temperature. Below this temperature, quantum fluctuations become important and tunneling phenomena may cause the system to relax [112]. In the antiferromagnetic spin ring system

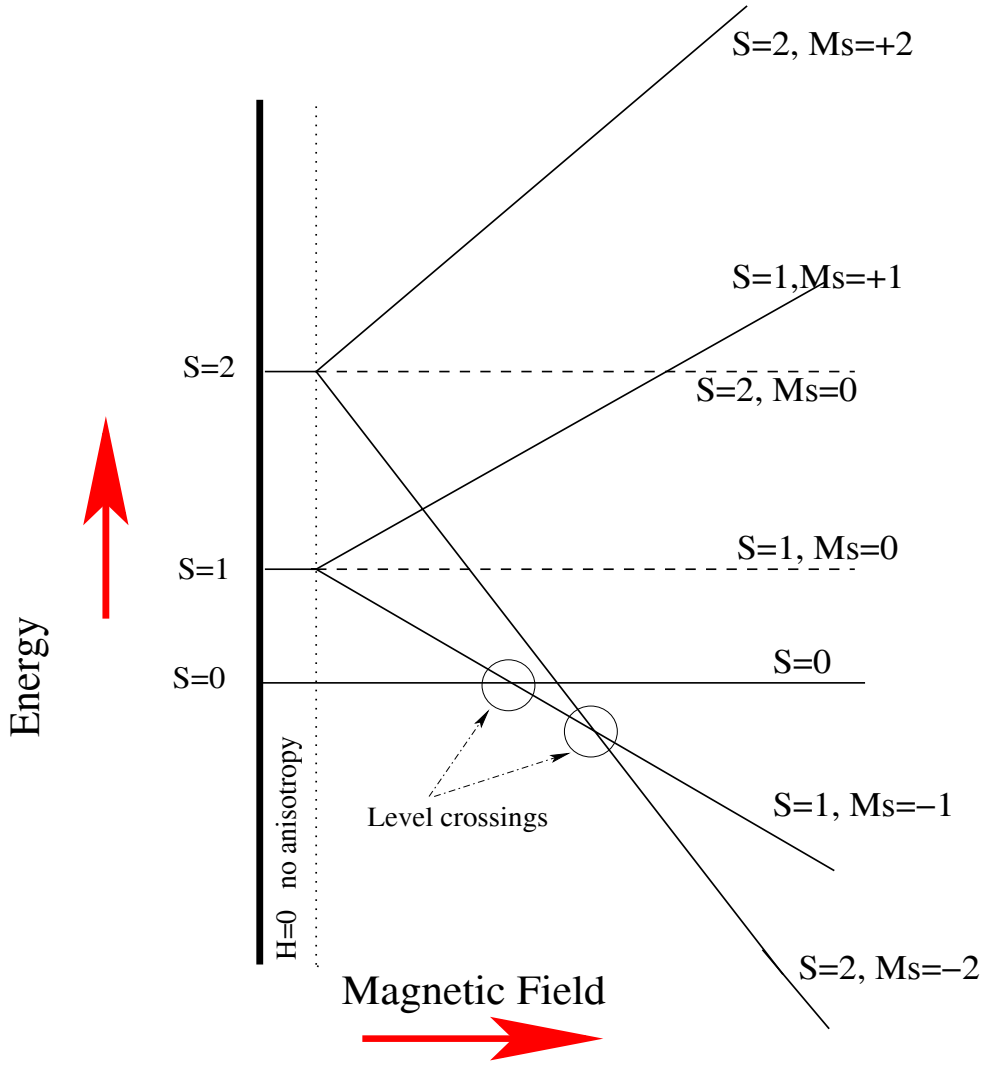

Figure 4.3.: Energy levels vs. magnetic field for the lower energy eigenvalues for the lower three values of total spin S (0,1,2), for the AFM ring system of $\{Cr_8\}$.

with a $S = 0$ singlet ground state and a $S = 1$ triplet excited state, an external applied magnetic field B removes the residual degeneracy of the triplet state and induces multiple level-crossings at specific magnetic field values. However, the ground state of the compound changes from $S = 0$ to $S = 1$ at B_1, from $S = 1$ to $S = 2$ at B_2, and so on. Because of the anisotropy, the values of B_i depend on the angle between B and the molecular axis z [92, 93].

In figure 4.3, we represent the dependence of the energy levels on magnetic field B for the lower three values of total spin S $(0, 1, 2)$, for the AFM ring system of $\{Cr_8\}$. The spectrum shows the two level crossings which we try to investigate in this work through proton spin-lattice relaxation rate.

4.3. T_1^{-1} vs B in heterometallic $\{MCr_7\}$ wheels

The proton spin-lattice relaxation rate of the mother substance $\{Cr_8\}$ has been investigated experimentally in great detail [108, 109], but predominantly as a function of temperature for certain small applied magnetic fields. In the following, having determined the Heisenberg exchange parameters of several heterometallic $\{MCr_7\}$ wheels, chapter 3, we investigate the behavior of the relaxation rate as a function of magnetic field according to the formula (4.14), given in sec. 4.1.2. In this formula, we allow transitions which deviate up to ε from strict energy conservation using the Gaussian distribution function, in which we neglecte dependencies of ε on B or T and use the same value $\varepsilon = 0.2$ K for all calculations of T_1^{-1} versus B, and different once for the case of T_1^{-1} versus T, Sec. 4.4. For technical reasons, the calculation was performed for the lower five total spin quantum numbers S using the 20 lowest energy eigenstates of the spectrum of the compound under consideration, figures 3.3 - 3.4, chap. 3.

The magnetic field dependence of proton T_1^{-1} and static magnetization M according to the formula (2.33) at fixed temperature T of the compound $\{Cr_8\}$ for $g = 2$ is reported in Figure 4.4. T_1^{-1} shows three very well-defined peaks centered around the critical field values (B_c): 6.8, 14.9, and 21.49 T. These values correspond very closely to the fields where the thermodynamic steps were observed in magnetization, which are a consequence of quantum level crossing, Figure 4.4. When $B \rightarrow B_c$ a resonance condition occurs between the nuclear spin system and the magnetic molecule as a whole. The width of this peak is determined by the constant ε Eq. (4.14). T_1^{-1} values are dependent upon magnetic field strength, increasing field strength gives increasing T_1^{-1}, which means, at this specific strong magnetic field B values we have also levels crossing between exited states which have influence in the proton T_1^{-1} and give a short relaxation time.

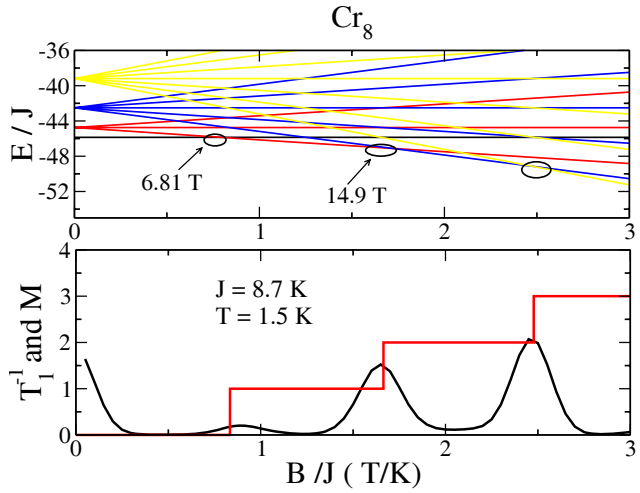

Figure 4.4.: Top panel: Zeeman splitting of the low-lying levels of $\{Cr_8\}$. The crossing fields are highlighted and the values of the two lowest fields given. Bottom panel: $(T = 0)$-magnetization (steps) and relaxation rate T_1^{-1} as function of the applied field normalized to the coupling J.

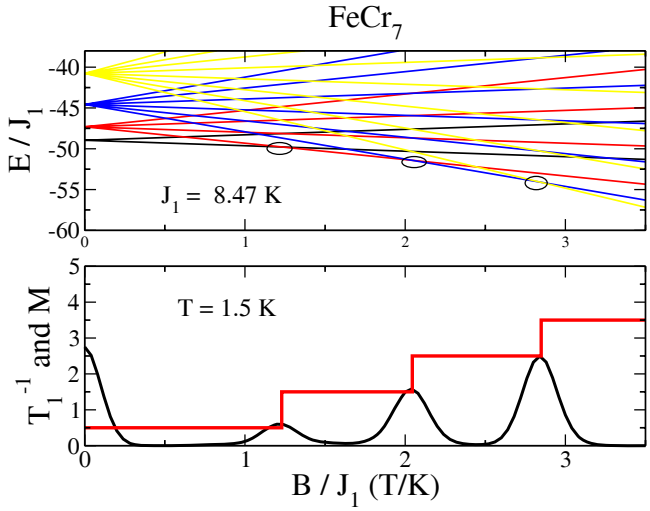

Figure 4.5.: Top panel: Zeeman splitting of the low-lying levels of $\{FeCr_7\}$. The crossing fields are highlighted and the values of the two lowest fields given. Bottom panel: $(T = 0)$-magnetization (steps) and relaxation rate T_1^{-1} as function of the applied field normalized to the coupling J_1.

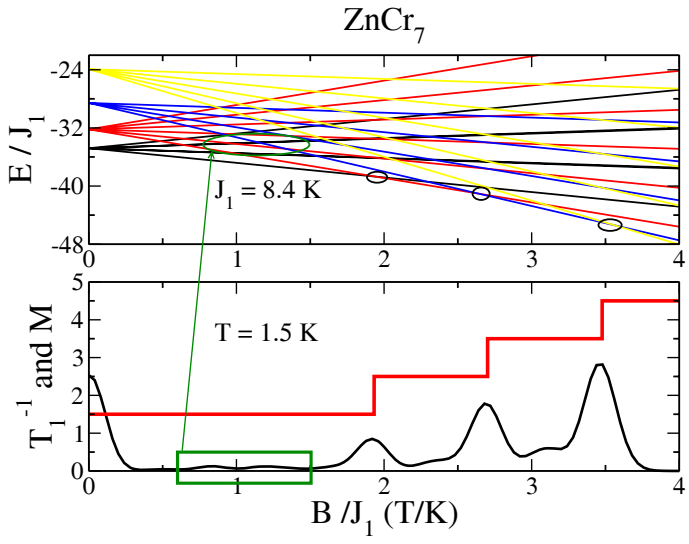

Figure 4.6.: Top panel: Zeeman splitting of the low-lying levels of $\{ZnCr_7\}$. The crossing fields are highlighted and the values of the two lowest fields given. Bottom panel: $(T = 0)$-magnetization (steps) and relaxation rate T_1^{-1} as function of the applied field normalized to the coupling J_1. The small peaks in the green box correspond to the crossing between the exited states.

The proton spin-lattice relaxation rate T_1^{-1} and static magnetization M versus applied magnetic field B for $\{CuCr_7\}$, $\{ZnCr_7\}$, $\{NiCr_7\}$, and $\{FeCr_7\}$ are shown in Figures 4.4 - 4.8. A g-value of $g = 2.1$ has been used for $\{NiCr_7\}$, in all other cases $g = 2$ has been assumed.
In Figures 4.6 and 4.7, T_1^{-1} show some small peaks at low applied magnetic field, these peaks are probably corresponding to transitions between exited levels. Reduced proton spin-lattice relaxation rates T_1^{-1} occur at certain level crossings, Figures 4.7 and 4.8.

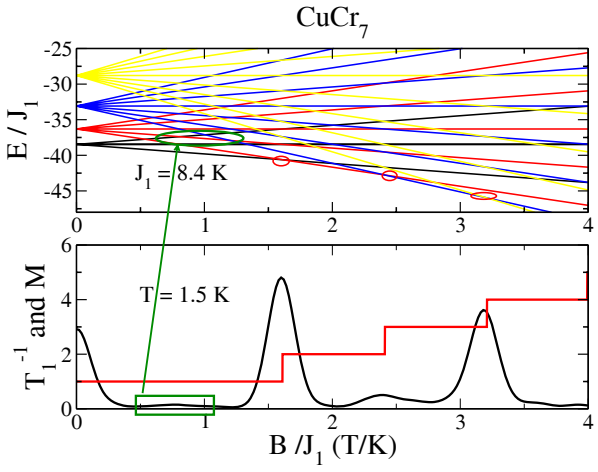

Figure 4.7.: Top panel: Zeeman splitting of the low-lying levels of $\{CuCr_7\}$. The crossing fields are highlighted and the values of the two lowest fields given. Bottom panel: $(T = 0)$-magnetization (steps) and relaxation rate T_1^{-1} as function of the applied field normalized to the coupling J_1. The small peaks in the box correspond to the crossing between the high levels.

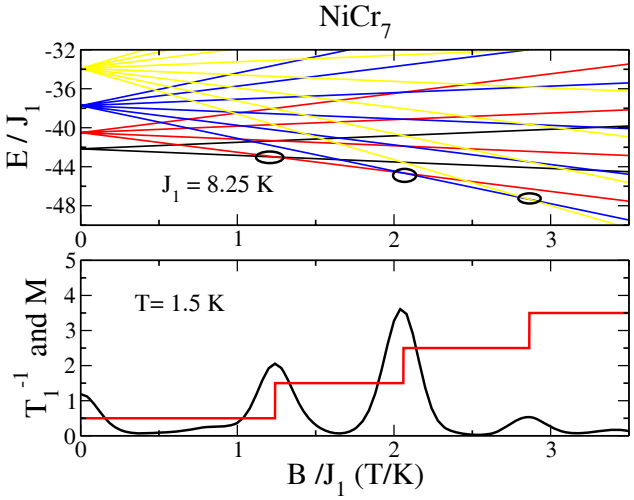

Figure 4.8.: Top panel: Zeeman splitting of the low-lying levels of $\{NiCr_7\}$. The crossing fields are highlighted and the values of the two lowest fields given. Bottom panel: $(T = 0)$-magnetization (steps) and relaxation rate T_1^{-1} as function of the applied field normalized to the coupling J_1.

4.4. Temperature dependence of T_1^{-1} in $\{Cr_8\}$

The temperature dependence of T_1^{-1} is also of great interest. Specifically, one can follow the spin dynamical behavior starting from the high-T regime, where the spins are uncorrelated, down to the lower temperatures where the correlations are governed by the strong exchange interactions. Mainly for the antiferromagnetic ring systems,

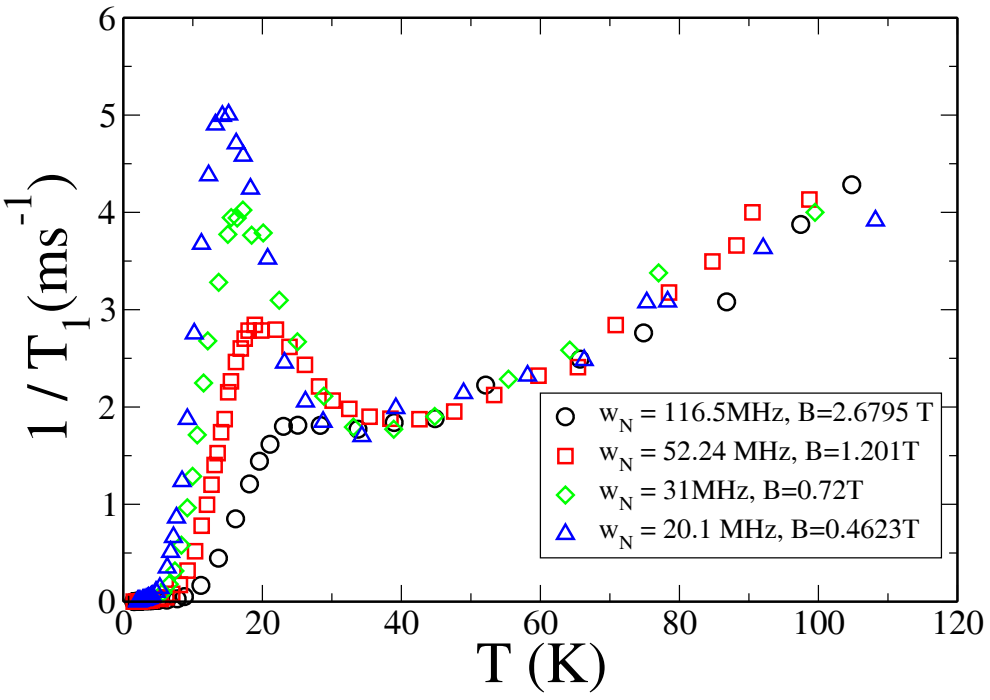

Figure 4.9.: The proton spin-lattice relaxation rate T_1^{-1} as function of the temperature T, for the anti-ferromagnetic ring system of $\{Cr_8\}$.

it has been found that the temperature dependence of T_1^{-1} resembles the behavior of the product $T\chi$, where $\chi(T)$ denotes the zero-field magnetic susceptibility [108]. The experimental data for T_1^{-1} for the AFM ring $\{Cr_8\}$ are shown in Fig. 4.9 for four choices of B [108]. In Figure 4.10 we present our data for the corresponding values of the spin-lattice relaxation rate obtained using the equation, Sec. 4.1.2:

$$\frac{1}{T_1} = \frac{A}{Z\varepsilon\sqrt{\pi}} \left(1 + e^{-\hbar\omega_N/k_BT}\right) \sum_{\mu,\nu} e^{-\beta E_\mu} \left(| < \psi_\mu | \underset{\sim}{G}^+ | \psi_\nu > | \right)^2$$

$$\exp\left\{-\frac{(g_N\mu_N * B - E_\nu(B=0) - [E_\mu(B=0) + g_e\mu_B B(M_\nu - M_\mu)])^2}{\hbar^2\varepsilon^2}\right\}, \quad (4.15)$$

where A is a fitting constant independent of both B and T. The results are represented by solid curves with different values of the parameter A and ε, which are constants determined by a best-fit procedure for the $\{Cr_8\}$ antiferromagnetic ring, and the results are given in Table 4.1 with the corresponding values of ε. We note that the temperature dependence of the spin-lattice relaxation rate is not adequately described by the common formula (4.15) at high T, this can be related that the calculation was performed just with the twenty low-energy levels of the five low number of subspaces with spin quantum number S (S=-1, 0, 1,2 and 3 respectively) for the antiferromagnetic ring system $\{Cr_8\}$. To describe the high temperature part we need the complete energy spectrum in our calculations. In Table 4.1 we give the values of the parameters for the $\{Cr_8\}$ anti-ferromagnetic ring.

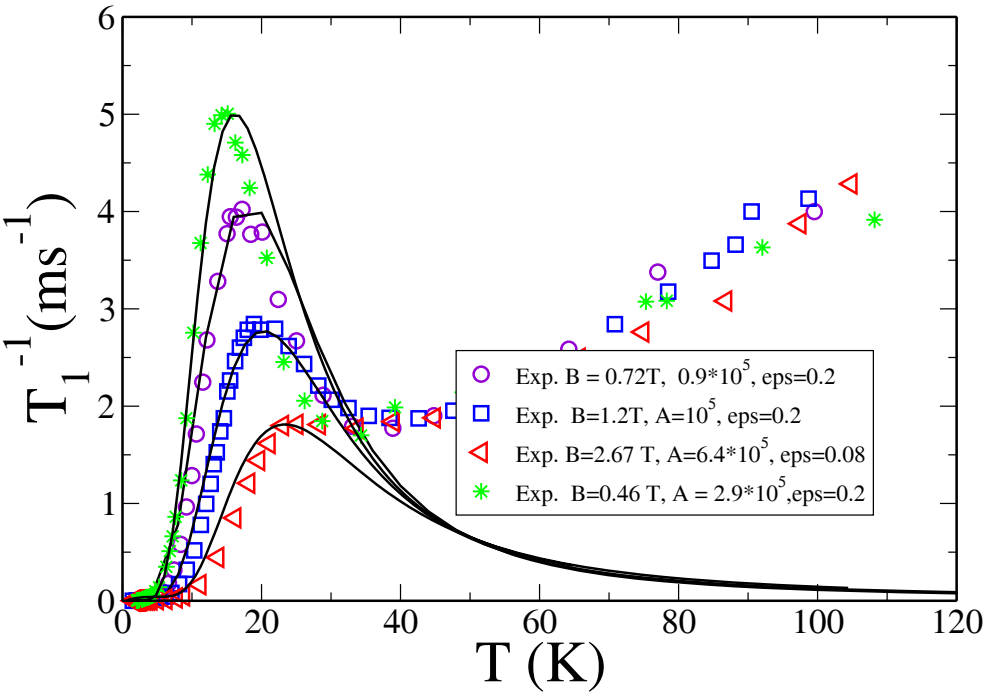

Figure 4.10.: The proton spin-lattice relaxation rate T_1^{-1} as function of the temperature T, for the anti-ferromagnetic ring system of $\{Cr_8\}$.

It should be mentioned that the parameter A varies, and this can be related to the quality of our Hamiltonian used in which the anisotropy term is neglected.

B(T)	A	ε
0.72	$0.9\text{x}10^5$	0.2
1.2	10^5	0.2
2.67	$6.4\text{x}10^5$	0.08
0.46	$2.9\text{x}10^5$	0.2

Table 4.1.: The values of the parameters obtained from the best fit of $1/\text{T}_1$ data using Eq. (4.15).

4.5. Results and Discussions

In the first part, we discussed the magnetic field dependence of the proton spin-lattice relation rate T_1^{-1} and of the end, we discussed the estimation of the T dependence of T_1^{-1} with our formulas (4.14) and (4.15), in which we have neglected the dependence of ε on B and T. We have used the same value $\varepsilon = 0.2$ K for all calculations of T_1^{-1} versus B, Eq. (4.14), and different once for T_1^{-1} versus T, Eq. (4.15). In the following we discuss the behavior of the relaxation rate as a function of magnetic field for a typical small temperature of $T = 1.5$ K [99]. This function highlights the behavior of the magnetic system at low-lying (dominantly ground state) Zeeman level crossings, since there resonant cross relaxation occurs. Experimentally such data are rarely accessible due to the fact that the level crossing fields are often outside the producible field range. In the case of $\{\text{Cr}_8\}$ [99] and Fe_{10} [53] these data could nevertheless be measured thanks to moderate exchange constants. One important result of these measurements is that the values of the level crossing fields for even-membered Heisenberg rings follow the Landé interval rule [53], which is nowadays understood as rotational modes [64], rotation of the Néel vector [113, 114] or tower of states [113, 115].

The behavior of the relaxation rate and static magnetization as a function of magnetic field for a typical small temperature of $T = 1.5$ K for $\{\text{Cr}_8\}$ and heterometallic $\{\text{MCr}_7\}$ are given in Figures 4.4 - 4.8. An obvious difference between $\{\text{Cr}_8\}$ and the heterometallic MCr_7 wheels is demonstrated by the fact that all of the discussed wheels have ground states with non-vanishing total spin. Therefore, for $\{\text{FeCr}_7\}$ (Fig. 4.5), $\{\text{ZnCr}_7\}$ (Fig. 4.6), $\{\text{CuCr}_7\}$ (Fig. 4.7), and $\{\text{NiCr}_7\}$ (Fig. 4.8) resonant relaxation occurs already at very low magnetic fields, which expresses itself in the pronounced maximum seen around $B = 0$ in Figs. 4.5 - 4.8. The second deviation

from the behavior of $\{Cr_8\}$ consists in pronounced differences of the maximum rates at higher Zeeman level crossings in the cases of $\{CuCr_7\}$ and $\{NiCr_7\}$ [98]. Within the employed framework and the assumed approximations the relaxation at the crossing between $S = 1$ and $S = 2$ in $\{CuCr_7\}$ (Fig. 4.7) appears to be rather small. The same is true for the relaxation at the crossing between $S = 5/2$ and $S = 7/2$ in $\{NiCr_7\}$ (Fig. 4.8).

Details about the NMR measurements of temperature dependence of the proton spin-lattice relaxation rate (T_1^{-1}) can be found in Refs. [116, 83]. The experimental data for T_1^{-1} versus temperature for different B are given in Figure 4.9. The general behavior found in AFM rings is that T_1^{-1} is approximately proportional to χ T, where χ is the magnetic susceptibility. However, a long-standing unexplained feature is that for a number of AFM rings T_1^{-1} shows a strong peak at temperature of the order of J/k_B. The peaks are superimposed with our calculation, using our formula (4.14) which has its origins from Moriya theory, sec. 4.1.2. The results are represented by solid curves in Figure 4.10. The coefficient A are determined when the data for diferent values of B are fitted separately, given in Table 4.1. It is noted that the parameter A varies and also ε, possibly due to the quality of our Hamiltonian where we neglected the anisotropy term. The interested reader is referred to Refs. [108, 109] for more discussing about temperature and field dependencies of T_1^{-1}.

4.6. Conclusion

To conclude, we have presented a theoretical description of the proton spin-lattice relaxation rate T_1^{-1} at low temperature and employed in molecular heterometallic $\{Cr_7M\}$ wheels where M = Fe, Ni, Cu, and Zn. In all rings the curves of T_1^{-1} vs applied magnetic field B are peaked at values close to the fields for which the thermodynamic steps were observed in the magnetization. This means that the level crossings and the nearly degenerate molecular levels of different rings are strongly coupled to the movement of nuclear spins. Furthermore, for $\{CuCr_7\}$ and $\{NiCr_7\}$ unexpectedly reduced proton spin-lattice relaxation rates T_1^{-1} occur at certain level crossings. Experimental confirmation to see whether this behavior could be experimentally verified or whether the additional anisotropic terms in the Hamiltonian [92, 93, 94, 29, 51] alter the picture completely would be very interesting for the validation of theoretical models. One of the main physical ingredients in this study has been the understanding from the beginning that due to the discrete character of the magnetic energy spectra and the phenomene of ground state degeneracy in molecular magnets, one needs to take into account the broadening effects of the interaction of the molecular levels and nuclear spins.

5. Magnetic properties of the new dodecanuclear $\{ Ni_{12} \}$

In the preceding chapters we have described the magnetic properties of molecular rings of heterometallic Cr_7M Wheels. In this study the new dodecanuclear $[Ni_{12}CO_3(OMe)_{12}(OAc)_9(\text{trans-tach})_6]$ cluster containing up to 370 atoms, Figure 5.1, will be investigated.
First, we establish the magnetic properties of these interacting spin systems using a theoretical description based on the Heisenberg model and, second, we present ESR spectroscopy measurements in this compound, in which we can estimate the g-value and the zero field splitting. This compound was recently presented by Geoffrey

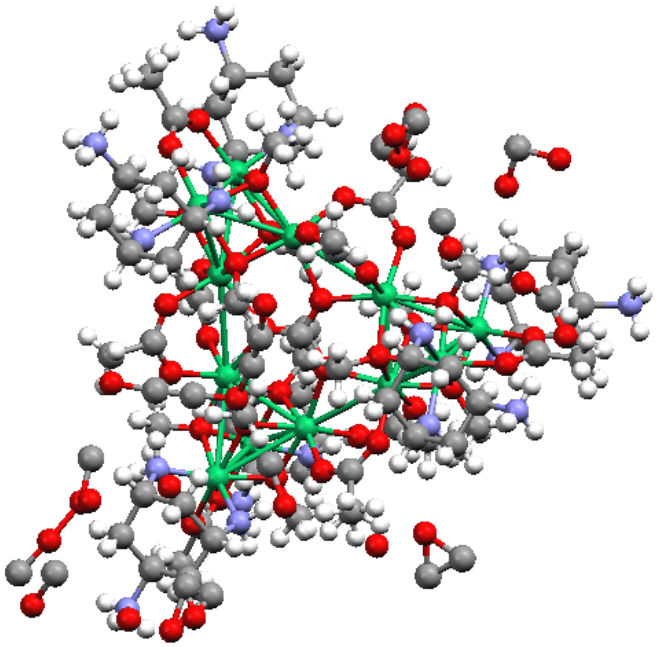

Figure 5.1.: Structure of $[Ni_{12}CO_3(OMe)_{12}(OAc)_9(\text{trans-tach})_6]$ molecular magnets, where: Ni^{+2}=green, O=red, N=light blue sticks, C=grey.

J. T. Cooper *et al.* (University of Glasgow, UK and Ames Laboratory, Iowa State University, USA). $\{Ni_{12}\}$ comprises a central CO_3^{2-} anion bridging three $\{M_4OMe_4\}$ cubanes [117], further linked by nine acetate anions and six trans-tach molecules. The nickel content in the crystalline materials was determined by Flam Atomic Absorption experiments which show that the mixed clusters contain the same ratio of metals as the starting reaction mixtures.

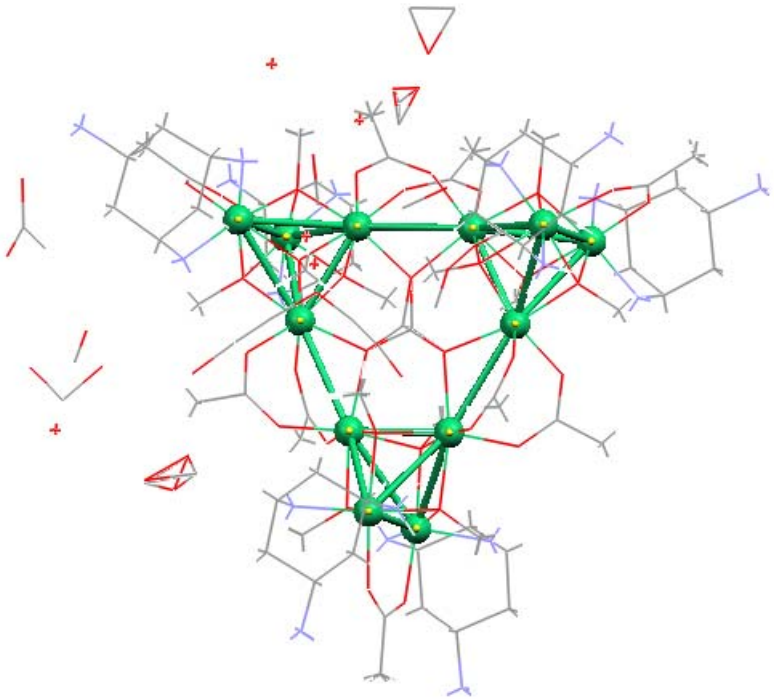

Figure 5.2.: Structure of $\{Ni_{12}\}$ molecular magnets. The 12 Ni ions with spin 1 are represented by large green spheres.

5.1. Theoretical model

The Hamiltonian of the $\{Ni_{12}\}$ spin system in the presence of a uniform external magnetic field B along the z-axis is given by

$$\underset{\sim}{H} = \sum_{u \neq v}^{N} J_{uv} \;\; \vec{S}(u) \cdot \vec{S}(v) + D \sum_{u}^{N} \underset{\sim}{S}_z^2(u) + g\mu_B B \sum_{u}^{N} \underset{\sim}{S}_z(u), \tag{5.1}$$

where the first term denotes the isotopic Heisenberg Hamiltonian in which J_{uv} is a symmetric matrix containing the exchange energy parameters between nearest neighbor spins at sites u and v. The matrix elements J_{uv} are positive for anitiferromagnetic interaction. The individual spin operators $\vec{S}(u)$ and $\vec{S}(v)$ are the 12 intrinsic spins with S =1 and they are given in units of $\hbar$. The second term describes the single-site anisotropic contribution. Due to the large size of the molecule, the anisotropic directions are simplified to be all equal to the z axis and the strength D is taking the same for all sites u. The third part is a Zeeman term which describes the interaction with the external magnetic field B and single spectroscopic splitting factor g. Neglecting the other directions of anisotropy axis and the strength D as well is taking the same for all sites. The Hamiltonian commutes with the square $\vec{S}^2$ and the z-component $\underset{\sim}{S}_z$ of the total spin. According to the symmetries existing in the molecule, we can only use the two symmetry operations represented in Figure 5.3, mirror symmetry in the tetrahedra and the rotational symmetry of the tetrahedra with $\pi/3$. The both operations are given by the symmetry operator $\underset{\sim}{T}$ being defined as

$$\begin{aligned} &\underset{\sim}{T}\,|\,m_1, m_2, m_3, m_4, m_5, m_6, m_7, m_8, m_9, m_{10}, m_{11}, m_{12}\,\rangle \\ &= |\,m_9, m_{10}, m_{11}, m_{12}, m_1, m_3, m_2, m_4, m_5, m_6, m_7, m_8\,\rangle. \end{aligned} \tag{5.2}$$

The common eigenstates for the operator $\underset{\sim}{H}$ are shifted into another. The symmetry operations there are repeated 6 times, until we have arrive at the eigenvalue equations. Then the complete Hilbert space can be decomposed into mutually orthogonal subspaces, where all energy eigenvalues and eigenvectors can be computed.

5.2. Energy spectrum of Ni_{12}

We have used different exchange parameters, a ferromagnetic one in the tetrahedra and an anti-ferromagnetic one between them, Figure 5.3. Note that the operator $\underset{\sim}{\mathcal{H}}$ is defined on a Hilbert space of dimension $3^{12} = 531441$.
We have evaluated the complete energy spectrum for the physical system Ni_{12} using numerical exact diagonalisation. The low-energy part of the spectra with and without anisotropy, are represented in Figure 5.4. Our calculations indicates that the ground state has a spin $S = 0$ without anisotropy ($D = 0$), and show degenerate ground state with spin $S = 2$ in the present of anisotropy ($D/k_B = -2.75K$).

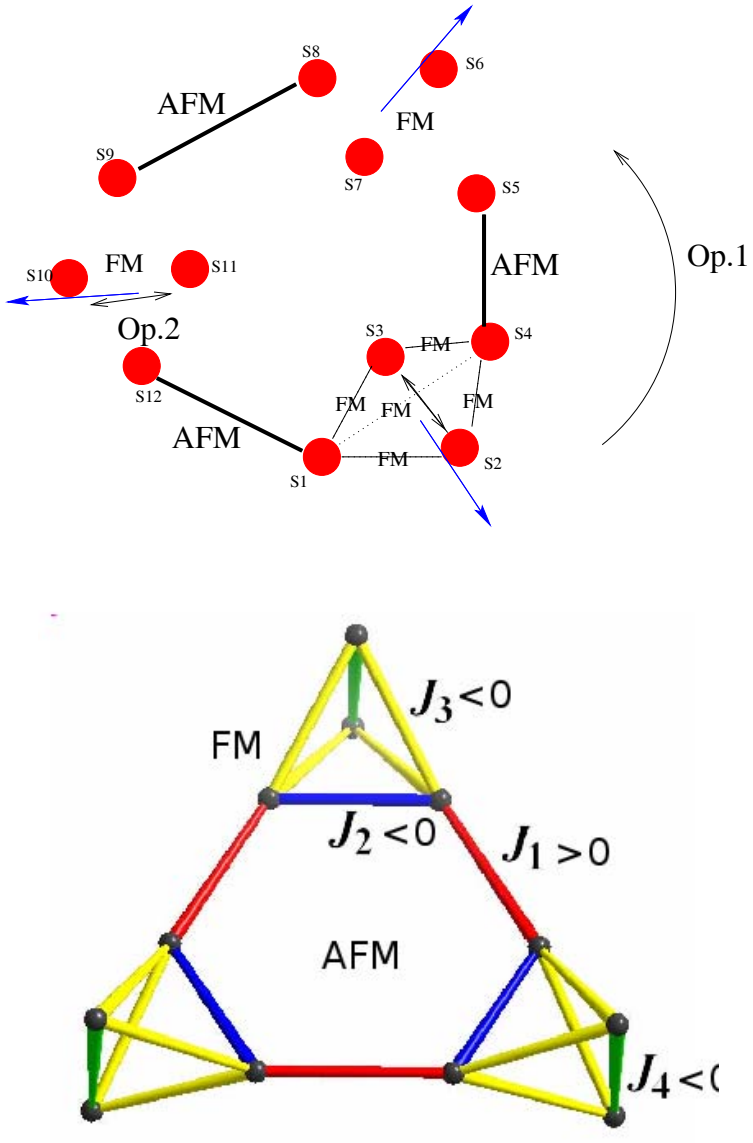

Figure 5.3.: Schematic representation of the symmetry operations and the exchange couplings used in our calculation for the molecular magnet {Ni_{12}}. Op.1: rotation of the tetrahedra by $\pi/3$ and Op.2: mirror symmetry inside. Assignement of the exchange parameters J_{1-4} to the Ni_{12} spin system: J_1: red, J_2 blue, J_3 yellow, and J_4 green.

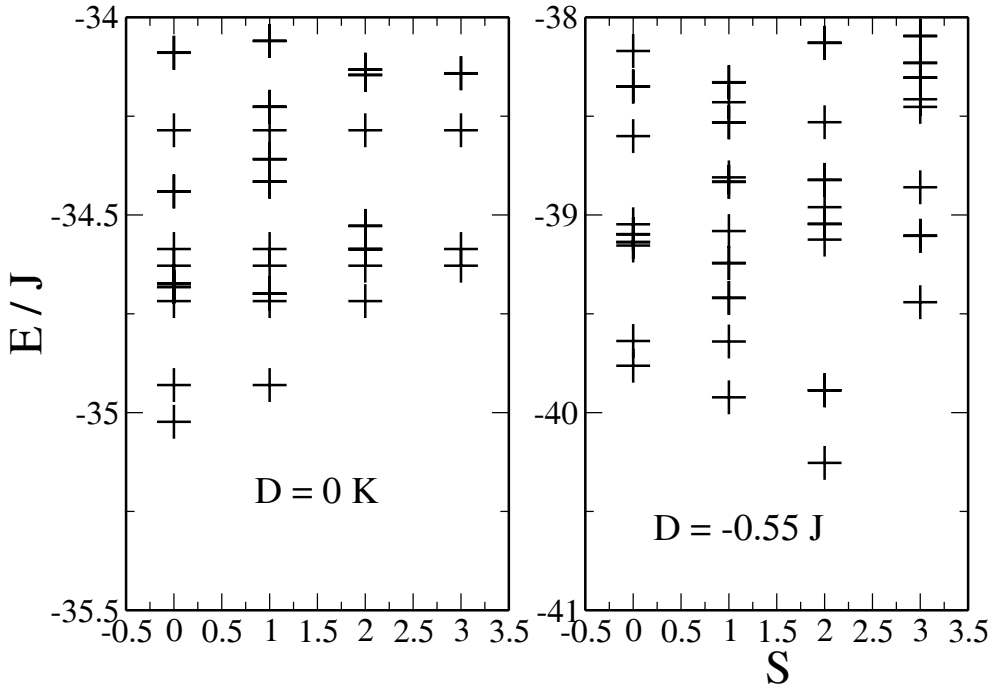

Figure 5.4.: The low part of energy spectrum for the magnetic molecular $\{Ni_{12}\}$. Using the interaction ($J_1 = 1.8J$, $J_2 = J$, $J_3 = 0.21J$, and $J_4 = 1.6J$) described in Figure 5.3: $D = 0$ (l.h.s) and $D = -0.55J$ with $J/k_B = 5K$ (r.h.s)

5.3. Temperature dependence of low field susceptibility in Ni_{12}

Low-field magnetic susceptibility data of $\{Ni_{12}\}$ in the range 2 - 290 K are dominated by antiferromagnetic intramolecular exchange, both antiferromagnetic and ferromagnetic exchange is observed, resulting in a maximum of T χ at 27 K, see Figure 5.6. In order to compare with the measured susceptibility we have used the equation (2.36).

In Figure 5.5 experimental data (diamonds) is shown for the temperature dependence of the magnetic susceptibility in the range below 70 K. With the Hamiltonian model Eq. (5.1) we have been able to determine a set of four exchange constants that give rise to results for the temperature-dependent susceptibility in quite good agreement with experimental results (see Figure 5.5): J_1, between adjacent Ni positions of neighboring Ni_4O_4 tetrahedra (inter-tetrahedra, mediated by the carbonate and two acetate bridges), J_2, between the two inner-face Ni positions (two

oxo and one carbonato bridges); J_3, between inner-face and outer-face Ni positions (one oxo and one methoxo bridge per Ni-Ni contact); J_4, between the two outer-face Ni centers (two methoxo bridges). The best theoretical fit between the cal-

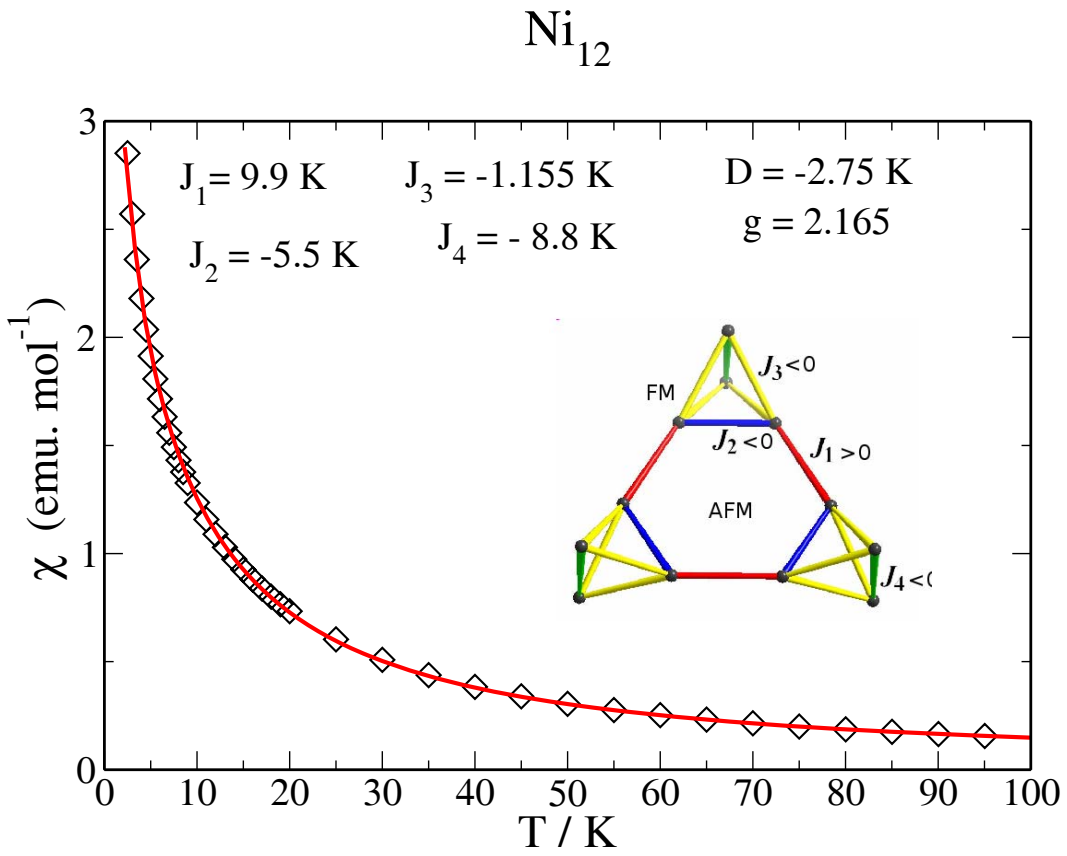

Figure 5.5.: Variation of $\mathcal{M}/B$ as a function of temperature T for {Ni_{12}}: The experimental data are given by black squares. The theoretical fit is depicted by red solid curve for $g = 2.165$, with $J_1/k_B = 9.9$ K, $J_2/k_B = -5.5$ K$J_3/k_B = -1.1155$ K, $J_4/k_B = -8.8$ K; $D/k_B = -2.75$ K and $B = 0.1$ T.

culated and measured susceptibility χ for the temperature range below 100 K is depicted by red solid curve within a Heisenberg model that adopts the numerical values of the four exchange constants J_{1-4}, resulted for the antiferromagnetic inter-tetrahedras ($J_1/k_B = 9.9$ K) and ferromagnetic intra-tetrahedras with strong variations of the individual exchange energies, reflecting ferro/antiferromagnetic composition between the involved exchange pathways, this leads to the following parameters ($J_2/k_B = -5.5$ K, $J_3/k_B = -1.1155$ K, and $J_4/k_B = -8.8$ K), $D/k_B = -2.75$ K and g = 2.165. It should be noted that Larry Engelhardt and Marshall Luban find

the following parameters ($J_1/k_B = 17.5$ K, $J_2/k_B = -9.5$ K, $J_3/k_B = -1.9$ K, and $J_4/k_B = -22$ K) by means of Quantum Monte Carlo [118].

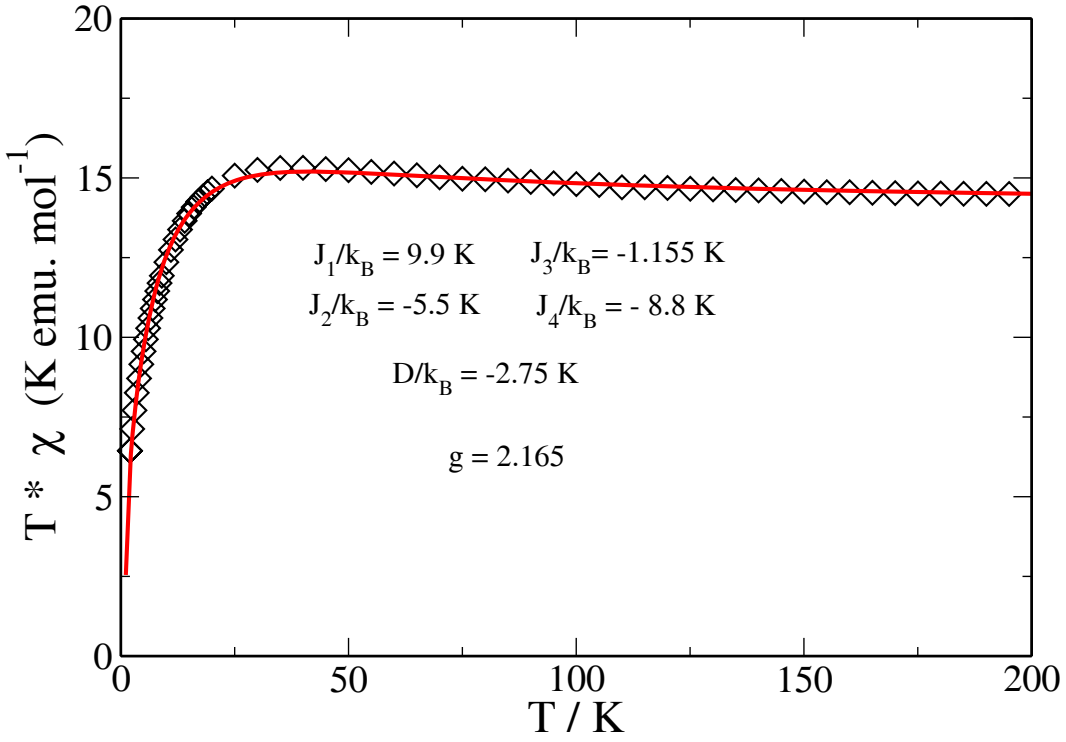

Figure 5.6.: Variation of $T\mathcal{M}/B$ as a function of temperature T for $\{Ni_{12}\}$: The experimental data are given by black squares. The theoretical fit is depicted by a solid curve for $J_1 = 9.9$ K, $J_2 = -5.5$ K$J_3 = -1.1155$ K, $J_4 = -8.8$ K; $D = -2.75$ K; $B = 0.1$ T and $g = 2.165$.

5.4. Magnetization vs magnetic field in Ni_{12}

After determining the exchange parameters fitting the low-field magnetic susceptibility we used the numerical calculation for the Hamiltonian so as to provide the full set of energy levels of Eq. (5.1). We find that in the absent of a magnetic field the ground state is degenerate and has a spin of $S = 2$ with anisotropy $D/k_B = -2.75K$, and the energy gap to the first excited state ($S = 1$) is 1.65 k_B K. We suppose now that T is maintained constant and we study the Zeeman splitting of energy levels as B is increased.

The hight field magnetization for powder sample {Ni_{12}} has been independently measured in pulsed magnetic field by Paul Kögerler (Ames University) as well as at the facility of the High Magnetic Field Laboratory (OHMFL) by Hiroyuki Nojiri (Tohoku University). The results of these two measurements are different, which is due probably to the quality of the powder sample used.

In Figure 5.7 we show magnetization as a function of applied external magnetic

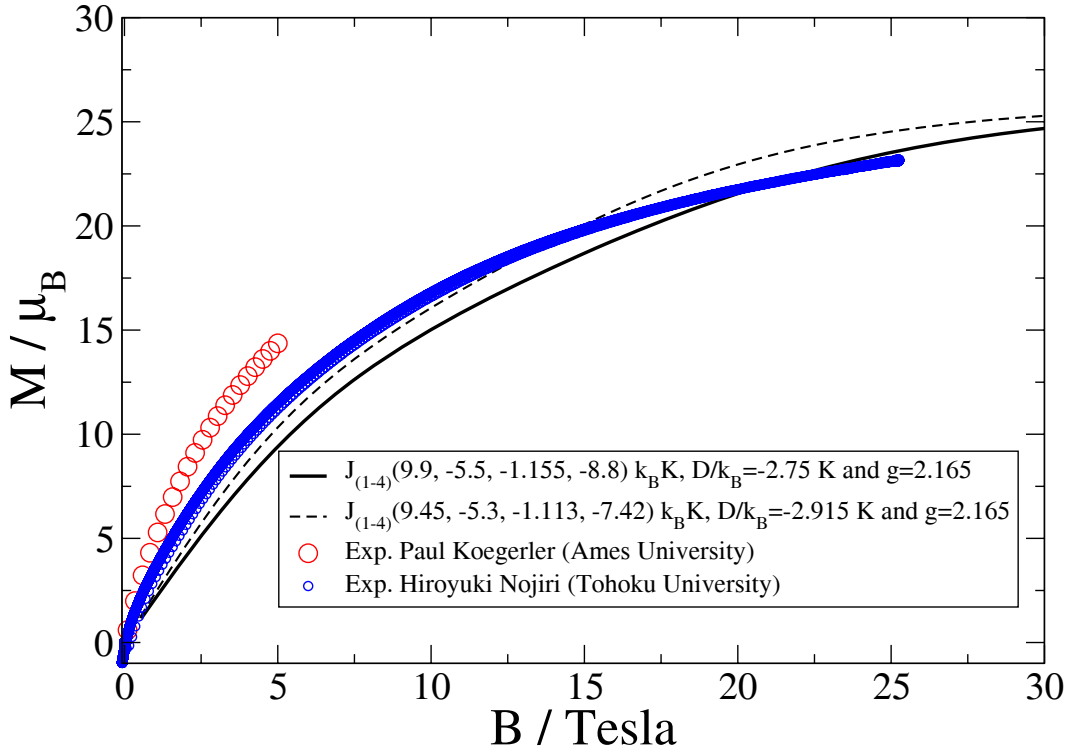

Figure 5.7.: Variation of magnetization as a function of applied magnetic field B for {Ni_{12}}: The experimental datas are given by the red and the blue colors. The theoretical fits are depicted by the solid curves.

field. The measurements which were performed at T =2 K are represented by blue squares (Tohoku University) and red circle (Ames University), the solid line corresponds to Eq. (2.33). We find that our fit is close to the measurement of Hiroyuki Nojiri (Tohoku University). Note that we were able to reproduce low field properties, Figure 5.6 using a simple Heisenberg Hamiltonian Eq. (5.1) but to get better fit for magnetization and understand the hight field properties, we suggest to use more elaborate models using anisotropy and include field-dependent parameters [8].

5.5. ESR measurements in $\{Ni_{12}\}$

A detailed analysis of the ESR measurement, using pulsed magnetic fields up to 30 T, was performed by the group of H. Nojiri, in the Institute for Material Research, Tohoku University (Japan). Far-infrared (FIR) radiation with frequency range of 95 - 381.5 GHz are supplied by an optically pumped FIR laser, Gunn oscillators and backward traveling wave tubes.

The results of the temperature dependence of the ESR spectra at 190 GHz are plotted in Figure 5.9. The signal shows a typical Lorentzian line shape. In Figure 5.8 we represent the radiation dependence of ESR spectra at T=1.5 T. Figure 5.10 shows the dependences of the observed ESR resonance frequencies Sub (circles) and Main (squares) on the magnetic field.

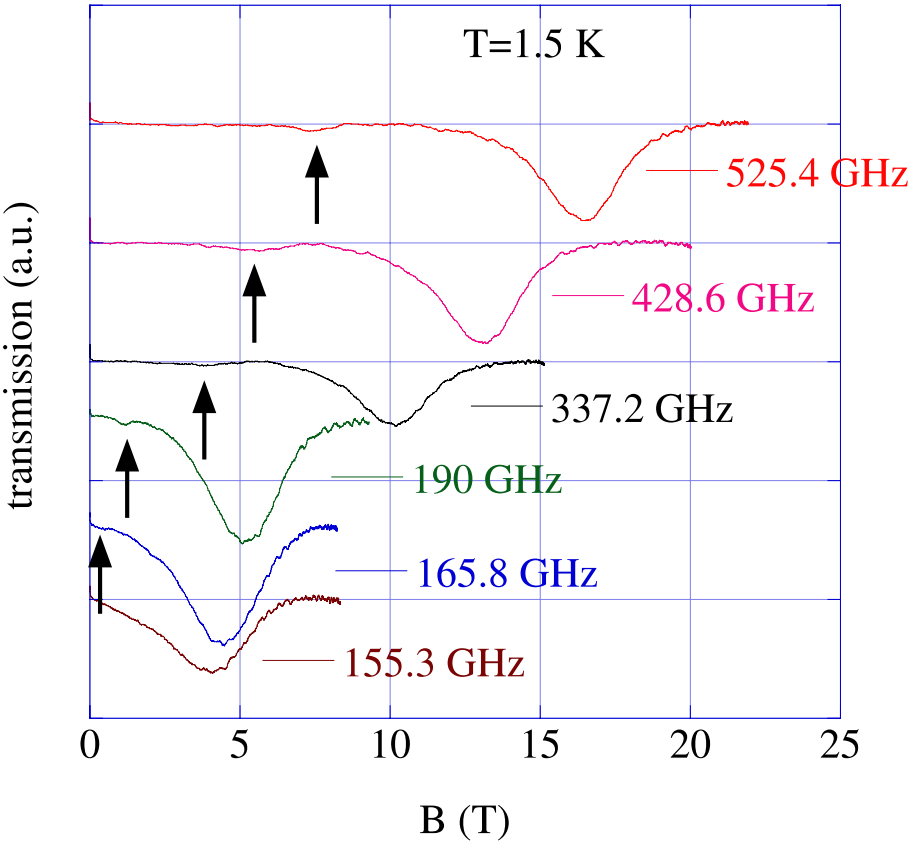

Figure 5.8.: Frequency dependence in EPR measurement.

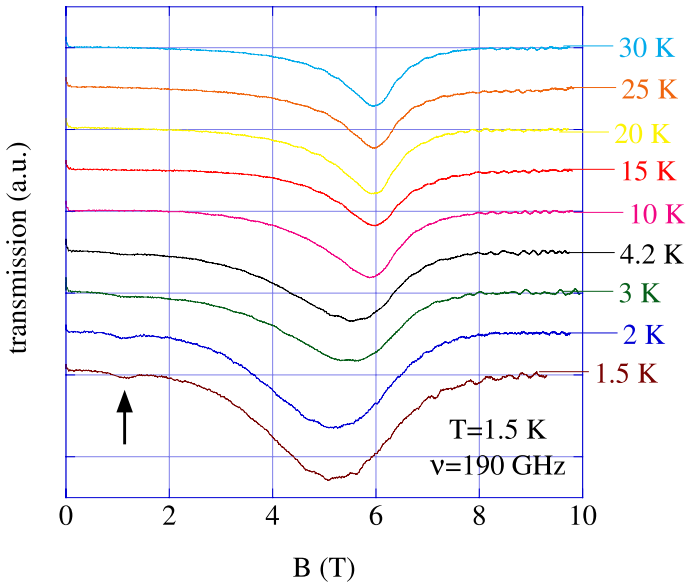

Figure 5.9.: Temperature dependence

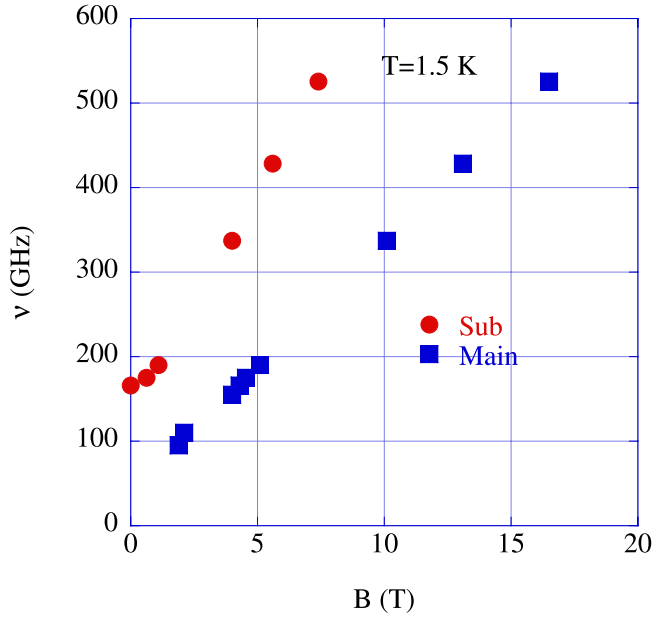

Figure 5.10.: The figure shows the dependence of the observed EPR resonance frequencies with magnetic field B, where Main (blue squares), correspond to Δ S_z =1 and the Sub (red circles) to Δ S_z =2.

We note that in figure 5.10 two different slopes can be assigned to the data, one corresponding to Δ M =1 (blue squares) and the (red circles) to Δ M =2. These dependencies can be explained by looking at the Zeeman level scheme of the simple Heisenberg model as it is represented in Fig. 5.11. The g-value can be easily deduced from the slope of the curves and gives a value around 2.2.

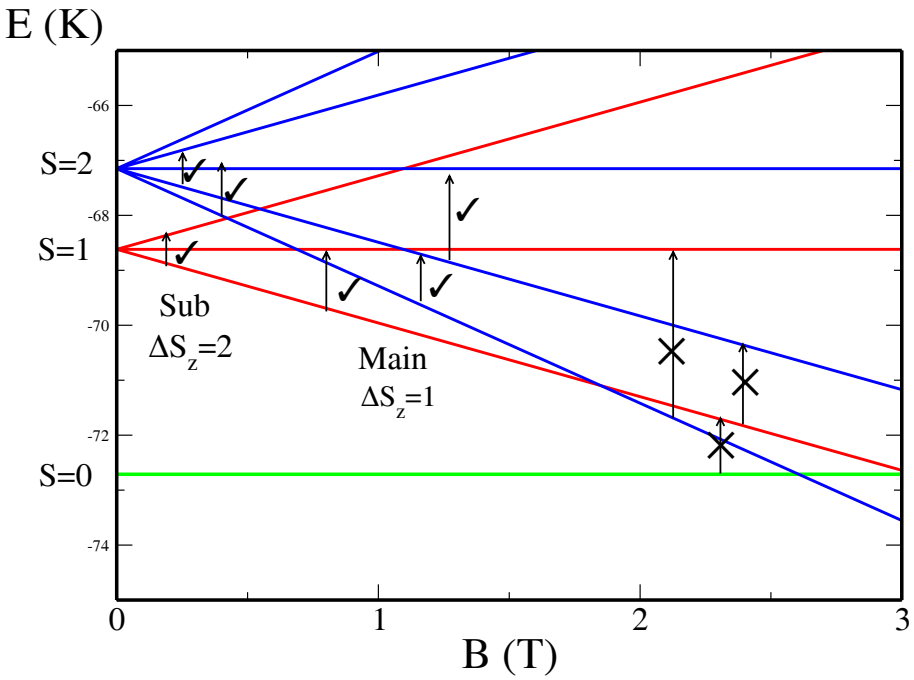

Figure 5.11.: The figure shows schematically the Zeeman level splittings in the Heisenberg model together with the assignments of allowed transitions for Δ S_z =1 (Main) and the Δ S_z =2 (Sub).

5.6. Results and Discussions

This chapter has two purposes. First, we have demonstrated that a treatment of the Heisenberg model on a Ni_{12} cluster leads to results in agreement with the measured magnetic susceptibility. Both antiferromagnetic and ferromagnetic exchange interactions are observed, ferro-interaction in the tetrahedra and an anti-ferromagnetic one between them. As discussed in Sec. 5.3, we have fitted the computed results to the experimental data by adjusting the exchange interaction J_{ij} (i$\neq$j), such that the computed susceptibility agrees with the experiment. The best fit reproduced using four exchange parameters $J_1/k_B = 9.9$ K, $J_2/k_B = -5.5$ K, $J_3/k_B = -1.1155$ K,

$J_4/k_B = -8.8$ K, $D/k_B = -2.915$ K, and $g = 2.165$ according to the Figure 5.3. The results of our exchange parameters describe well low field susceptibility, it fails to reproduce the high-field magnetization, Figure 5.7, which is due probably to the quality of our Hamiltonian using simple anisotropy D parallel to the easy axis z.

The second purpose of this chapter is to explain ESR spectroscopy in Ni_{12}, which is a very helpful method and provides more precise data even on the molecular orbital of the unpaired electron. The results of ESR measurements in the compound Ni_{12} show a movement of the peak in the 190 GHz, Figure 5.9. At low temperatures T, only a few levels contribute, therefore the influence of anisotropy is large. At high T, very many levels contribute in the compound and the anisotropic contributions average out, Figure 5.10. In Figure 5.9 the slope of the curves shows a value of g around 2.25 is quite reasonable and the zero-field splitting 2.4 K. It should be mentioned that this value is very large for this compound, because the gap between the ground state and the first exated state is about 1.65 K, and the pentuplet is 2.45 K. Usually g is isotropic for Ni, and then we must take into account the other anisotropy axis in our model. But since the total dimension of Hilbert space is 531441 levels, therefore we could not do calculation including different directions of anisotropy parameter terms. It should be noted that, due to some ferromagnetic interactions in the three tetrahedra of the compound, we have basically no low-lying gaps and the levels are very dense. Therefore, this reason why the magnetization curve is featureless, Figure 5.7. To clarify this phenomenon, futher work is needed.

5.7. Conclusion

In conclusion, we have studied in detail the magnetic interactions in the $\{Ni_{12}\}$ cluster, which shows ferromagnetic interaction in the tetrahedra and a anti-ferromagnetic one between them. We have provided a comprehensive description of the magnetic susceptibility and the high-field magnetization. We have presented ESR spectroscopy measurements in $\{Ni_{12}\}$, which gives an estimation for a g-value around 2.2 K and zero field splitting around 2.4 K, which we are not able to describe only with anisotropic contribution with directions simplified to be all equal to the z axis.

6. Wheel-shaped tungstophosphate $[Cu_{20}Cl(OH)_{24}(H_2O)_{12}(P_8W_{48}O_{184})]^{25-}$ ($Cu_{20}P_8W_{48}$)

This study reports and examines the magnetic properties of the new large wheel-shaped tangstophosphate $[Cu_{20}Cl(OH)_{24}(H_2O)_{12}(P_8W_{48}O_{184})]^{25-}$ ($Cu_{20}P_8W_{48}$), Figure 6.1, in short Cu_{20} which was recently synthesized [119]. This study has been undertaken because studies of the magnetic exchange in simple polynuclear paramagnetic clusters are a topic of current focus in magnetochemistry [120]. The solid solution like structure of Cu_{20} allows studies of catalysis, ion exchange, gas storage, and medicine.

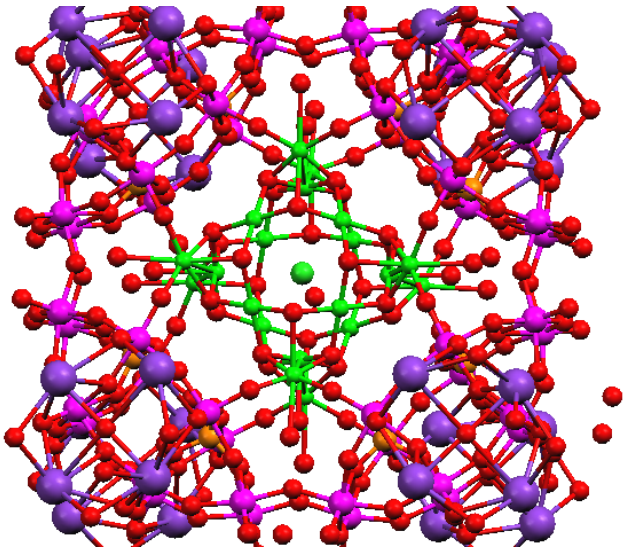

Figure 6.1.: Structure of $[Cu_{20}Cl(OH)_{24}(H_2O)_{12}(P_8W_{48}O_{184})]^{25-}$ ($Cu_{20}P_8W_{48}$) molecular magnets. Where: Cu^{+2}=20 small green, O=red, Cl=violet, P=yellow, W=bright vilet.

The electrochemical characterization and electrocatalytic properties of this system was investigated by Cyclic Voltammetry (CV) and Controlled Potential Coulometry

(CPC) in pH 0 and pH 5 media [121]. They found that in both media the cyclic voltammograms are dominated by the current intensities of processes attributed to the reduction of Cu^{2+} centers. Controlled potential coulometry indicates that all the Cu^{2+} centers within the supramolecular complex remain electroactive.

The model we adopt for describing the magnetic properties of the molecule cluster Cu_{20} is the Heisenberg spin Hamiltonian together with a Zeeman term of an applied magnetic field along the z-axis given by

$$\underset{\sim}{H} = \sum_{u \neq v}^{N} J_{uv} \ \vec{S}(u) \cdot \vec{S}(v) + g\mu_B B \sum_{u}^{N} \underset{\sim}{S}_z(u), \tag{6.1}$$

where the individual spin operators are those for intrinsic spin $S = 1/2$ given in units of $\hbar$, and g is the spectroscopic splitting factor.

Due to the complexity of this system with a very large size of the molecule and

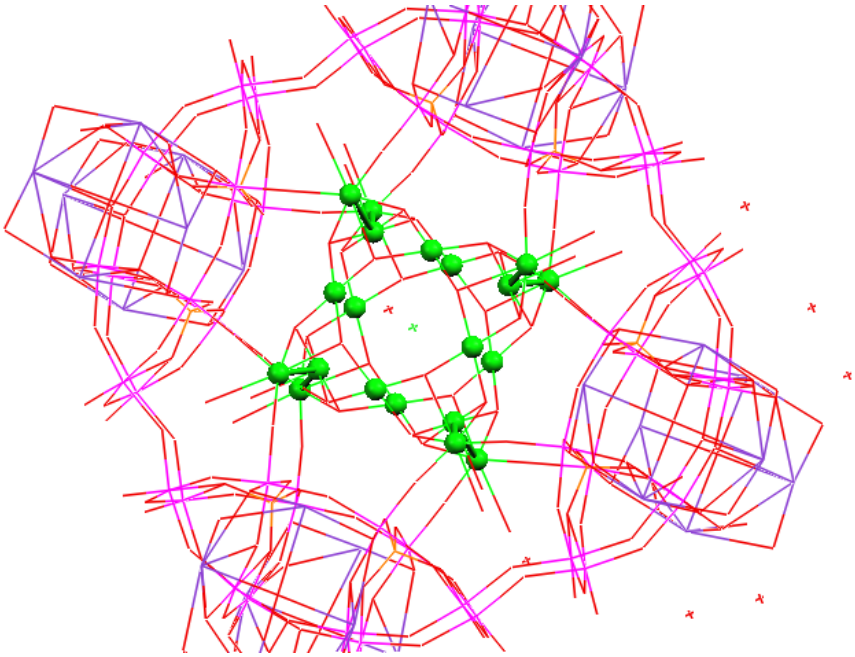

Figure 6.2.: Structure of $\{Cu_{20}\}$ molecular magnets.

consequently also of the related Hilbert space with dimension of 2^{20}, we approximate the spin system by a smaller one. Then, using numerically exact diagonalization of the Heisenberg model, we calculate the energy spectrum for various possible couplings, and compare our findings to the available low-field susceptibility data as well as to high-field magnetization measurements.

6.1. Approximation with single spin 1/2 impurity

The deliberate use of substitutional impurities in the compounds has been a topic of great interest because of their a valuable tool for controlled studies [122, 123, 124]. Doping of nommagnetic Zn ions in antiferromagnetic CuO_2 planes is known to lead to a surprisingly large reduction of T_c (T_c orthorhombic-to-tetragonal structural transition) [124] and induces local strangered magnetic moments around the impurity sites [123]. It has now become quite standard to analyze the local magnetic moments around static magnetic and nonmagnetic impurities in an aniferromagnetic background for deeper understanding of the correlated states [125, 126].
The low-temperature thermodynamics low-field susceptibility exhibits a Curie-like behaviour ($\chi \propto \frac{1}{T}$), which suggests a non-negligible impurity contribution [127].

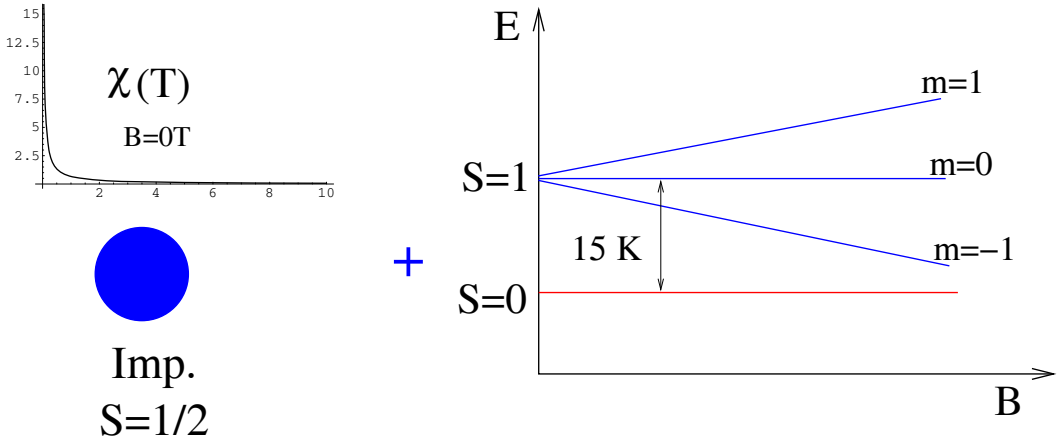

Figure 6.3.: single spin 1/2 impurity plus one singlet-triplet gap of 15K.

Eventually, we have approximated the system $\{Cu_{20}\}$ with a single spin 1/2 impurity plus one singlet-triplet gap of 15K. Figure 6.4 shows an excellent agreement between theory and experiment for the applied magnetic field dependence of the magnetization.
For the temperature dependence of the low-field susceptibility, we were not able to reproduce the fit so well because higher-lying levels are missing, Figure 6.5.

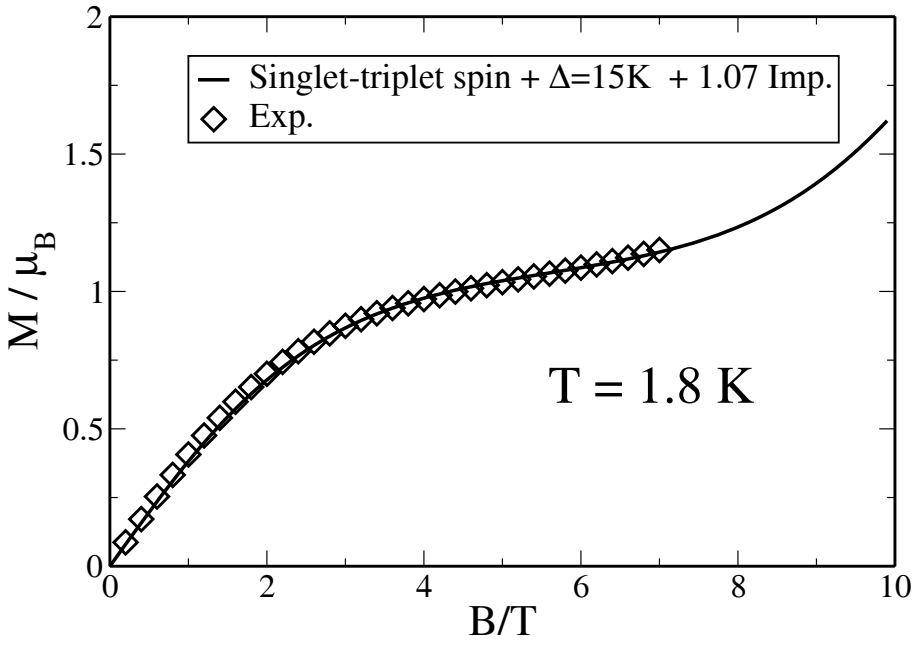

Figure 6.4.: Magnetization vs applied magnetic field B for $\{Cu_{20}\}$.

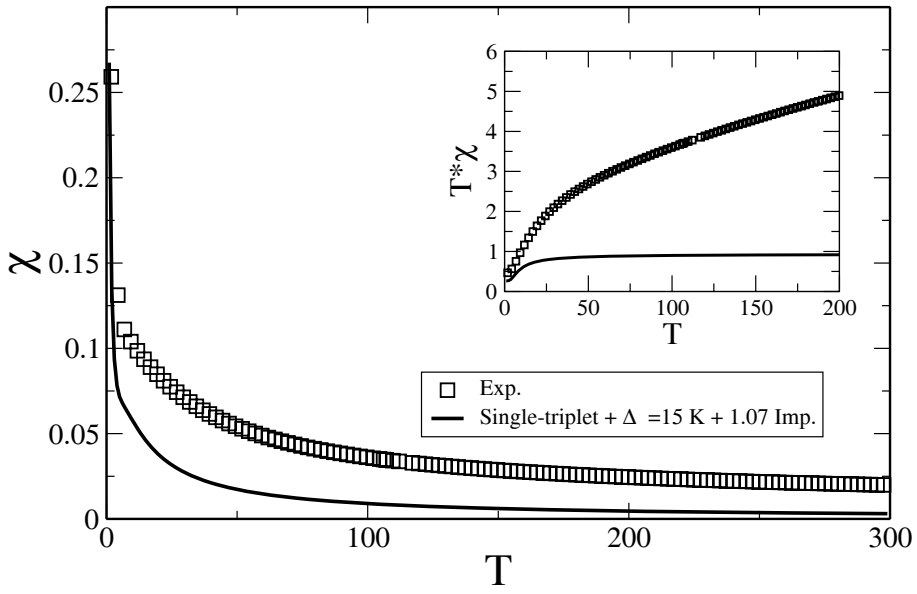

Figure 6.5.: low-field susceptibility vs. temperature.

6.2. Approximations with 4 spins 3/2 and 8 spins Cu 1/2

The distance between the 3 Cu ions in the triads is only 2.81 Å. We assume that they interact strongly and can be treated as one effective spin. We suppose that the three spins would survive magnetic only if all Cu ions of the triads couple ferromagnetically, which we can approximate with one spin $S = 3/2$. From this, we can easily model the system with 4 spins 3/2 and eight central "cage" Cu ions, as shown in Figure 6.6. The operator $\underset{\sim}{H}$ corresponding to this approximation is defined on a Hilbert space of dimension 4^4 x $2^8 = 65536$. Using the numerical exact diagonalization method, we have been able to estimate the numerical values of the two exchange constants ($J_1 = 20$ K and $J_2 = 15$ K) which provide a reasonable temperature-dependent susceptibility in good agreement with the experimental results, Figure 6.7.

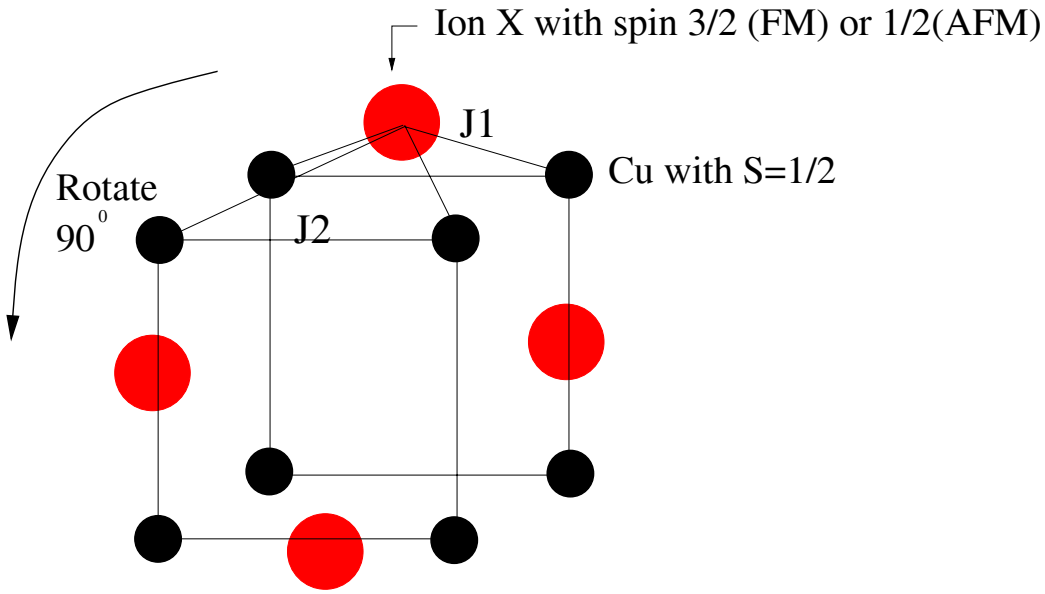

Figure 6.6.: Schematic representation of symmetry operation (rotation of the X ion by $\pi/4$) and the exchange coupling used in our calculation for molecular magnetic $\{Cu_{20}\}$

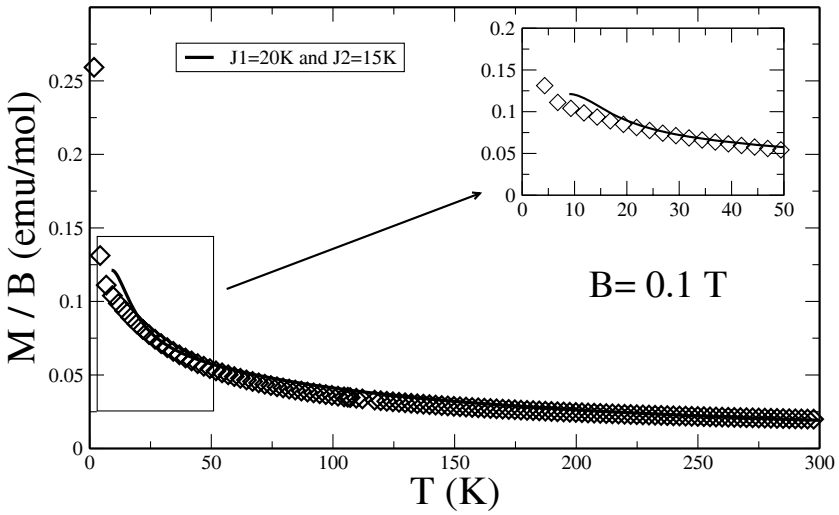

Figure 6.7.: Variation of $\mathcal{M}/B$ as a function of temperature T for $\{Ni_{12}\}$: The experimental data are given by black squares. The theoretical fits are depicted by solid curve for AFM interactions: $J_1 = 20$ K and $J_2 = 15$ K black solid curve, $B = 0.1$ T and $g = 2$.

6.3. Symmetry of Cu_{20} with 20 spins 1/2

We idealize the structure as 20 Cu ions which are situated at the vertices of regular triads and squares, Figure 6.8. The ion spins interact with each other via an istropic Heisenberg exchange and with a uniform external magnetic field B whose direction defines the z axis, Eq. (6.1), which yield the operator $\underset{\sim}{H}$ defined on the Hilbert space of dimension 2^{20} =1048576.

We suppose that the triads interact with the cage just with one spin Fig. 6.8, which mean that we can used symmetry of the 2 other spins around the interacted one. According to this approximation and the symmetries existing in the molecule, we can use only two symmetry operations represented in Figure 6.8: mirror symmetry in the triads and rotational symmetry of the triads by π /4. Fortunately, we may finally decompose the complete Hilbert space into the mutually orthogonal subspaces, where all energy eigenvalues and eigenvectors can be computed, using complex*16 numbers requiring 9 GB RAM.

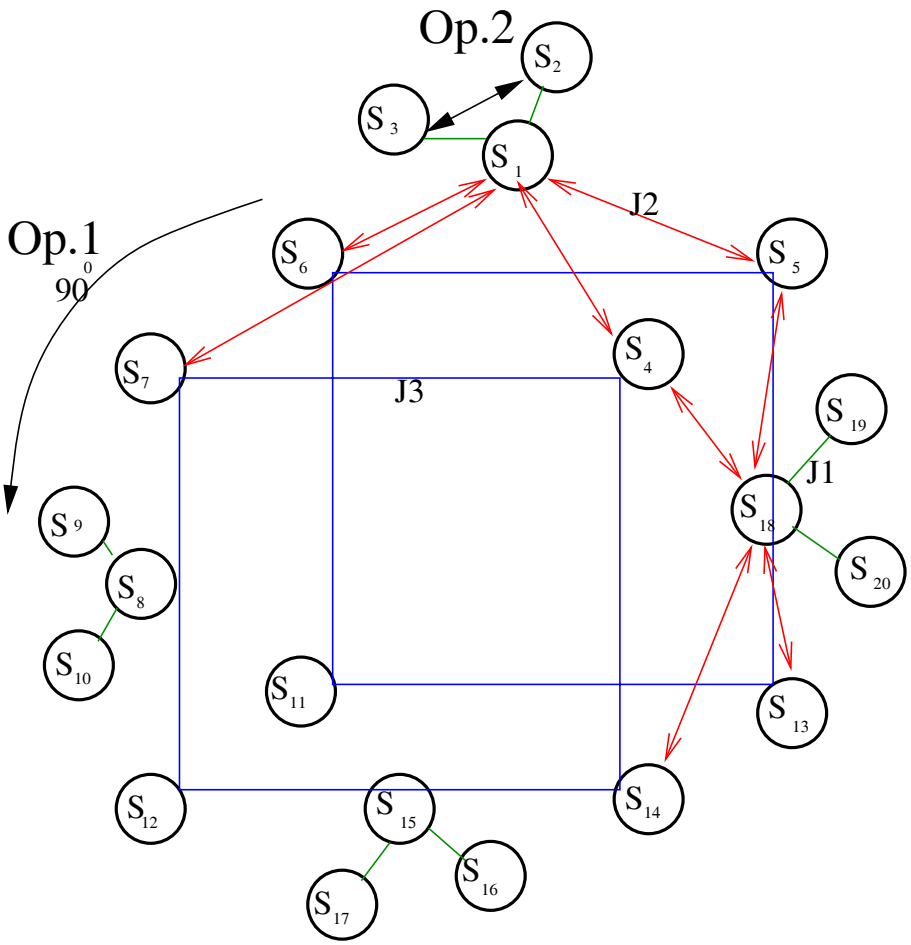

Figure 6.8.: Schematic representation of symmetry operations and the exchange coupling used in our calculation for a molecular magnetic $\{Cu_{20}\}$ with 20 spins 1/2. Op.1: rotation of the triads by $\pi/4$ and Op.2: mirror symmetry inside. The exchange parameters used: J_1: green, J_2 red, and J_3 blue.

6.4. Conclusion

In this work we have investigated the magnetic properties of $Cu_{20}P_8W_{48}$. Due to the very large size of the molecule, we have approximated the spin system by a smaller one. First with single spin 1/2 impurity plus one singlet-triplet system with a gap of 15 K. Second, we have approximated with 4 spins $3/2 + 8$ spin 1/2 where we found that the best fit is ferromagnetic interaction in the triads which are antiferromagnetic to the eight central "cage" Cu and antiferromagnetic inside of the cage.

7. Summary and conclusion

Molecular magnetic clusters are a fundamental interest, which offer the prospect of new applications and also allow to test basic theories of magnetism. In this work we have simply presented a few examples, in which we have investigated there magnetic properties: Wheel-shaped tungstophosphate $[Cu_{20}Cl(OH)_{24}(H_2O)_{12}(P_8W_{48}O_{184})]^{25-}$ ($Cu_{20}P_8W_{48}$) , dodecanuclear cluster $[Ni_{12}CO_3(OMe)_{12}(OAc)_9(\text{trans-tach})_6]$, and the heterometallic $\{Cr_7M\}$ wheels, in which one of the Cr^{III} ions of Cr_8 has been replaced by an ion M (M $\equiv$ Fe, Cu, Zn, Ni, ion) with this extra-spin acting as local probe for the spin dynamics. Such systems have been synthesized recently and they are well described using the Heisenberg spin Hamiltonian with a Zeeman term of an applied magnetic field along the z-axis. Using the numerical exact diagonalization method, we have calculated the energy spectrum and the eigenstates for different compounds, and we have used them to study the magnetic properties and thermodynamic properties such as magnetization and susceptibility.

First, we have presented the concept of the theoretical modeling method for calculating in detail the magnetic properties described by the Heisenberg model of interacting spins. We have provided a comprehensive description of the magnetic susceptibility and reexamined the available experimental data [29] and presented the exchange parameters of molecular magnetic rings of heterometallic $\{Cr_7M\}$. In order to study these different systems we have used a mirror symmetry operation around the doping ion M, we have evaluated the different energy spectra and used these energy eigenvalues to adjust the curves of $T * M/B$ and M/B versus T, with the experiment ally measured data. The data of different rings were well fitted using two exchange parameters. Our key results are that the magnetic ground state depends highly on the value of the extra spin quantum number M and in the case of $\{FeCr_7\}$ the iron-chromium exchange is different from the chromium-chromium exchange in contrast to the other cases. A detailed analysis of the magnetic propertis in dodecanuclear $\{Ni_12\}$ shows that both antiferromagnetic and ferromagnetic exchange interactions contribute, ferro-interaction in the tetrahedra and a anti-ferro. one between them. However, we have provided a description of the magnetic susceptibility and the high-field magnetization. For wheel-shaped tungstophosphate $\{Cu_{20}\}$, due to the complexity of this system with a very large size of the Hilbert space with a dimension of 2^{20}, we have approximated the spin system by a smaller one. Then, using numerically exact diagonalization of the Heisenberg model, we have calculated the energy spectrum for various possible couplings, and compared our findings to the available low-field susceptibility data as well as to high-field magnetization measure-

ments.

The spin dynamics of the heterometallic $\{Cr_7M\}$ has been characterized through the proton spin lattice relaxation rate, T_1^{-1}. A detailed of a theoretical account of what the proton spin-lattice relaxation rate T_1^{-1} probes in magnetic molecule systems has been performed, via general arguments based on Monriya's theory. We have defined the quantity T_1^{-1} as the various spectral functions of the magnetic molecule evaluated at the nuclear Larmor frequency ω_L, and investigated this quantity as a function of the applied magnetic field at low temperature regimes, as well as a function of temperature at low field in molecular $\{Cr_8\}$, heterometallic $\{Cr_7M\}$ wheels, and we have explained accordingly the above findings.

Indeed, in all rings the curves of T_1^{-1} vs the applied magnetic field B for low temperatures shows a strong enhancement at values close to the fields where the steps were observed in the magnetization at low temperature which correspond also to the resonant relaxation. This means that the level crossing and the nearly degenerate molecular levels of different rings are strongly coupled to the movement of nuclear spins. However, it appears that $\{CuCr_7\}$ and $\{NiCr_7\}$ show an unexpectedly reduced relaxation rate occuring at certain level crossings, which would be very interesting and helpful to see whether this behavior could be experimentally verified or whether the additional anisotropic terms in the Hamiltonian [92, 93, 94, 29, 51] alter the picture completely. For the temperature dependence of T_1^{-1}, we have reproduced just the low temperature part of the experiment results in $\{Cr_8\}$. Note that we were not able to reproduce the high temperature part and that for the reason of time calculation, where we was limited to the lowest part of the spectrum and just for the five lowest subspaces of spin quantum number S, we neglected dependencies of ε on B or T in the equation (4.14). Netherless, there are still open theoretical questions comparing to the experimental evidence of T_1^{-1}. For example, the difference that seems to exist between molecules with spins $S = 1/2$ and molecules with $S > 1/2$, and the temperature dependence of frequency ω [108], in which the spin-phonon interaction seem to play role. What mediates the dynamics in resonant tunneling of magnetization? What determines the magnetic reorientation barrier?.

The most remarkable conclusion of the present work is that our model for proton T_1^{-1} based on Moriya's theory, describes well the behaviors of T_1^{-1} vs applied magnetic field B which are peaked at certain level crossings for all different heterometallic rings, and we find a good agreement between our theoretical data with the experiment for the temperature dependence. Future work will focus on studying dynamical effects of quantum mechanical in the vicinity of the level crossing and to compare our approach with the topological theory of reference [108], in which they employed a number of simple symmetry arguments and considering several specific cases, including the spin-phonon interactions, and geometrical coefficients about the

distances and the various angles of the protons with respect to the electronic spin sites.

The next few years are certain to see an increased effort in the direction of magnetic molecular clusters, the hope of course is that magnetic structures can be designed according to the desired magnetic properties. A particularity important issue is to find well characterized compounds for which one could obtain precise information on both the ground state and the excited states of a strongly coupled paramagnetic system. This goal is not close at all, it requires further understanding of the interplay of magneto-chemistry and magnetic phenomena, which can be clarify with Density Functional Theory (DFT) or other ab-initio methods [128, 129, 130, 131, 132], in which the ground state energy of many electron system depends only on a electronic density.

A. Basic of Feynman thermodynamic path-integral

This appendix gives a brief general review of the basic theory of path-integral used in quantum Monte Carlo. The path-integral method allow for simulations at non-zero temperatures, without the necessity for considering individual excited states and without construction of trial wave functions. The Static and dynamical properties of a quantum system in thermal equilibrium are obtainable from the thermal density matrix $\mathrm{e}^{-\beta \underset{\sim}{H}}$, chapter 2. The expectation value of an operator $\underset{\sim}{A}$,

$$< \underset{\sim}{A} > = \frac{1}{Z} \mathrm{Tr} \left\{ \underset{\sim}{A} \rho(\vec{r}, \vec{r}^{\,\prime}; \beta) \right\} \tag{A.1}$$

where $\rho(\vec{r}, \vec{r}^{\,\prime}; \beta)$ is the position-space density matrix given

$$\rho(\vec{r}, \vec{r}^{\,\prime}; \beta) = \langle \vec{r} \,|\, e^{-\beta \underset{\sim}{H}} \,|\, \vec{r}^{\,\prime} \rangle \tag{A.2}$$

and

$$Z = \mathrm{Tr} \rho(\vec{r}, \vec{r}^{\,\prime}; \beta) = \mathrm{Tr} \left(e^{-\beta \underset{\sim}{H}} \right) \tag{A.3}$$

where $\vec{r} = \{\mathrm{r}_1, \ldots, \mathrm{r}_N\}$ and r_i is the position of the i^{th} particle.

the fact that $\underset{\sim}{H}$ usually contains two possibly non-commutating parts $\underset{\sim}{\Omega}$ and $\underset{\sim}{\Upsilon}$, representing the kinetic and the potential energy operators, presents serious problem for the calculation of the density matrix. A very common approach to solve this problem is to separate the two part of the Hamiltonian. Using the exact operator identity one gets

$$\exp\left(-\beta(\underset{\sim}{\Omega} + \underset{\sim}{\Upsilon})\right) = \exp\left(-\beta \underset{\sim}{\Omega}\right) \exp\left(-\beta \underset{\sim}{\Upsilon}\right) \exp\left(-\frac{\beta^2}{2} \left[\underset{\sim}{\Omega}, \underset{\sim}{\Upsilon}\right]\right) \tag{A.4}$$

This equation can be rewritten

$$\exp\left(-\beta(\underset{\sim}{\Omega} + \underset{\sim}{\Upsilon})\right) = \exp\left(-\frac{\beta}{M} \underset{\sim}{\Omega}\right) \exp\left(-\frac{\beta}{M} \underset{\sim}{\Upsilon}\right) \exp\left(-\frac{\beta^2}{2M^2} \left[\underset{\sim}{\Omega}, \underset{\sim}{\Upsilon}\right]\right) \tag{A.5}$$

and it has been shown by E. Trotter [133] that the commutator term becomes much smaller than the others for $\mathrm{M} \to \infty$ and can thus be ignored, one does not have to worry:

$$\exp\left(-\beta(\underset{\sim}{\Omega} + \underset{\sim}{\Upsilon})\right) = \lim_{M \to 0} \left[\exp\left(-\frac{\beta}{M} \underset{\sim}{\Omega}\right) \exp\left(-\frac{\beta}{M} \underset{\sim}{\Upsilon}\right)\right]^M + O\left(\frac{\beta^3}{M^2}\right) \tag{A.6}$$

This equation is correct to the order ($\frac{\beta^3}{M^2}$). The parameter M is usually called the number of timeslics. More detailed description can be found in references [134, 135, 136, 137].
Using Trotter's approach, the partition function can be written as

$$Z = \mathrm{Tr}\left[\lim_{M\to 0}\left[\exp\left(-\frac{\beta}{M}\underset{\sim}{\Omega}\right)\exp\left(-\frac{\beta}{M}\underset{\sim}{\Upsilon}\right)\right]^M + O\left(\frac{\beta^3}{M^2}\right)\right] \tag{A.7}$$

with $\underset{\sim}{\Omega} = \frac{\hbar^2}{2m}$ and $\underset{\sim}{\Upsilon} = \mathrm{V}(\vec{r})$

For slowly varying potentials, Takahshi and Imada have shown that replacing the potential energy term by an effective potential reduces the computing time significantly [137, 138, 133]. They introduced

$$\underset{\sim}{H}_0 = \underset{\sim}{\Upsilon} + \frac{1}{24}\left(\frac{\beta}{M}\right)^2\left[\underset{\sim}{\Upsilon},\left[\underset{\sim}{\Omega},\underset{\sim}{\Upsilon}\right]\right] \tag{A.8}$$

which is identical to the case presented here

$$\underset{\sim}{H}_0 = V(\vec{r}) + \frac{\hbar^2}{24m}\left(\frac{\beta}{M}\right)^2\left(\frac{\delta V(\vec{r})}{\delta\vec{r}}\right)^2 \tag{A.9}$$

Using this approach, an equation equivalent to Feynman's approach [139] for the partition function of a one particle system in position space can be written [140]

$$\begin{aligned} Z = \int\left[\prod_{\gamma=1}^{M} d\vec{r}(\gamma)\right]\prod_{\alpha=1}^{M}\Big[\langle\,\vec{r}(\alpha+1)\,|\exp\left(-\frac{\beta}{M}\underset{\sim}{\Omega}\right) \\ |\,\vec{r}(\alpha)\,\rangle\mathrm{x}\langle\,\vec{r}(\alpha)\,|\exp\left(-\frac{\beta}{M}\underset{\sim}{\Upsilon}\right)\,|\,\vec{r}(\alpha)\,\rangle\Big] + O\left(\frac{\beta^3}{M^2}\right) \end{aligned} \tag{A.10}$$

$$\begin{aligned} = \left(\frac{Mm}{2\pi\beta\hbar^2}\right)^{3M/2}\int\left[\prod_{\gamma=1}^{M} d\vec{r}(\gamma)\right]\Bigg[\exp\Bigg(-\sum_{\alpha=1}^{M}\frac{Mm}{2\beta\hbar^2}(\langle\,\vec{r}(\alpha+1)\,|\,-\vec{r}(\alpha))^2 \\ -\frac{\beta}{M}\sum_{\alpha=1}^{M}V(\vec{r}(\alpha))\Bigg)\Bigg] + O\left(\frac{\beta^3}{M^2}\right). \end{aligned} \tag{A.11}$$

For $M\to\infty$ this formula becomes exact and coincides with the famous formula of Kac and Feynman [141]. The number of times M is the source of the relative error of the simulation. While the kinetic energy term is proportional to M/β, and potential energy term is proportional to β/M. To achive a uniform convergence of both parts

of Eq.(A.11), the quotient β/M is kept constant. This results in a higher number of timeslices for low temperatures and in an increasing computational effort.
For a system of N electrons in an external potential, the Feynman path integral can be written as [140]

$$Z = \left(\frac{1}{N!}\right)^M \int \left[\prod_{\gamma=1}^{M}\prod_{i=1}^{N} \mathrm{d}\vec{r_i}(\gamma)\right] \prod_{\alpha=1}^{M} \det(A(\alpha,\alpha+1)) \\ \exp\left[-\frac{\beta}{M}\sum_{\alpha=1}^{M} V\left(\vec{r_1}(\alpha),\ldots,\vec{r_N}(\alpha)\right)\right] + O\left(\frac{\beta^3}{M^2}\right) \tag{A.12}$$

with the NxN-dimensional matrix

$$(A(\alpha,\alpha+1))_{k,l} = \begin{cases} \langle\, \vec{r}_k(\alpha) \,|\, \exp\left(-\frac{\beta}{M}\frac{p^2}{2m} \,|\, \vec{r}_l(\alpha+1)\,\rangle\right) & : S_k = S_l \\ 0 & : S_k \neq S_l \end{cases} \tag{A.13}$$

$S_{k,l} = \pm 1/2$ denotes the spin of the electron.
This is the famous mapping from a quantum system to a classical system.

B. Spin function and spin-orbit coupling

This appendix gives a brief general review of the spin function of one electron and spin orbital coupling.

Spin orbital of a **one-electron system**

$$\psi(\vec{r})\psi(\sigma) = \psi_{n,l,m_l}(\vec{r})\psi(\sigma) \tag{B.1}$$

$$= \underbrace{R_{n,l}(r)Y^l_{m_l}(\theta,\phi)}_{\text{atomic orbital}}\,\psi(\sigma) \tag{B.2}$$

Spin function

$$\psi(\sigma) \equiv |sm_s> \begin{cases} m_s = \frac{1}{2}: & \alpha \\ m_s = -\frac{1}{2}: & \beta \end{cases} \tag{B.3}$$

$$\underset{\sim}{\vec{S}}^2|Sm_s> = s(s+1)\hbar^2|Sm_s> \quad \text{with } s = \frac{1}{2} \tag{B.4}$$

$$\underset{\sim}{S_z}|Sm_s> = m_s\hbar|Sm_s> \quad \text{with } m_s = \pm\frac{1}{2} \tag{B.5}$$

$$\underset{\sim}{S_\pm}|Sm_s> = (s(s+1) - m_s(m_s \pm 1))^{1/2}\hbar|Sm_s \pm 1> \tag{B.6}$$

$$\tag{B.7}$$

Spin-orbit coupling results on account of the interaction of the electron's magnetic spin moment $\vec{\mu_s}$

$$\vec{\mu_s} = -\frac{e}{2m_e}g\vec{S} = \gamma_e g\vec{S} \tag{B.8}$$

Caused by the circulating charged particle. Only certain orientations between $\vec{l}$ and $\vec{s}$ are allowed given by the vector sum

$$\vec{j} = \vec{l} + \vec{s}, \begin{cases} j = l+s, l+s-1, \ldots, |l-s| \\ ass = 1/2 \rightarrow j = l \pm 1/2 \end{cases} \tag{B.9}$$

$$m_j = m_l + m_s \tag{B.10}$$

$$\underset{\sim}{\vec{j}}^2 = \underset{\sim}{j_x}^2 + \underset{\sim}{j_y}^2 + \underset{\sim}{j_z}^2 \tag{B.11}$$

$$\underset{\sim}{j_+} = \underset{\sim}{j_x} + i\underset{\sim}{j_y} \tag{B.12}$$

$$\underset{\sim}{j_-} = \underset{\sim}{j_x} - i\underset{\sim}{j_y} \tag{B.13}$$

$$\underset{\sim}{\vec{j}}^2 |jm_j> = j(j+1)\hbar^2 |jm_j> \tag{B.14}$$

$$\underset{\sim}{j_z} |jm_j> = m_j\hbar |jm_j> \tag{B.15}$$

$$\underset{\sim}{j_\pm} |jm_j> = (j(j+1) - m_j(m_j \pm 1))^{1/2}\hbar |jm_j \pm 1> \tag{B.16}$$

$$\tag{B.17}$$

operator of spin-orbit coupling

$$\underset{\sim}{H_{so}} = \xi(r)\underset{\sim}{\vec{l}}.\underset{\sim}{\vec{s}} \tag{B.18}$$

where

$$\xi r = -\frac{e}{2m_e^2c^2}\frac{1}{r}\frac{\delta V(r)}{\delta r} \tag{B.19}$$

Many electron atoms

The total orbital angular momentum and its projection are expressed through the sums

$$\vec{L} = \sum_i \vec{l_i} \tag{B.20}$$

$$L_z = \sum_i l_i^z \tag{B.21}$$

and they are quantised through the quantum numbers L and M_L, respectively

$$<\vec{L}> = \sqrt{L(L+1)}\hbar \tag{B.22}$$

$$<L_z> = M_L\hbar \tag{B.23}$$

$$L = \sum_i l_i$$
$$\text{and} \quad M_L = -L, -L+1 \ldots, -1, 0, +1, \ldots, L-1, L \tag{B.24}$$

$L = \sum_i l_i$ and $M_L = -L, -L+1 \ldots, -1, 0, +1, \ldots, L-1, L$
The same for the total spin angular momentum $\vec{S}$, its projection S_z and the corresponding quantum numbers S and M_S. Atomic spin-orbitals various configuration functions

$$|\, \psi_u(M_L, M_S) \,\rangle \rightarrow |\, M_L, M_S \,\rangle \tag{B.25}$$

These are eigenfunction of the operators of the projection of the total orbital angular momentum $\underset{\sim}{L}_z$ and the projection of the total spin angular momentum $\underset{\sim}{S}_z$.

$$\underset{\sim}{L}_z \,|\, \psi_u(M_L, M_S) \,\rangle = M_{Lu}\hbar \,|\, \psi_u(M_L, M_S) \,\rangle \tag{B.26}$$

$$\underset{\sim}{S}_z \,|\, \psi_u(M_L, M_S) \,\rangle = M_{Su}\hbar \,|\, \psi_u(M_L, M_S) \,\rangle \tag{B.27}$$

A proper linear combination of these functions

$$|\, L, M_L, S, M_S \,\rangle = \sum_u C_u \,|\, \psi_u(M_L, M_S) \,\rangle \tag{B.28}$$

yields the proper eigenfunctions of the operators $\underset{\sim}{L}^2$ and $\underset{\sim}{S}^2$ as required for eigenfunctions of many-electron atoms

$$\underset{\sim}{L}^2 \,|\, L, M_L, S, M_S \,\rangle = L(L+1)\hbar^2 \,|\, L, M_L, S, M_S \,\rangle \tag{B.29}$$

$$\underset{\sim}{S}^2 \,|\, L, M_L, S, M_S \,\rangle = S(S+1)\hbar^2 \,|\, L, M_L, S, M_S \,\rangle \tag{B.30}$$

The combination coefficients can be determined as follows. By substituting the expansion we have

$$\underset{\sim}{L}^2 \sum_u C_u \,|\, \psi_u \,\rangle = L(L+1)\hbar^2 \sum_u C_u \,|\, \psi_u \,\rangle \tag{B.31}$$

and by multiplying from the left side by the bra vector $\langle\, \psi_v \,|$ a homogeneous system of linear equations is obtained.

$$\sum_u C_u \left[\langle\, \psi_v \,|\, \underset{\sim}{L}^2 \,|\, \psi_u \,\rangle - L(L+1)\hbar^2 \delta_{vu} \right] = 0 \tag{B.32}$$

and analogously

$$\sum_u C_u \left[\langle \psi_v \,|\, \underset{\sim}{S}^2 \,|\, \psi_u \rangle - S(S+1)\hbar^2 \delta_{vu} \right] = 0 \tag{B.33}$$

The solution of these equations is straightforward. The linear combination of the configuration functions means, in fact, a configuration interaction. This is one way of overcoming the one-electron approximation.

Hund's rules

$$\mu = g_J \sqrt{J(J+1)} \mu_B \tag{B.34}$$

except $4f^4$, $4f^5$, $4f^6$ systems
with Landé factor

$$g_J = 1 + \frac{J(J+1) + S(S+1) - L(L+1)}{2J(J+1)} \tag{B.35}$$

S,J,L correspond to the total spin angular momentum, the total orbital angular momentum and total angular momentum, respectively, of the ground state.

Bibliography

[1] S. Sun, C. B. Murray, D. Weller, L. Folks, and A. Moser. *Science*, 287:1989, 2000.

[2] Dante Gatteschi, Andrea Caneschi, L. Pardi, and Roberta Sessoli. Large clusters of metal ions: The transition from molecular to bulk magnets. *Science*, 265:1054, 1994.

[3] Roberta Sessoli, Dante Gatteschi, Andrea Caneschi, and M. A. Novak. Magnetic bistability in a metal-ion cluster. *Nature*, 365:141–143, 1993.

[4] Dante Gatteschi. Molecular magnetism: a basis for new materials. *Adv. Mater.*, 6:635, 1994.

[5] Achim Müller, Sabyasachi Sarkar, Syed Qaiser Nazir Shah, Hartmut Bögge, Marc Schmidtmann, Shatarupta Sarkar, Paul Kögerler, B. Hauptfleisch, A.X. Trautwein, and V. Schünemann. Archimedean synthesis and magic numbers: "sizing" giant molybdenum-oxide-based molecular spheres of the keplerate type. *Angew. Chem., Int. Ed.*, 38:3238, 1999.

[6] ed. By E. Coronado, P. Delhaes, D. Gatteschi, and J. S. Miller. Molecular magnetism: From molecular assemblies to the devices. *NATO ASI Series E, Kluwer Academic Publishing*, 321, 1996.

[7] Science 25 January 2002J:581. *Science*, 295:581, 2002.

[8] J. Schnack, M. Brüger, M. Luban, P. Kögerler, E. Morosan, R. Fuchs, R. Modler, Hiroyuki Nojiri, Ram C. Rai, Jinbo Cao, J. L. Musfeldt, and Xing Wei. 2005.

[9] Swapan K. Pati and C. N. R. Rao. Role of the spin magnitude of the magnetic ion in determining the frustration and low-temperature properties of kagome lattices. *J. Chem. Phys.*, 123:234703, 2005.

[10] J. R. Friedman, V. Patel, W. Chen, S. K. Tolpygo, and J. E. Lukens. *Nature*, 406:43, 2000.

[11] J. Tejada, J. M. Hernandez, and E. del Barco. *J. Magn. Magn. Mater.*, 197:552, 1999.

[12] L. Thomas, F. Lionti, R. Ballou, D. Gatteschi, R. sessoli, and B. barbara. *Nature*, 383:145, 1996.

[13] *http://msmd.ims.ac.jp/molspin/03mokuteki_e.html*.

[14] R.E.P. Winpenny. *Adv, Inorg. Chem.*, 52:1, 2001.

[15] Dante Gatteschi and Roberta Sessoli. Quantum tunneling of magnetization and related phenomena in molecular materials. *Angew. Chem., Int. Edit.*, 42:268–297, 2003.

[16] Dante Gatteschi and Roberta Sessoli. *J. Magn. Magn. Mater*, 1030:272–276, 2004.

[17] Achim Müller, F. Peters, M.T. Pope, and Dante Gatteschi. Polyoxometalates: very large clusters - nanoscale magnets. *Chem. Rev.*, 98:239, 1998.

[18] E. Coronado, P. Delhaes, Dante Gatteschi, and J.S. Miller, editors. *Localized and Itinerant Molecular Magnetism: From Molecular Assemblies to the Devices*, volume 321 of *NATO Advanced Studies Institute, Series E: Applied Sciences*, Dordrecht, 1996. Kluwer Academic.

[19] Achim Müller, Marshall Luban, Christian Schröder, Robert Modler, Paul Kögerler, Maria Axenovich, Jürgen Schnack, Paul C. Canfield, Sergei Bud'ko, and Neil Harrison. Classical and quantum magnetism in giant keplerate magnetic molecules. *Chem. Phys. Chem.*, 2:517, 2001.

[20] X.G. Wang and P. Zanardi. Quantum entanglement and bell inequalities in heisenberg spin chains. *Phys. Lett. A*, 301:1–6, 2002.

[21] X.G. Wang. Thermal and ground-state entanglement in heisenberg xx qubit rings. *Phys. Rev. A*, 66:034302, 2002.

[22] Achim Müller and J. Döring. *Angew. Chem., Int. Ed. Engl.*, 27:1721, 1988.

[23] T. Lis. Preparation, structure, and magnetic properties of a dodecanuclear mixed-valence manganese carboxylate. *Acta Chrytallogr. B*, 36:2042, 1980.

[24] C. Delfs, Dante Gatteschi, L. Pardi, Roberta Sessoli, K. Wieghardt, and D. Hanke. Magnetic properties of an octanuclear iron(iii) cation. *Inorg. Chem.*, 32:3099, 1993.

[25] Andrea Caneschi, Andrea Cornia, Antonio C. Fabretti, Dante Gatteschi, and Wanda Malavasi. Polyiron(iii)-alkoxo clusters: A novel trinuclear complex and its relevance to the extended lattices of iron oxides and hydroxides. *Inorg. Chem.*, 34:4660, 1995.

[26] Oliver Waldmann, J. Schülein, R. Koch, Paul Müller, Ingo Bernt, Rolf W. Saalfrank, Hans Peter Andres, Hans U. Güdel, and P. Allenspach. Magnetic anisotropy of two cyclic hexanuclear fe(iii) clusters entrapping alkaline ions. *Inorg. Chem.*, 38:5879, 1999.

[27] Bernd Pilawa, R. Desquiotz, M.T. Kelemen, M. Weickenmeier, and A. Geisselman. Magnetic properties of new fe_6 (triethanolaminate(3-))$_6$ spin clusters. *J. Magn. Magn. Mater.*, 177:748, 1997.

[28] Darine Jabbour, Binrta Keita, Louis Nadjo, Ulrich Kortz, and Sib Sankar Mal. *Electrochemistry Communications*, 2005.

[29] Finn K. Larsen, Eric J. L. McInnes, Hassane El Mkami, Jacob Overgaard, Stergios Piligkos, Gopalan Rajaraman, Eva Rentschler, Andrew A. Smith, Graham M. Smith, Val Boote, Martin Jennings, Grigore A. Timco, and Richard E. P. Winpenny. Synthesis and characterization of heterometallic Cr_7M wheels. *Angew. Chem. Int. Ed.*, 42:101, 2003.

[30] D. Awschalom and N. Samarth and D. Loss. Semiconductor spintronics and quantum computation. *Springer, Berlin*, 2002.

[31] Leuenberger M. N. and Daniel Loss. Quantum computing in molecular magnets. *Nature*, 410:789–793, 2001.

[32] Florian Meier and Daniel Loss. Electron and nuclear spin dynamics in antiferromagnetic molecular rings. *Phys. Rev. Lett.*, 86:5373–5376, 2001.

[33] Florian Meier and Daniel Loss. Coherent spin quantum dynamics in antiferromagnetic rings. *Physica B*, 329-333:1140–1141, 2003.

[34] S. Carretta, E. Liviotti, N. Magnani, P. Santini, and G. Amoretti. *Phys. Rev. Lett.*, 92:207205, 2004.

[35] A.Aharoni. Introduction to the theory of ferromagnetism. *Oxford University Press Inc., New York*, 1998.

[36] J. von delft and C. L. Henley. *Phys. Rev. Lett.*, 69:3236, 1992.

[37] A. Garg. *Europhys. Lett.*, 22:205, 1993.

[38] J. B. Goodenough. Magnetism and the chemical bond. *Magnetism and the Chemical Bond, Wiley-Interscience, New York*, 1963.

[39] A. H. Morrish. Magnetism and the chemical bond. *Physical prinsiples of Magnetism, Wiley, New York*, 1965.

[40] L. Néel. *Magnetism and local molecular field, Science*, 174:985–92, 1971.

[41] A. Auerbach. Interacting electrons and quantum magnetism. *springer, New York*, 1994.

[42] W. Heisenberg. *Z. Physik*, 49:619, 1928.

[43] P. A. M. Dirac. *Proc. Roy. Soc. London Ser. A*, 123:714, 1929.

[44] C. Herring. *Rev. Mod. Phys.* , 34:631, 1962.

[45] P. W. Anderson. *in solid state Physics, edited by F. Seitz and D. Turnbull (Academic Press, New york)*, 14, chap. 2:99, 1963.

[46] Jeremy Levy. Quantum information processing with ferroelectrically coupled quantum dots. *Phys. Rev. A*, 64:052306, 2001.

[47] D. Gatteschi *et al. Chem. Soc. Rev.*, 25:101, 1996.

[48] A. Cornia, A. G. M. Jansen, and M. Affronte. Magnetic anisotropy of fe6 and fe10 molecular rings by cantilever torque magnetometry in high magnetic fields. *Phys. Rev. B*, 60:12177, 1999.

[49] B. Normand, X. Wang, X. Zotos, and Daniel Loss. Magnetization in molecular iron rings. *Phys. Rev. B*, 63:184409, 2001.

[50] M.Affronte, J. C. Lasjaunias, A. Cornia, and A. Caneschi. Low-temperature specific heat of fe6 and fe10 molecular magnets. *Phys. Rev. B*, 60:1161–1166, 1999.

[51] R. Caciuffo, T. Guidi, G. Amoretti, S. Carretta, E. Liviotti, P. Santini, C. Mondelli, G. Timco, C. A. Muryn, and R.E.P. Winpenny. Spin dynamics of heterometallic cr_7m wheels (m = mn, zn, ni) probed by inelastic neutron scattering. *Phys. Rev. B*, 2004. submitted; cond-mat/0412169.

[52] Oliver Waldmann, R. Koch, S. Schromm, J. Schülein, Paul Müller, Ingo Bernt, Rolf W. Saalfrank, F. Hampel, and E. Balthes. Magnetic anisotropy of a cyclic octanuclear fe(iii) cluster and magneto-structural correlations in molecular ferric wheels. *Inorg. Chem.*, 40:2986, 2001.

[53] M.-H. Julien, Z.H. Jang, Alessandro Lascialfari, Ferdinando Borsa, M. Horvatić, Andrea Caneschi, , and Dante Gatteschi. Proton nmr for measuring quantum level crossing in the magnetic molecular ring fe10. *Phys. Rev. Lett.*, 83:227, 1999.

[54] Klaus Bärwinkel, Heinz-Jürgen Schmidt, and Jürgen Schnack. Structure and relevant dimension of the heisenberg model and applications to spin rings. *J. Magn. Magn. Mater.*, 212:240, 2000.

[55] Dimitris Kouzoudis. Exact analytical partition function and energy levels for a heisenberg ring of $n = 6$ spin 1/2 sites. *J. Magn. Magn. Mater.*, 189:366, 1998.

[56] J.C. Bonner and M.E. Fisher. Linear magnetic chains with anisotropic coupling. *Phys. Rev.*, 135:A640, 1964.

[57] Klaus Fabricius, Ute Löw, K.-H. Mütter, and Peer Ueberholz. Complete solution of the antiferromagnetic heisenberg rings with $n = 12$–16 sites. *Phys. Rev. B*, 44:7476, 1991.

[58] Klaus Fabricius, Ute Löw, and Joachim Stolze. Dynamic correlations of antiferromagnetic spin-$\frac{1}{2}$ xxz chains at arbitrary temperature from complete diagonalization. *Phys. Rev. B*, 55:5833, 1997.

[59] Efstratios Manousakis. The spin-$\frac{1}{2}$ heisenberg antiferromagnet on a square lattice and its application to the cuprous oxides. *Rev. Mod. Phys.*, 63:1, 1991.

[60] A. Müller *et al. Angew. Chem. Int. Ed.*, 38:3238, 1999.

[61] W. Feller. An introduction to probability theory and its applications. *3 ed. (John Wiley, Sons, New York)*, 1, 1968.

[62] Philipp Gütlich, Andreas Hauser, and Hartmut Spiering. Thermisch und optisch schaltbare eisen(ii)-komplexe. *Angew. Chem.*, 106:2109, 1994.

[63] J. Schnack. Quantum theory of molecular magnetism. *Magnetism goes Nano, Eds. Stefan Blgel, Thomas Brckel, Claus M. Schneider, Lecture Manuscripts of the 36th Spring School of the Institute of Solid State Research, Jlich, ISBN 3-89336-381-5*, 2005.

[64] Jürgen Schnack and Marshall Luban. Rotational modes in molecular magnets with antiferromagnetic heisenberg exchange. *Phys. Rev. B*, 63:014418, 2001.

[65] Klaus Bärwinkel, Peter Hage, Heinz-Jürgen Schmidt, and Jürgen Schnack. Exact quantum numbers for relative ground states of frustrated heisenberg spin rings. *Phys. Rev. B*, 68:054422, 2003.

[66] Cornelius Lanczos. An iteration method for the solution of the eigenvalue problem of linear differential and integral operators. *J. Res. Nat. Bur. Stand.*, 45:255–282, 1950.

[67] Jane K. Cullum and Ralph A. Willoughby. *Lánczos Algorithms for Large Symmetric Eigenvalue Computations*, volume I. Birkhäuser, Boston, 1985.

[68] Steven R. White. Density-matrix algorithms for quantum renormalization groups. *Phys. Rev. B*, 48:10345, 1993.

[69] David P. Landau and Kurt Binder. A guide to monte carlo simulations in statistical physics. *Cambridge University Press, CB2 2RU, UK*, 2000.

[70] R. Blankenbecler, D. J. Scalapino, and R. L. Sugar. Monte carlo calculation of coupled boson-fermion systems. *Phys. Rev. D*, 24:2278, 1981.

[71] K. Takegahara. Quantum monte carlo of the degenerate anderson model with cubic crystal field. *J. Phys. Soc. Jpn.*, 62:1736, 1993.

[72] A. Georges, G. Kotliar, W. Krauth, and M. J. Rozenberg. Dynamical mean-field theory of strongly correlated fermion systems and limit of infinite dimensions. *Rev. Mod. Phys.*, 68:13, 1996.

[73] S. Fahy, X. W. Wang, and Steven G. Louie. Variational quantum monte carlo nonlocal pseudopotential approach to solids: Formulation and application to diamond, graphite, and silicon. *Phys. Rev. B*, 42:3503, 1990.

[74] Umrigar C. J., Nightingale M. P., and Runge K. J. Spin contamination in quantum monte carlo wave functions. *J. Chem. Phys.*, 99:2865, 1993.

[75] L. Mitas and R. M. Martin. Quantum monte carlo of nitrogen: atom, dimer, atomic and molecular solids. *Phys. Rev. Lett.*, 72:2438, 1994.

[76] J. C. Grossman. Benchmark quantum monte carlo calculations. *J. Chem. Phys.*, 117:1434, 2002.

[77] L. Gunther and B. Barbara. for an overview, see e.g., *quantum tunneling of magnetization* and references therein,. *Kluwer, Dordrecht, The Netherlands*, 1994.

[78] Alain Chiolero and Daniel Loss. Macroscopic quantum coherence in molecular magnets. *Phys. Rev. Lett.*, 80:1998, 1998.

[79] A. Garg. *Europhys. Lett.*, 22:205, 1993.

[80] W. Wernsdorfer and R. Sessoli. *Sience*, 284:133, 1999.

[81] N. Bloembergen, E. M. Purcell, and R. V. Pound. Relaxation effects in nuclear magnetic resonance absorption. *Phys. Rev.*, 73:679, 1948.

[82] A. Müller, R. Sessoli, E. Krickemeyer, H. Bögge, J. Meyer, D. Gatteschi, L. Pardi, J. Westphal, K. Hovemeier, R. Rohlfing, and J. Döring. *Inorg. Chem.*, 36:5239, 1997.

[83] A. Lascialfari, D. Gatteschi, F. Borsa, and A. Cornia. Spin dynamics in mesoscopic size magnetic systems: A $\hat{\text{h}}$ nmr study in rings of iron (iii) ions. *Phys. Rev.B*, 55:14341, 1997.

[84] J. Padilla, D. Gatteschi, and P. Chaudhuri. *Inorg. Chim. Acta*, 260:217, 1997.

[85] H. Lopez Sandoval, R. Contreras, A. Escuer, R. Vicente, S. Bernes, H. Noth, G. J. Leigh, and N. Barba Behrens. *J. Chim. Soc. Daltan Trans*, page 2648, 2002.

[86] M. Oshikawa and I. Affleck. Low temperature electron spin resonance theory for half integer spin antiferromagnetic chains. *Phys. Rev. Lett.*, 82:5136, 1999.

[87] A. De Martino, R. Egger, K. Hallberg, and C. A. Balseiro. *Phys. Rev. Lett.*, 88:116401, 2002.

[88] J. Overgaard, B. B. Iversen, S. P. Palii, G. A. Timco, N. V. Gerbeleu, and F. K. Larsen. Magnetic properties of new fe_6 (triethanolaminate(3-))$_6$ spin clusters. *Chem. Eur. J.*, 8:2775, 2002.

[89] Andres H., Basler R., Blake A. J., C. Cadiou, G. Chaboussant, C. M. Grant, H. U. Gudel, M. Murrie, S. Parsons, C. Paulsen, F. Semadini, V. Villar, W. Wernsdorfer, and R. E. P. Winpenny. Studies of a nickel-based single-molecule magnet. *Chem. Eur. J.*, 8:4867–4876, 2002.

[90] G. Amoretti, S. Carreta, R. Caciuffo, H. Casalta, A. Cornia, M. Affronte, and D. Gatteschi. *Phy. Rev. B*, 64:104403, 2001.

[91] S. Carreta, E. Liviotti, G. Aoretti, R. Cornia, D. Gatteschi, J. Kulda, and E. Liviotti. *Appl. Phys. A (Suppl.)*, 74:S929, 2002.

[92] J. van Slageren, Roberta Sessoli, Dante Gatteschi, A. A. Smith, M. Helliwell, R. E. P. Winpenny, A. Cornia, A. L. Barra, A. G. M. Jansen, E. Rentschler, and G. A. Timco. Magnetic anisotropy of the antiferromagnetic ring [cr(8)f(8)piv(16)]. *Chem. Eur. J.*, 8:277–285, 2002.

[93] S. Carretta, J. van Slageren, T. Guidi, E. Liviotti, C. Mondelli, D. Rovai, A. Cornia, A. L. Dearden, F. Carsughi, M. Affronte, C. D. Frost, R. E. P. Winpenny, Dante Gatteschi, G. Amoretti, and R. Caciuffo. Microscopic spin hamiltonian of a cr_8 antiferromagnetic ring from inelastic neutron scattering. *Phys. Rev. B*, 67:094405, 2003.

[94] M. Affronte, T. Guidi, R. Caciuffo, S. Carretta, G. Amoretti, J. Hinderer, I. Sheikin, A. G. M. Jansen, A. A. Smith, Richard E. P. Winpenny, J. van Slageren, and Dante Gatteschi. Mixing of magnetic states in a cr_8 molecular ring. *Phys. Rev. B*, 68:104403, 2003.

[95] M. Affronte, T. Guidi, R. Caciuffo, S. Carretta, G. Amoretti, J. Hinderer, I. Sheikin, A. A. Smith, R. E. P. Winpenny, J. van Slageren, and Dante Gatteschi. Level crossing in a molecular cr_8 ring. *J. Magn. Magn. Mater.*, 272-76:1050–1051, 2004.

[96] F. Troiani, A. Ghirri, M. Affronte, S. Carretta, P. Santini, G. Amoretti, S. Piligkos, G. Timco, and R. E. P. Winpenny. Molecular engineering of antiferromagnetic rings for quantum computation. 2004. cond-mat/0405507.

[97] A. Bencini and D. Gatteschi. *EPR of exchange Coupled Systems, Springer, Berlin*, 1989.

[98] M. Allalen and J. Schnack. Theoretical estimates for proton-nmr spin-lattice relaxation rates of heterometallic spin rings. 2005. cond-mat/0504658.

[99] A. Lascialfari, F. Borsa, M. H. Julien, E. Micotti, D. Furukawa, Z. H. Jang, A. Cornia, Dante Gatteschi, M. Horvatic, and J. Van Slageren. Spin dynamics at level crossing in molecular af rings probed by nmr. *J. Magn. Magn. Mater.*, 272-76:1042–1047, 2004.

[100] Principles of Nuclear Magnetism A. Abragam. *Principles of Nuclear Magnetism, (Clarendon Press, Oxford), 1961.*

[101] A. Lascialfari, Z. H. Jang, F. Borsa, D. Gatteschi, A. Cornia, D. Rovai, A. Caneschi, and P. Carretta. *Phys. Rev. B*, 61:6839, 2000.

[102] F. Borsa and M. Mali. *Phys. Rev. B*, 9:2215, 1974.

[103] R. Basler, G. Chaboussant, A. Sieber, A. Andres, M. Murrie, P. KÖgerler, H. Bögge, D. C. Crans, E. Krickemeyer, S. Janssen, H. Mutka, A. Müller, and H. Güdel. *Inorg. Chem*, 42:5675–5685, 2002.

[104] B. J. Suh, D. Procissi, P. Kögerler, E. Micotti, A. Lascialfari, and F. Borsa. *ICM, Rome*, 2003.

[105] F. Borsa and A. Rigamonti. *in Magnetic resonance of phase transitions, edit by F. J. Owens, C. P. Poole, Jr., and H. A. Farach(Academic, new York)*, page 79, 1979.

[106] T. Moriya. Nuclear magnetic relaxation in antiferromagnets. *Prog. Theor. Phys.*, 16:23, 1956.

[107] A. Abragam. *The Principles of Nuclear Magnetism.* Clarendon, Oxford, 1961.

[108] S. H. Baek, Marshall Luban, A. Lascialfari, E. Micotti, Y. Furukawa, Ferdinando Borsa, Joris van Slageren, and A. Cornia. Scaling behavior of the proton spin-lattice relaxation rate in antiferromagnetic molecular rings. *Phys. Rev. B*, 70:134434, 2004.

[109] P. Santini, S. Carretta, E. Liviotti, G. Amoretti, P. Carretta, and E. Micotti M. Filibian, A. Lascialfari. *Phys. Rev. Lett.*, 94:077203, 2005.

[110] J. von Neumann and E. P. Wigner. *Phys. Z*, 30:467, 1929.

[111] A. Garg. *Phys. Rev. B*, 51:15161, 1995.

[112] S. Miyashita, K. Saito, and H. e Raedt. *Phys. Rev. Lett.*, 80:1525, 1998.

[113] P. W. Anderson. *Phys. Rev*, 86:694, 1952.

[114] Oliver Waldmann, T. Guidi, S. Carretta, C. Mondelli, and A. L. Dearden. Elementary excitations in the cyclic molecular nanomagnet cr8. *Phys. Rev. Lett.*, 91:237202, 2003.

[115] P. Azaria, B. Delamotte, and D. Mouhanna. *Phys. Rev. Lett.*, 70:2483, 1993.

[116] A. Lascialfari F. Borsa and Y. Furukawa. *cond-mat/0404379*, 2004.

[117] G. Seeber, P. Kögerler, B. M. Kariuki, and L. Cronin. Chem. Commun., 2004.

[118] Larry Engelhardt, Marshall Luban, and Paul Kögerler. 2005. private communications.

[119] Sib Sankar Mal and Ulrich Kortz. *Angrew. Chem. Int. Ed.*, 44:2, 2005.

[120] O. Kahn. *Chem. Phys. Rev.*, 265:165, 1997.

[121] D abbour, B. Keita, L. Nadjo, U. Kortz, and S. S. Mal. The wheel shaped cu 20tungstophosphate, redox and electrocatalytic properties. *Electrochem. Comm.*, 7:841–847, 2005.

[122] O. P. Vajk *et al. Science*, 295:1691, 2002.

[123] A. V. Mahajan *et al. Phys. Rev. Lett.*, 72:3100, 1994.

[124] G. Xiao, M. Z. Cieplak, A. Gavrin, F. H. Streitz, A. Bakhshai, and C. L. Chien. *Phys. Rev. Lett.*, 60:146, 1988.

[125] S. T. Ting *et al. Phys. Rev. B.*, 46:11772, 1992.

[126] M. Corti *et al. Phys. Rev. B.*, 52:4226, 1995.

[127] Satoshi Fujimoto and Sebatian Eggert. *Phys. Rev. Lett.*, 92:037206, 2004.

[128] E. Ruiz, P. Alemany, S. Alvarez, and J. Cano. Toward the prediction of magnetic coupling in molecular systems: Hydroxo- and alkoxo-bridged cu(ii) binuclear complexes. *J. Am. Chem. Soc.*, 119:1297–1303, 1997.

[129] E. Ruiz, J. Cano, S. Alvarez, and P. Alemany. Magnetic coupling in end-on azido-bridged transition metal complexes: A density functional study. *J. Am. Chem. Soc.*, 120:11122–11129, 1998.

[130] M. R. Pederson, N. Bernstein, and J. Kortus. Fourth-order magnetic anisotropy and tunnel splittings in mn-12 from spin-orbit-vibron interactions. *Phys. Rev. Lett.*, 89:097202, 2002.

[131] J. Kortus, C. S. Hellberg, and M. R. Pederson. Hamiltonian of the v-15 spin system from first-principles density-functional calculations. *Phys. Rev. Lett.*, 86:3400–3403, 2001.

[132] Jens Kortus, T. Baruah, N. Bernstein, and M. R. Pederson. Magnetic ordering, electronic structure, and magnetic anisotropy energy in the high-spin mn-10 single molecule magnet. *Phys. Rev. B*, 66:092403, 2002.

[133] H. F. Trotter. On the product of semi groups of operators. *Proc. Math. Soc. Am.*, 10:565, 1959.

[134] G. Roepstorff. *Path integral approach to quantum physics. Springer Verlag*, 1996.

[135] H. Kleinert. Pfadintegrale in quantenmechanik, statistik und polymerphysik. bi wissenschaftsverlag. 1993.

[136] D.M. Ceperley. Path integrals in the theory of condensed helium. *Rev. Mod. Phys.*, 67:279, 1995.

[137] H. De Raedt and A. Lagendijk. Monte carlo calculation of the thermodynamic properties of a quantum model. *Phys. Rev. Lett.*, 47:77, 1981.

[138] H. Kono, A. Takasaka, and S. H. Lin. Monte carlo calculation of the quantum partition function via path integra. *J. Chem. Phys.*, 88:6390, 1988.

[139] R.P. Feynman. Space time approach to non relativistic quantum mechanics. *Rev. Mod. Phys.*, 20:367, 1948.

[140] M. Takahashi and M. Imada. *Phys. Soc. Jpn*, 53:936, 1984.

[141] M. Kac. ondistricution of certain wiener functionals. *Trans. Math. Soc. Am.*, 65:1, 1949.

Acknowledgements

This thesis has been prepared during the past three years in the group *Macroscopic systems and quantum theory* at the physics department of the University of Osnabrück. I am indebted to many people for their help and guidance during the time which I spent working on this PhD thesis.

First of all, I am particularly very grateful to Apl Prof. Jürgen Schnack, my supervisor, for his continuous support the project and innumerable stimulating discussions on fascinating problems with powerful ideas and his unmatched enthusiasm, and I enjoyed working with him very much.
I would like to thank Prof. Klaus Bärwinkel and Apl Prof. H.-J. Schmidt both provided an active and friendly environment for my work which helped making my research enjoyable and successful. I also appreciate the collaboration with M. Exler, who provided his extensive computer support.
In addition, I would like to express my thanks to Dr. Andrei V. Postnikov, Prof. Marshall Luban, Dr. Bernd Pilawa as well as Prof. Richard Winpenny for fruitful discussions, and Prof. Eva Rentschler for providing the susceptibility data of heterometallic wheels. Prof. Ulrich Kortz and Prof. Naresh Dalal are acknowledged for collaboration and providing the wheel-shaped Tungstophosphate.
Furthermore, I want to thank Dr. Lee Cronin and Dr. Paul Kögerler for providing dodecanuclear cluster and Prof. H. Nojiri for the ESR measurements.
I should like to acknowledge many people who made my time in the group interesting and enjoyable. I am grateful to M. Brüger, P. Hage, R. Steinigeweg, F. Homann, F. Ouchni, F. Hesmer, P. Shchelokovskyy. I want also to thank T. Mehaddene, S. Lounis, B. Belhadji and O. Adjaoud.

This work was supported by the Ph.D. program of the University of Osnabrück. I am indebted to the coordinator Dr. Wolfgang Mikosch, for leading and organizing a series of very useful scientific seminars and language courses, I want to thank all the students for the pleasant atmosphere during the lectures, seminars and workshops. The financial support is gratefully acknowledged.

Finally, I want to thank my family and special thank for my parents.

Eidesstattliche Erklärung

Hiermit erkläre ich an Eides Statt, die vorliegende Abhandlung selbständig und ohne unerlaubte Hilfe verfasst, die benutzten Hilfsmittel vollständig angegeben und noch keinen Promotionsversuch unternommen zu haben.

Osnabrück, 03/05/2006

Mohammed Allalen